

HYBRID VECTOR CONTROL FOR INDUCTION MOTOR

A DISSERTATION

*Submitted in partial fulfilment of the
requirements for the award of the degree*

of

MASTER OF TECHNOLOGY

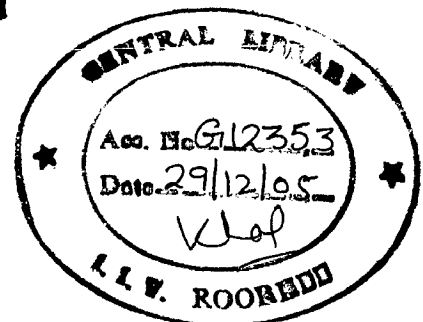
in

ELECTRICAL ENGINEERING

(With Specialization in Power Apparatus and Electric Drives)

By

DHIRENDRA SINGH



**DEPARTMENT OF ELECTRICAL ENGINEERING
INDIAN INSTITUTE OF TECHNOLOGY ROORKEE
ROORKEE-247 667 (INDIA)**

JUNE, 2005

18

CANDIDATE'S DECLARATION

I hereby declare that the work, which is being presented in the dissertation entitled "HYBRID VECTOR CONTROL FOR INDUCTION MOTOR" towards partial fulfillment of the requirement for the award of degree of **Master of Technology in Electrical Engineering** with specialization in **Power Apparatus and Electrical Drives**, submitted to the Department of Electrical Engineering, Indian Institute of Technology, Roorkee, is an authentic record of my own work carried out from July 2004 to June 2005, under the guidance of **Assoc. Prof. S.P. Singh**, Department of Electrical Engineering, IIT, Roorkee.

I have not submitted the matter embodied in this dissertation for the award of any other degree or diploma.

Date: 24.06.2005

Place: Roorkee

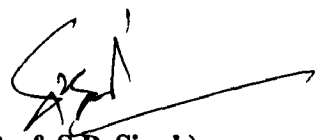

(DHIRENDRA SINGH)

CERTIFICATE

This is to certify that the above statement made by the candidate is correct to the best of my knowledge.

Date: 24.06.2005

Place: Roorkee


(Assoc. Prof. S.P. Singh)
Department Electrical Engineering
IIT Roorkee
Roorkee- 247667
INDIA

ACKNOWLEDGEMENT

The work presented in this paper is carried out at the Department of Electrical Engineering at the IIT Roorkee.

I wish to express my deep sense of gratitude to Assoc. Prof. S. P. Singh, Department of Electrical Engineering, IIT Roorkee for his unfailing inspiration, whole-hearted co-operation and pain staking supervision for this thesis work. His encouragement and incisive comments gave immense confidence to complete this work. His guidance, enthusiasm; encouragement and vast knowledge have been invaluable throughout the course of this thesis work.

I am very grateful to Prof. H. O. Gupta, Head of the department of Electrical Engineering, who supported my effort.

Thanks are due to those who in some way or the other assisted me in preparing this thesis work.

Date-24.06.2005
Place: Roorkee


(DHIRENDRA SINGH)

ABSTRACT

In this thesis work, first the dynamic modeling of the induction motor has been described because per-phase equivalent circuit analysis it is not appropriate to predict dynamic performance of the motor. In order to understand and analyze vector control of induction motors the dynamic model is necessary. Machine is modeled in stator reference frame since it is easier to describe the characteristics of induction motor. Also the machine is modeled in relatively simple terms by using the concept of space vectors and d-q variables.

II In the next part of the thesis, general principle and various concepts of vector control have been described. Then direct vector control (DVC) has been simulated and analyzed. For the rotor flux position angle estimation, here motor terminal voltages (v_{ds} , v_{qs}) and current (i_{ds} , i_{qs}) has been used and rotor flux based calculations are made. Machine is modeled in stator reference frame using state space vectors for viewing actual behavior of inputs and outputs. In direct vector control, only inverse Clark's and Park's transformation are required because torque current and flux current commands are set by using PI controllers. But direct vector suffers from low speed and zero speed problems. Because at these speeds stator voltages, currents and frequency becomes very low and it becomes difficult to sense these quantities. Moreover parameter variation effect of resistance R_s and inductances L_{sl} , L_{rl} and L_m tends to reduce the accuracy of estimated signals.

In the next part of the thesis indirect vector control scheme has been simulated and analyzed. This scheme uses rotor speed signal for the estimation of rotor flux position estimation in whole speed range. Here also the machine is modeled in stator reference frame for the same reason as stated above. Since the commanded torque producing and flux producing current are DC signals, so the stator three phase currents are transformed into synchronous frame dq-currents. For this Clark's and Park's transformations are used. Again for PWM control the actual dq-current that corresponds to input variables (ω_{ref} and T_L) are converted into stationary reference frame by using inverse Clark's and Park's transformations. Parameter variation effects of rotor resistance R_r has also been analyzed

both in open loop and closed loop and a method called model reference adaptive control has been used for compensation of rotor resistance mismatch. Since indirect vector control scheme uses rotor speed signal so speed sensing encoders becomes costly and more complex at higher speeds.

In the last of this work, hybrid vector control scheme has been designed and simulated. Hybrid vector controlled drive utilizes both direct and indirect vector control schemes according to speed variation. This drive system is rotor flux oriented in whole speed range and primarily aimed for electric vehicle type applications, which requires dynamic torque control even at zero speed or low speed. The drive system controls the speed and torque separately in a decoupled manner. This rotor flux oriented drive starts at zero speed in indirect vector control mode , transits to direct vector control mode as the speed develops, and then transits back to indirect vector control mode as the speed approaches to zero. The operation of drive in four quadrants has also been analyzed.

CONTENTS

Candidate's Declaration	I
Acknowledgement	II
Abstract	III
Contents	V
List of symbols	VIII
List of figures	XI
Introduction	1
I. Historical review	1
II. Literature Review	5
III. Structure of thesis	8
IV. Aim of Thesis	10
Chapter 1 – Induction Motor Model, Generalities	11
1.1 Dynamic modeling of Induction motor	11
1.2 Space phasor modeling of Induction motor	14
1.3 Simulink design of Space Phasor model of Induction motor	18
1.4 Simulation results	20
1.4.1 Free acceleration characteristics	20
1.4.2 Rated Load characteristics	25
1.5 Interim conclusions	26
Chapter 2 – Field Oriented Control. Principle and Generalities	27
2.1 Principle of Field Oriented Control	27
2.2 Phasor diagram of Vector Control	28
2.3 Space vector definition and projection	29
2.4 The (a, b, c) → (α, β) projection (Clarke transformation)	30

2.5 The $(\alpha, \beta) \rightarrow (d, q)$ projection (Park transformation)	30
2.6 The $(d, q) \rightarrow (\alpha, \beta)$ projection (inverse Park transformation)	31
2.7 The basic scheme for the FOC	32
2.8 The inputs for the FOC	34
2.9 Interim conclusions	35
Chapter 3 – Direct Vector Control	36
3.1 Principle of Direct Vector Control.	36
3.2 Rotor Flux Vector Estimation	37
3.2.1 Terminal Voltage Model	37
3.3 PWM Voltage Source Inverter	40
3.2.1 Simulink design of PWM inverter	42
3.4 The PI Controller	42
3.4.1 Simulink Design of PI Controllers	43
3.4.1.1 Torque and Speed PI controller	43
3.4.1.2 Torque current PI controller	44
3.4.1.3 Flux current PI controller	44
3.5 Simulation results	45
3.5.1 Speed response analysis under no load condition ($T_l = 0$)	45
3.5.2 Torque response analysis under no load condition ($T_l = 0$)	52
3.5.3 Response under speed reversal ($T_l = 0$)	53
3.5.4 Response under load condition	56
3.6 Interim conclusions	60
Chapter 4 – Indirect Vector Control	61
4.1 Principle of Indirect Vector Control	61
4.2 Indirect Vector Control Scheme	62
4.3 SIMULINK design of Indirect Vector Control scheme	64
4.4 Response under No load condition	65

4.4.1	Speed response analysis	65
4.4.2	Torque response analysis	67
4.5	Response under reverse Motoring Operation	73
4.6	Response under load condition	76
4.7	Response during field weakening mode	81
4.8	Parameter Sensitivity of the Indirect Vector Control Scheme	82
4.8.1	Response of Uncompensated System	83
4.9	Parameter Sensitivity Compensation	86
4.9.1	Slip gain tuning based on MRAC	86
4.9.2	Response of compensated system	88
4.10	Parameter sensitivity effect on closed loop speed control system	91
4.11	Interim conclusions	95
 Chapter 5 – Hybrid Vector Control		96
5.1	Introduction	96
5.2	Simulation results	97
5.3	Response under four quadrant operation	107
5.3.1	Response during first quadrant operation	108
5.3.2	Response during second quadrant operation	110
5.3.3	Response during third quadrant operation	113
5.3.4	Response during fourth quadrant operation	114
5.4	Interim conclusions	115
 Chapter 6 – Conclusions and Scope for future work		116
 References		
 Appendixes 1		
 Appendixes 2		

LIST OF SYMBOLS

T_e	Electromagnetic torque of motor
T_{load}	Load torque reference
λ_r	Rotor flux linkage
i_{qs}	q-axis component of stator current in stator reference frame
i_{ds}	d-axis component of stator current in stator reference frame
V_s	Stator voltage
v_{qs}	q-axis stator voltage in stator reference frame
v_{ds}	d-axis stator voltage in stator reference frame
v_{qs}^e	q-axis stator voltage in synchronous reference frame
v_{ds}^e	d-axis stator voltage in synchronous reference frame
i_s	Stator current
i_T	Torque component of stator current
i_f	Flux component of stator current
θ_e	Field angle
θ_s	Stator phase angle
θ_T	Torque angle
θ_{sl}	Slip angle
θ_r	Rotor position angle
ω_s	Synchronous frequency
ω_{sl}	Slip frequency
ω_r	Rotor frequency
ω_{ref}	Reference speed signal

$i_{s\alpha}$	Component of stator current in $\alpha\beta$ – reference frame
$i_{s\beta}$	Component of stator current in $\alpha\beta$ – reference frame
i_{sdref}	d-axis stator flux reference current component
i_{sqref}	q-axis stator torque reference current component
v_{sdref}, v_{sqref}	d, q-axis stator voltage reference
i_{qe}^*, i_{de}^*	Torque command and flux command current (synchronous reference frame).
$\lambda_{dr}^s, \lambda_{qr}^s$	Rotor d, q-axis flux in stator reference frame
i_a, i_b, i_c	Stator phase currents
i_{dr}^s, i_{qr}^s	Rotor d-axis and q-axis current in stator reference frame
R_s	Stator resistance
R_r	Rotor resistance
R_{rc}	Rotor resistance used in vector controller
L_r	Rotor inductance in Henry
L_{rc}	Rotor inductance used in vector controller
L_s	Stator inductance in Henry
L_m	Magnetizing inductance in Henry
L_{mc}	Magnetizing inductance used in vector controller
L_{ls}	Stator leakage inductance
p	Number of poles
$\lambda_{ds}^s, \lambda_{qs}^s$	Stator d-axis and q-axis flux in stator reference frame
λ_s	Stator flux
$\lambda_{dm}, \lambda_{qm}$	Magnetizing flux
$\sin \theta_e, \cos \theta_e$	Unit vectors
K_{ps}, K_{is}	Proportional and integral gain of speed PI controller

K_{p1}, K_{i1}	Proportional and integral gain of torque current PI controller
K_{p2}, K_{i2}	Proportional and integral gain of flux current PI controller
λ_{rc}	Commanded value of rotor flux
T_{rc}	Rotor time constant used in vector controller
ω_b	Base speed of motor

ABBREVIATIONS

FOC	Field Oriented Control
DVC	Direct Vector Control
IVC	Indirect Vector Control
PI	Proportional and Integral controller

LIST OF FIGURES

- Figure (1.1): Stator and rotor windings of a two phase induction motor
- Figure (1.2): Space phasor model of induction motor
- Figure (1.3): Flux and current relation block
- Figure (1.4): Stator phase A current under free acceleration
- Figure (1.5): Stator phase B current under free acceleration
- Figure (1.6): stator phase C current under free acceleration
- Figure (1.7): Torque response under free acceleration
- Figure (1.8): Speed response under free acceleration
- Figure (1.9): Stator d-axis flux response during free acceleration
- Figure (1.10): Stator q-axis flux response during free acceleration
- Figure (1.11): Stator flux response during free acceleration
- Figure (1.12): Rotor flux response during free acceleration
- Figure (1.13): Stator phase A current under rated load condition
- Figure (1.14): Torque-speed characteristic during rated load condition
- Figure (1.15): Speed response during rated load condition
- Figure (2.1): Phasor diagram of the vector controller
- Figure (2.2): Stator current space vector and its component in (a,b,c)
- Figure (2.3): Stator current space vector and its components in (α and β)
- Figure (2.4): Stator current space vector and its component in (α , β) and in the d, q rotating reference frame
- Figure (2.5): Basic scheme of vector control for AC machines
- Figure (3.1): Simulink diagram for direct vector control scheme
- Figure (3.2): $d^s - q^s$ and $d^e - q^e$ phasors showing correct rotor flux orientation
- Figure (3.3): Basic scheme of PWM inverter
- Figure (3.4): Simulink design of triangular wave generation
- Figure (3.5): Simulink design of sinusoidal PWM inverter

- Figure (3.6): Simulink design of speed PI controller for torque command
- Figure (3.7): Simulink design of current PI controller for i_{qe} component
- Figure (3.8): Simulink design of current PI controller for i_{de} component
- Figure (3.9) Speed response under no load condition
- Figure (3.10) Shows unit vector signals in correct phase position
- Figure (3.12) Shows unit vector signals in correct phase position
- Figure (3.14) Stator phase A current
- Figure (3.15) Stator phase B current
- Figure (3.16) Stator phase C current
- Figure (3.17) Stator flux response (no load condition)
- Figure (3.18) Rotor flux response (no load condition)
- Figure (3.19) Torque response under no load condition
- Figure (3.20) Speed response during reverse motoring (no load condition)
- Figure (3.21) Speed and torque response during reverse motoring operation
- Figure (3.22) Unit vector signal $\sin \theta_c$ during reverse motoring operation
- Figure (3.23) Unit vector signal $\cos \theta_c$ during reverse motoring operation
- Figure (3.22) Speed response under load condition
- Figure (3.24) Stator phase A current during reverse motoring operation
- Figure (3.25) Torque response under load condition
- Figure (3.26) Speed response under load condition
- Figure (3.27) Speed and torque response under load condition
- Figure (3.28) Unit vector signal $\cos \theta_c$ and λ_{dr} under load condition
- Figure (3.29) Unit vector signal $\sin \theta_c$ and λ_{qr} under load condition
- Figure (3.30) Rotor flux (λ_r) response under load condition
- Figure (4.1) Phasor diagram of indirect vector control
- Figure (4.2) Simulink diagram for indirect vector control scheme
- Figure (4.3) Speed response during no load condition

- Figure (4.4) Torque response during no load condition
- Figure (4.5) stator phase currents response during no load condition
- Figure (4.6): Rotor flux response
- Figure (4.7): Unit vector $\sin\theta_e$ and λ_{qr} during no load condition
- Figure (4.8): Unit vector $\cos\theta_e$ and λ_{dr} during no load condition
- Figure (4.9): Stator flux response during no load condition
- Figure (4.10): Stator dq-current response during no load condition
- Figure (4.11): Stator d-axis voltage
- Figure (4.12): Stator q-axis voltage
- Figure (4.13): Speed response during reverse motoring operation
- Figure (4.14): Torque response during reverse motoring operation
- Figure (4.15): Response of unit vector $\sin\theta_e$ and λ_{qr} during reverse motoring operation
- Figure (4.16): Response of unit vector $\cos\theta_e$ and λ_{dr} during reverse motoring operation
- Figure (4.17) Stator phase current response during reverse motoring operation
- Figure (4.18): Field angle (θ_e) variation during reverse motoring operation
- Figure (4.19): Response of rotor speed under load condition
- Figure (4.20): Torque response under load torque of 100 N·m
- Figure (4.21): Response of $\sin\theta_e$ and λ_{qr}
- Figure (4.22): Response of $\cos\theta_e$ and λ_{dr}
- Figure (4.23): Stator phase current response
- Figure (4.24): Speed and torque response under dynamic load condition
- Figure (4.25): Rotor speed above rated speed
- Figure (4.26): Rotor flux (λ_r) response
- Figure (4.27): Torque response for different values of rotor resistance
- Figure (4.28): Rotor flux response for different values of rotor resistance
- Figure (4.29): Stator q-axis current response

- Figure (4.30): Stator d-axis current response
- Figure (4.31): Speed response for different values of rotor resistance
- Figure (4.32): Slip gain tuning by model reference adaptive control principle
- Figure (4.33): Torque response ($R_r = 0.5 * R_{rc}$)
- Figure (4.34): Rotor d-axis flux response ($R_r = 0.5 * R_{rc}$)
- Figure (4.35): Rotor q-axis flux response ($R_r = 0.5 * R_{rc}$)
- Figure (4.36): Torque response ($R_r = 1.5 * R_{rc}$)
- Figure (4.37): Rotor d-axis flux response ($R_r = 1.5 * R_{rc}$)
- Figure (4.38): Rotor q-axis flux response ($R_r = 1.5 * R_{rc}$)
- Figure (4.39): Speed response for different values of rotor resistance
- Figure (4.40): Torque response for different values of rotor resistance
- Figure (4.41): Commanded Torque response for different values of rotor resistance
- Figure (4.42): Stator flux response for different values of rotor resistance
- Figure (4.43): Rotor flux response for different values of rotor resistance
- Figure (5.1): IVC – DVC transition control diagram
- Figure (5.2): Simulink diagram for hybrid vector control
- Figure (5.3): Response of Transition signal
- Figure (5.4): Speed response
- Figure (5.5): Torque response
- Figure (5.6): Response of $\cos \theta_e$
- Figure (5.7): Response of $\sin \theta_e$
- Figure (5.8): Response of rotor dq-flux
- Figure (5.9): Response of stator dq- current
- Figure (5.10): Speed response
- Figure (5.11): Torque response
- Figure (5.12): Stator d-axis current response
- Figure (5.13): Stator q-axis current response
- Figure (5.14): Speed response in forward and reverse motoring mode

- Figure (5.15): Torque response in forward and reverse motoring mode
- Figure (5.16): Unit vectors response in forward and reverse motoring mode
- Figure (5.17): Stator dq-current response in forward and reverse motoring mode
- Figure (5.18): Speed (above) and Torque (below) response in 1st quadrant
- Figure (5.19): Response of Rotor flux (above) and Unit vectors (below) in 1st quadrant
- Figure (5.20): Response of stator dq-current in 1st quadrant
- Figure (5.21): Speed response in 2nd quadrant
- Figure (5.22): Torque response in 2nd quadrant
- Figure (5.23): Response of $\cos\theta_e$ and λ_{dr} in correct phase sequence
- Figure (5.24): Response of $\sin\theta_e$ and λ_{qr} in correct phase sequence
- Figure (5.25): Speed (above) and Torque (below) response in 3rd quadrant
- Figure (5.26): Speed (above) and Torque (below) response in 4th quadrant

INTRODUCTION

I. Historical review

The history of electrical motors goes back as far as 1820, when Hans Christian Oersted discovered the magnetic effect of an electric current. One year later, Michael Faraday discovered the electromagnetic rotation and built the first primitive D.C. motor. Faraday went on to discover electromagnetic induction in 1831, but it was not until 1883 that Tesla invented the A.C asynchronous motor [28]. Currently, the main types of electric motors are still the same, DC, AC asynchronous and synchronous, all based on Oersted, Faraday and Tesla's theories developed and discovered more than a hundred years ago.

Since its invention, the AC asynchronous motor, also named induction motor, has become the most widespread electrical motor in use today. At present, 67% of all the electrical energy generated is converted to mechanical energy for utilization. These facts are due to the induction motors advantages over the rest of motors. The main advantage is that induction motors do not require an electrical connection between stationary and rotating parts of the motor. Therefore, they do not need any mechanical commutator (brushes), leading to the fact that they are maintenance free motors. Induction motors also have low weight and inertia, high efficiency and a high overload capability. Therefore, they are cheaper and more robust, and less prone to any failure at high speeds. Furthermore, the motor can work in explosive environments because no sparks are produced. Taking into account all the advantages as outlined above, induction motors must be considered the perfect electrical to mechanical energy converter.

However, mechanical energy is more than often required at variable speeds, where the speed control system is not a trivial matter. The only effective way of producing an infinitely variable induction motor speed drive is to supply the induction motor with three phase voltages of variable frequency and variable amplitude. A variable frequency is required because the rotor speed depends on the speed of the rotating magnetic field provided by the stator [9] [3]. A variable voltage is required because the motor impedance reduces at low frequencies and consequently the current has to be limited by means of reducing the supply voltages [26] [27].

Before the days of power electronics, a limited speed control of induction motor was achieved by switching the three-stator windings from delta connection to star connection, allowing the voltage at the motor windings to be reduced. Induction motors are also available with more than three stator windings to allow a change of the number of pole pairs. However, a motor with several windings is more expensive because more than three connections to the motor are needed and only certain discrete speeds are available. Another alternative method of speed control can be realized by means of a wound rotor induction motor, where the rotor winding ends are brought out to slip rings. However, this method obviously removes most of the advantages of induction motors and it also introduces additional losses. By connecting resistors or reactances in series with the stator windings of the induction motors, poor performance is achieved. At that time the above described methods were the only ones available to control the speed of induction motors, whereas infinitely variable speed drives with good performances for DC motors already existed. These drives not only permitted the operation in four quadrants but also covered a wide power range. Moreover, they had a good efficiency, and with a suitable control even a good dynamic response. However, its main drawback was the compulsory requirement of brushes [22] [31].

With the enormous advances made in semiconductor technology during the last 20 years, the required conditions for developing a proper induction motor drive are present. These conditions can be divided mainly in two groups: The decreasing cost and improved performance in power electronic switching devices. The possibility of implementing complex algorithms in the new microprocessors. However, one precondition had to be made, which was the development of suitable methods to control the speed of induction motors, because in contrast to its mechanical simplicity their complexity regarding their mathematical structure (multivariable and non-linear) is not a trivial matter [21]. It is in this field, that considerable research effort is devoted. The aim being to find even simpler methods of speed control for induction machines. One method, which is popular at the moment, is Vector Control [1] [2] [3] [9]. Historically, several general controllers have been developed:

Scalar controllers: Despite the fact that “Voltage-Frequency” (V/f) is the simplest controller, it is the most widespread, being in the majority of the industrial applications. It is known as a

scalar control and acts by imposing a constant relation between voltage and frequency. The structure is very simple and it is normally used without speed feedback. However, this controller doesn't achieve a good accuracy in both speed and torque responses, mainly due to the fact that the stator flux and the torque are not directly controlled. Even though, as long as the parameters are identified, the accuracy in the speed can be 2% (except in a very low speed), and the dynamic response can be approximately around 50ms [9].

Direct Torque Control (DTC): This method has emerged over the last decade to become one possible alternative for speed control of Induction Machines. Its main characteristic is the good performance, obtaining results as good as the classical vector control. DTC has certain advantages over vector control scheme like absence of coordinate transformation, absence of PID controller for motor torque and flux.

Vector Controllers: Vector control or field orientation control, is a method in which the motor input currents are adjusted to set a specific angle between fluxes produced in the rotor and stator windings in a manner that follows from the operation of a dc machine. More formally, the approach applies direct-quadrature (d-q) two-axis analysis methods directly to the torque control problem if open loop or speed control, if closed loop. When the dynamic equations for an induction motor is transformed by means of well-known rotating transformation methods into a reference frame that coincides with rotor flux, the results become similar to the dynamic behavior of a dc machine. This allows the ac motor's stator current to be separated into flux-producing component and an orthogonal torque producing component, analogous to a dc machine field current and armature current. The key to field-oriented control is knowledge of the rotor flux position angle with respect to the stator. Methods in which rotor flux is sensed by flux sensing coils or it is calculated by motor terminal voltages or currents, are generally termed "direct vector control" (DVC) methods. It is also possible to compute the angle from shaft position information, provided other motor parameters are known. This approach is generally termed "indirect vector control" (IVC), and is the basis of most commercial drives based on the field orientation concept. Whatever the field-orientation approach, once the flux angle is known, an algorithm performs the transformation from three-phase stator currents into the orthogonal torque- and flux-producing

components. Control is then performed in these components, and an inverse transformation is used to determine the necessary three-phase currents or voltages [1] [5] [6] [7]. Accuracy of vector control scheme can reach values such as 0.5% regarding the speed and 2% regarding the torque, even when at stand still

Vector Controllers main features are as follows:

- a. Full motor torque capability at low speed.
- b. Better dynamic performance.
- c. Higher efficiency for each operation point in a wide speed range.
- d. Decoupled control of torque and flux.
- e. Four quadrant operation.

However, some disadvantages are also present such as:

- a. Relatively low dynamic performance due to PI current regulator.
- b. Parameter detuning causes high torque and flux magnitude error.
- c. The main disadvantages are the huge computational capability required and the compulsory good identification of the motor parameters

II. Literature Reviews

Vagati, A. (1984), suggested strategically mixing both the voltage model and current model equations in flux estimation in order to reduce the parameter variation effect.

Bose, K. (1986), proposed another hybrid vector controlled scheme which is basically direct vector control scheme with stator flux orientation in whole velocity range, but uses indirect vector control scheme only for start-up at zero-velocity and shut down, where direct and indirect modes are changed discontinuously.

Schauder, C. (1989), proposed speed estimation by MRAC (model reference adaptive control) method where the speed dependent current model flux estimator tracks the voltage model based flux estimator.

C. C. Chan (1990) described an effective method for rotor resistance identification for the purpose of improving the performance of vector control of induction motor drives. The method is mathematically derived from proper selection of coordinate axes and utilization of the steady-state model of the induction motor.

Kubota, H. (1991), proposes a speed adaptive flux observer which has some degree of robustness for parameter variation.

Kanokvate Tungpimolrut (1993), solve the problem of performance degradation due to parameter variations in an indirect vector control of induction motor, by a novel and simple rotor circuit time constant compensation method. The proposed method is based on regulating the energy stored in the magnetizing inductance by utilizing the information from terminal voltages and currents.

Katsunori TANIGUCHI and Atoushi OKUMURA (1993) described a new PWM method to reduce the torque ripple in the induction motor without producing an optional pulsating wave in a dc link.

De Doncker (1994), proposed a vector control scheme where orientation could be changed between rotor flux, stator flux and air-gap flux, and making transition of indirect vector

control scheme in a low velocity range to direct vector control scheme in high velocity range.

Fang-Zheng Peng (1994) has proposed a new approach to estimate induction motor speed from measured terminal voltages and currents for tachless vector control. The proposed approach is based on observing the counter electromotive force vector or the instantaneous reactive power of the rotor flux.

Kanokvate Tungpimolrut (1994) had described a novel and simple estimation method for the rotor circuit time constant to solve the problem of performance degradation due to parameter variations in an indirect vector control of an induction motor. The proposed method was based on regulating the energy stored in the magnetizing inductance.

Tajima, T. (1996), proposed another switching type hybrid vector control scheme where two methods of generating synchronous angular velocity in indirect form were used and they are discontinuously switched to each other before and after zero-crossing of synchronous angular velocity.

Bimal K. Bose (1997) had described a fuzzy logic-based on-line efficiency optimization control for an indirect vector-controlled induction motor drive.

Kwanghee Nam (1998) had proposed a series R - L model that accounts for the effects of the iron loss in electric vehicle (EV) motors that are characterized by their low inductance and high current density. He had derived a rotor-flux-oriented vector control scheme for the series model and analyzes the flux error, orientation angle error, and torque error caused by iron loss.

Yen-Shin Lai (1998) had explained a unified approach for modeling and vector control of induction motors (IM) using state variables.

L. Romeral , gives a general overview of the motion control system blocks, especially that related with motor considerations and torque control.

Dal Y. Ohm (2000) has described dynamic and state space vector model of induction motor in order to understand and analyze vector control of induction motors. He had also explained the fundamental dynamic mechanism of the motor in the synchronous frame and the basic principles of vector control in general terms.

Shinnaka, S. (2002), proposed a seamless hybrid vector control scheme without velocity and position sensors in pure rotor flux orientation using a frequency hybrid approach. It was completely free from variation of rotor electrical parameters.

M. A. DENAI (2002) had designed intelligent control systems combining conventional control techniques with fuzzy logic and neural networks. Such a hybrid implementation leads to a more effective control design with improved system performance and robustness. Two control approaches were developed and applied to adjust the speed of the drive system. The first control design combines the variable structure theory with fuzzy logic concept and the second approach was a fuzzy state feedback controller that was based on pole placement technique.

Juanjuan Sun and Yongdong Li (2002) had worked out a method for the performance improvement of the Voltage-Oriented Vector Control of induction motor which presents the merits of constant stator flux control, simple calculation and easy implementation. In this method, the d-axis of synchronous reference frame was oriented in the direction of the stator voltage vector, and then a control strategy peculiar to the induction motor was obtained.

Takaharu Takeshita, Yoshiki Nagatoshi, and Nobuyuki Matsui (2002) had worked out a sensorless vector control scheme for low speed drive. The sensorless algorithmic was based on the estimation of the secondary speed emf that leads the secondary magnetic flux by an angle $\pi/2$.

Xing Yu and Matthew W. Dúnnigan (2002) had explained a novel rotor resistance identification method for an indirect rotor flux-orientated controlled induction machine drive. A decoupled synchronous voltage control scheme was used to achieve a fast, accurate current control response and indicates the relative thermal change of the rotor resistance. A model reference adaptive control scheme was used to track the variation of the rotor resistance.

Burak Ozpineci (2003) explained a modular Simulink implementation of an induction machine model in a step-by-step approach. With the modular system, each block solves one of the model equations; therefore, unlike black box models, all of the machine parameters are accessible for control and verification.

III. - Structure of the thesis

The work presented in this thesis is organized in five main chapters. These five chapters are structured as follows.

Chapter 1 is entitled “Induction Motor Model Generalities”. It introduces a mathematical model of cage rotor induction motor. Different ways of implementing these models are presented as well as some simulations corroborating its validity. In this chapter all simulations are obtained from MATLAB/Simulink. The elements of space pharos notation are also introduced and used to develop a compact notation.

Chapter 2 is entitled “Vector Control, Principles and Generalities”. It is devoted to introduce Vector Control or Field Oriented Control (FOC) strategies. It includes:

- a) Introduction to Field oriented control (FOC)
- b) Space vector definition and projection
- c) Clarke transformation and Park Transformation
- d) Inverse Park Transformation
- e) Basic scheme for the FOC

Chapter 3 is entitled “Direct Vector Control”. It covers a full and in-depth description of Direct Vector Control (DVC) scheme. At the end of the chapter simulated results are presented for different load and speed conditions. Interim conclusions and limitations of direct vector control scheme have been listed at the end.

Chapter 4 is entitled “Indirect Vector Control”. It covers a full and in-depth description of Indirect Vector Control (IVC). At the end of the chapter simulated results are presented for

different load and speed conditions. This chapter also includes the behavior of FOC under parameter detuned condition. Then a method (called MRAC for parameter variation) is described for the compensation of FOC. At the end of the chapter simulated results are presented for uncompensated and compensated system, both under open loop and closed loop, for different load and speed conditions.

Chapter 5 is entitled "Hybrid Vector Control". It covers a full and in-depth description of a rotor flux oriented drive system which starts at zero speed in indirect vector control mode, transits to direct vector control mode as the speed develops, and then transits back to indirect vector control mode at zero speed. Hence this control scheme overcomes the limitations of direct and indirect vector control scheme. At the end of the chapter simulated results are presented for different load and speed conditions.

In **Chapter6**, entitled "Conclusions and scope for future works", all achievements are summarized and appropriate conclusions are drawn.

Finally, all PC programs used in the implementation of DVC, IVC and Hybrid vector control schemes are listed in the appendixes.

IV. - Aim of the thesis

The present thesis deals with the development of Hybrid Vector Control of induction motor that has improved performance compared to the DVC and IVC drive control system. The main improvement has been the torque ripple reduction during startup and other transient conditions. Also, a scheme for tuning of the indirect vector controller is also developed which improves the drive performance when motor rotor resistance changes and become different from vector controller parameter.

CHAPTER 1

INDUCTION MOTOR MODEL, GENERALITIES

1.1 Dynamic Modeling of Induction Motor.

The steady state model is useful for studying the performance of machine in steady state. This implies that all electrical transients are during load changes and stator frequency variation. Such variation arises in application involving variable speed drives. The dynamic model considers the instantaneous effects of varying voltage/currents, stator frequency and torque disturbances. The dynamic model of induction motor model is desired because of the conceptual simplicity obtained with two sets of windings, one on the stator and other on the rotor. The dynamic model of induction motor is derived by using a two phase motor in direct and quadrature axes [9] [26].

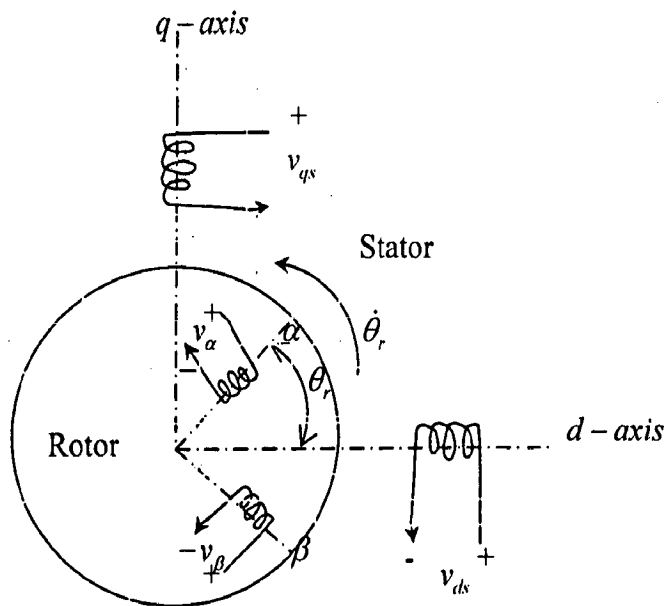


Figure (1.1): Stator and rotor windings of a two phase induction motor

A two-phase induction machine with stator and rotor windings is shown in figure (1.1). The windings are displaced in space by 90 electrical degrees, and the rotor winding, α , is at an angle θ_r from the stator d-axis winding. It is assumed that the d-axis is leading the q-axis for

clockwise direction of rotation of the rotor. If the clockwise phase sequence is dq , the rotating magnetic field will be revolving at the angular speed of the supply frequency but counter to the phase sequence of the supply. Therefore rotor is pulled in the direction of the rotating magnetic field. The currents and voltages of the stator and rotor windings are marked in the figure (1.1). θ_r is the electrical rotor position at any instance, obtained by multiplying the rotor mechanical position by pairs of electrical poles. The terminal voltages of the rotor and stator windings can be expressed as the sum of voltage drops in resistances and rates of change of flux linkages, which are the products of currents and inductances. The equations are as follows:

$$v_{qs} = R_q i_{qs} + p(L_{qq} i_{qs}) + p(L_{qd} i_{ds}) + p(L_{q\alpha} i_{\alpha}) + p(L_{q\beta} i_{\beta}) \quad (1.1)$$

$$v_{ds} = R_d i_{ds} + p(L_{dq} i_{qs}) + p(L_{dd} i_{ds}) + p(L_{d\alpha} i_{\alpha}) + p(L_{d\beta} i_{\beta}) \quad (1.2)$$

$$v_{\alpha} = R_{\alpha} i_{\alpha} + p(L_{\alpha q} i_{qs}) + p(L_{\alpha d} i_{ds}) + p(L_{\alpha\alpha} i_{\alpha}) + p(L_{\alpha\beta} i_{\beta}) \quad (1.3)$$

$$v_{\beta} = R_{\beta} i_{\beta} + p(L_{\beta q} i_{qs}) + p(L_{\beta d} i_{ds}) + p(L_{\beta\alpha} i_{\alpha}) + p(L_{\beta\beta} i_{\beta}) \quad (1.4)$$

Where p is the differential operator $\frac{d}{dt}$, and the various inductances are explained as follows. v_{qs} , v_{ds} , v_{α} , v_{β} are the terminal voltages of the stator q-axis and d-axis, and rotor α and β windings, respectively. i_{qs} and i_{ds} are the stator q axis and d axis current, respectively. i_{α} and i_{β} are the rotor α and β windings currents, respectively. $L_{\alpha\alpha}$, $L_{\beta\beta}$, L_{qq} and L_{dd} are the stator q and d axis winding and rotor α and β winding self inductances, respectively.

Under assumption of uniform air gap, the self inductances are independent of angular positions; hence they are constant:

$$L_{\alpha\alpha} = L_{\beta\beta} = L_{rr} \quad (1.5)$$

$$L_{dd} = L_{qq} = L_s \quad (1.6)$$

The mutual inductances between stator windings and rotor windings are zero. This leads to the following simplification:

$$L_{\alpha\beta} = L_{\beta\alpha} = 0 \quad (1.7)$$

$$L_{dq} = L_{qd} = 0 \quad (1.8)$$

The mutual inductances between stator and rotor windings are function of rotor position θ_r , so

$$L_{\alpha d} = L_{d\alpha} = L_{sr} \cos \theta_r \quad (1.9)$$

$$L_{\beta d} = L_{d\beta} = L_{sr} \sin \theta_r \quad (1.10)$$

$$L_{\alpha q} = L_{q\alpha} = L_{sr} \sin \theta_r \quad (1.11)$$

$$L_{\beta q} = L_{q\beta} = -L_{sr} \cos \theta_r \quad (1.12)$$

Where L_{sr} is the peak value of the mutual inductance between a stator and a rotor winding. Substituting equations from (1.5) to (1.12) into equations from (1.1) to (1.4) results in a system of differential equations with time varying equations. The resulting voltage equations are as follows:

$$v_{qs} = (R_s + L_s p)i_{qs} + L_{sr} p(i_{\alpha} \sin \theta_r) - L_{sr} p(i_{\beta} \cos \theta_r) \quad (1.13)$$

$$v_{ds} = (R_s + L_s p)i_{ds} + L_{sr} p(i_{\alpha} \cos \theta_r) - L_{sr} p(i_{\beta} \sin \theta_r) \quad (1.14)$$

$$v_{\alpha} = L_{sr} p(i_{qs} \sin \theta_r) + L_{sr} p(i_{ds} \cos \theta_r) + (R_r + L_r p)i_{\alpha} \quad (1.15)$$

$$v_{\beta} = -L_{sr} p(i_{qs} \cos \theta_r) + L_{sr} p(i_{ds} \sin \theta_r) + (R_r + L_r p)i_{\beta} \quad (1.16)$$

Where $R_s = R_q = R_d$

$$R_r = R_{\alpha} = R_{\beta}$$

When these equations are transformed into stationary d- and q- axis, these becomes in matrix form as follows:

$$\begin{bmatrix} v_{qs} \\ v_{ds} \\ v_{qr} \\ v_{dr} \end{bmatrix} = \begin{bmatrix} R_s + L_s p & 0 & L_m p & 0 \\ 0 & R_s + L_s p & 0 & L_m p \\ L_m p & -L_m \dot{\theta}_r & R_r + L_r p & -L_r \dot{\theta}_r \\ L_m \dot{\theta}_r & L_m p & L_m \dot{\theta}_r & R_r + L_r p \end{bmatrix} \begin{bmatrix} i_{qs} \\ i_{ds} \\ i_{qr} \\ i_{dr} \end{bmatrix} \quad (1.17)$$

Where $\dot{\theta}_r$ is the time derivative of θ_r and stator effective turns per phase equals to rotor effective turns per phase, $L_m = L_{sr}$, $R_r = R_{rr}$ and $L_r = L_{rr}$.

Equation (1.17) gives induction motor model in stator reference frame. Torque equation is

$$\text{given as } T_c = \frac{3}{2} \frac{P}{2} L_m (i_{qs} i_{dr} - i_{ds} i_{qr}) . \quad (1.18)$$

This model is used when stator variables are required to be actual i.e. the same in the actual machine stator. This model allows simulation of stator controlled induction motor drives, such as phase controlled and inverter- controlled induction motor drives because the input variables are well defined. For a balanced three phase supply

$$v_{qs} = v_{cs} \quad (1.19)$$

$$v_{ds} = \frac{(v_{cs} - v_{hs})}{\sqrt{3}} \quad (1.20)$$

The stator and rotor flux linkages equations can be written as

$$\lambda_{qs} = L_s i_{qs} + L_m i_{qr} \quad (1.21)$$

$$\lambda_{ds} = L_s i_{ds} + L_m i_{dr} \quad (1.22)$$

$$\lambda_{qr} = L_s i_{qr} + L_m i_{qs} \quad (1.23)$$

$$\lambda_{dr} = L_s i_{dr} + L_m i_{ds} \quad (1.24)$$

1.2 Space Phasor Model of Induction Motor.

The stator and rotor flux linkage phasors are the resultant stator and rotor flux linkages and are found by taking the vector sum of the respective d and q components of the flux linkages. Note that flux-linkage phasor describes its spatial distribution. In stead of using two axes such as d and q for a balanced poly phase machine, the flux-linkage phasor can be thought of as being produced by equivalent single phase stator and rotor windings. Such a representation has many advantages:

- a) The system of equations become compact and reduced from four to two;
- b) The system reduces to a two winding system like the dc machine-hence the apparent similarity of them in control to obtain a decoupled independent flux and torque control as in dc machine;
- c) A clear conceptualization of the dynamics of machine, because it is easier to visualize the interaction of two windings rather than four windings, resulting in an in-depth understanding of the dynamics process used in developing high performance control strategies;
- d) A meaningful interpretation of the eign values of the system, regardless of the reference considered.

Voltage equations:

The four dq-equations (1.17) are reduced to two space-phasor equations by the following steps:

$$v_{qs} = (R_s + L_s p)i_{qs} + L_m p i_{qr} \quad (1.25)$$

$$v_{ds} = (R_s + L_s p)i_{ds} + L_m p i_{dr} \quad (1.26)$$

$$v_{qr} = L_m p i_{qs} - \omega_r L_m i_{ds} + (R_r + L_r p)i_{qr} - \omega_r L_r i_{dr} \quad (1.27)$$

$$v_{dr} = L_m \omega_r i_{qs} + L_m p i_{dr} + \omega_r L_r i_{qr} + (R_r + L_r p)i_{dr} \quad (1.28)$$

Since v_{ds} and v_{qs} are in quadrature, so

$$v_s = v_{qs} - jv_{ds} \quad (1.29)$$

Or,

$$v_s = \{(R_s + L_s p)i_{qs} + L_m p i_{qr}\} - j\{(R_s + L_s p)i_{ds} + L_m p i_{dr}\} \quad (1.30)$$

$$v_s = \{(R_s + L_s p)i_{qs} - (R_s + L_s p) j i_{ds}\} + \{L_m p i_{qr} - L_m p j i_{dr}\} \quad (1.31)$$

$$v_s = (R_s + L_s p)\{i_{qs} - j i_{ds}\} + L_m p \{i_{qr} - j i_{dr}\} \quad (1.32)$$

$$v_s = (R_s + L_s p)i_s + L_m p i_r \quad (1.33)$$

Similarly for rotor voltage:

Since v_{dr} and v_{qr} are in quadrature, so

$$v_r = v_{qr} - jv_{dr} \quad (1.34)$$

So from equation (2.27) and (2.28)

$$v_r = \left\{ L_m p i_{qs} - \omega_r L_m i_{ds} + (R_r + L_r p) i_{qr} - \omega_r L_r i_{dr} \right\} - j \left\{ L_m \omega_r i_{qs} + L_m p i_{ds} + \omega_r L_r i_{qr} + (R_r + L_r p) i_{dr} \right\} \quad (1.35)$$

Or

$$v_r = (L_m p i_{qs} - j L_m p i_{ds}) + (-\omega_r L_m i_{ds} - L_m \omega_r j i_{qs}) + ((R_r + L_r p) i_{qr} - (R_r + L_r p) j i_{dr}) + (-\omega_r L_r j i_{qr} - \omega_r L_r i_{dr}) \quad (1.36)$$

Or

$$v_r = L_m p (i_{qs} - j i_{ds}) - j \omega_r L_m (i_{qs} - j i_{ds}) + (R_r + L_r p) (i_{qr} - j i_{dr}) - j \omega_r L_r (i_{qr} - j i_{dr}) \quad (1.37)$$

Or

$$v_r = (L_m p - j \omega_r L_m) i_s + ((R_r + L_r p) - j \omega_r L_r) i_r \quad (1.38)$$

By using equations from (1.21) to (1.24), flux linkage equations can be written as:

$$\begin{bmatrix} \lambda_{ds} \\ \lambda_{dr} \end{bmatrix} = \begin{bmatrix} L_{sl} + L_m & L_m \\ L_m & L_{rl} + L_m \end{bmatrix} \begin{bmatrix} i_{ds} \\ i_{dr} \end{bmatrix} \quad (1.39)$$

$$\begin{bmatrix} \lambda_{qs} \\ \lambda_{qr} \end{bmatrix} = \begin{bmatrix} L_{sl} + L_m & L_m \\ L_m & L_{rl} + L_m \end{bmatrix} \begin{bmatrix} i_{qs} \\ i_{qr} \end{bmatrix} \quad (1.40)$$

So,

$$\begin{bmatrix} i_{ds} \\ i_{dr} \end{bmatrix} = \begin{bmatrix} L_{sl} + L_m & L_m \\ L_m & L_{rl} + L_m \end{bmatrix}^{-1} \begin{bmatrix} \lambda_{ds} \\ \lambda_{dr} \end{bmatrix} \quad (1.41)$$

$$\begin{bmatrix} i_{ds} \\ i_{dr} \end{bmatrix} = \frac{1}{\Delta} \begin{bmatrix} L_{rl} + L_m & -L_m \\ -L_m & L_{sl} + L_m \end{bmatrix} \begin{bmatrix} \lambda_{ds} \\ \lambda_{dr} \end{bmatrix} \quad (1.42)$$

Similarly,

$$\begin{bmatrix} i_{qs} \\ i_{qr} \end{bmatrix} = \begin{bmatrix} L_{sl} + L_m & L_m \\ L_m & L_{rl} + L_m \end{bmatrix}^{-1} \begin{bmatrix} \lambda_{qs} \\ \lambda_{qr} \end{bmatrix} \quad (1.43)$$

$$\begin{bmatrix} i_{qs} \\ i_{qr} \end{bmatrix} = \frac{1}{\Delta} \begin{bmatrix} L_{rl} + L_m & -L_m \\ -L_m & L_{sl} + L_m \end{bmatrix} \begin{bmatrix} \lambda_{qs} \\ \lambda_{qr} \end{bmatrix} \quad (1.44)$$

Where $\Delta = [(L_{sl} + L_m)(L_{rl} + L_m) - L_m^2] = [L_{sl} \cdot L_{rl} + L_{sl} \cdot L_m + L_{rl} \cdot L_m]$

From equations (1.33) and (1.38) voltage equations in state space form can be written as

$$v_s = R_s i_s + \frac{d\lambda_s}{dt} + j\omega_k [B] \lambda_s \quad (1.45)$$

$$0 = R_r i_r + \frac{d\lambda_r}{dt} + j(\omega_k - \omega_m) [B] \lambda_r \quad (1.46)$$

where $B = \begin{bmatrix} 0 & -1 \\ 1 & 0 \end{bmatrix}$

$$i_s = [i_{ds} \quad i_{qs}] \quad i_r = [i_{dr} \quad i_{qr}]$$

$$v_s = [v_{ds} \quad v_{qs}] \quad \lambda_s = [\lambda_{ds} \quad \lambda_{qs}]$$

$$\lambda_r = [\lambda_{dr} \quad \lambda_{qr}]$$

$$v_r = 0; \text{ for squirrel cage rotor}$$

Electromagnetic torque developed is derived as

$$T_e = \frac{3}{2} \frac{p}{2} L_m \left[\text{img} (i_s \bar{i}_r) \right] \quad (1.47)$$

Or,

$$T_e = \frac{3}{2} \frac{p}{2} L_m \left[\text{img} \left\{ (i_{qs} - j i_{ds}) (i_{qr} + j i_{dr}) \right\} \right] \quad (1.48)$$

Or,

$$T_e = \frac{3}{2} \frac{P}{2} L_m (i_{qs} i_{dr} - i_{ds} i_{qr}) \quad (1.49)$$

And the mechanical equation for the torque is

$$T_e = 2J \left(\frac{d\omega_r}{dt} \right) + B_m \omega_r + T_l \quad (1.50)$$

where

$\omega_k \rightarrow$ Speed of reference frame

$\omega_r \rightarrow$ Speed of rotor

$B_m \rightarrow$ Frictional constant

1.3 Simulink design of induction motor space phasor model.

A three phase, 4-pole symmetrical induction motor has been simulated in the stationary frame. For small dynamic stability analysis, a synchronously rotating reference frame, yields steady state values of steady state voltages under balanced conditions. Here it is needed to build a model that includes the stator and rotor flux referenced along the d-q axes. This is because these values are used to calculate the voltages induced in the rotor. Once again, calculation are greatly simplified when all quantities are referred along the d-q reference frame, however, in this case, the d-q reference frame is stationary. Therefore, the angular position of the rotor is not required to make the transformations. The interior of the “induction machine block” in stationary frame is

shown in figure (1.2). Flux and current relation block is shown in figure (1.3). It uses equation (1.44). Torque subsystem uses equations from (1.50).

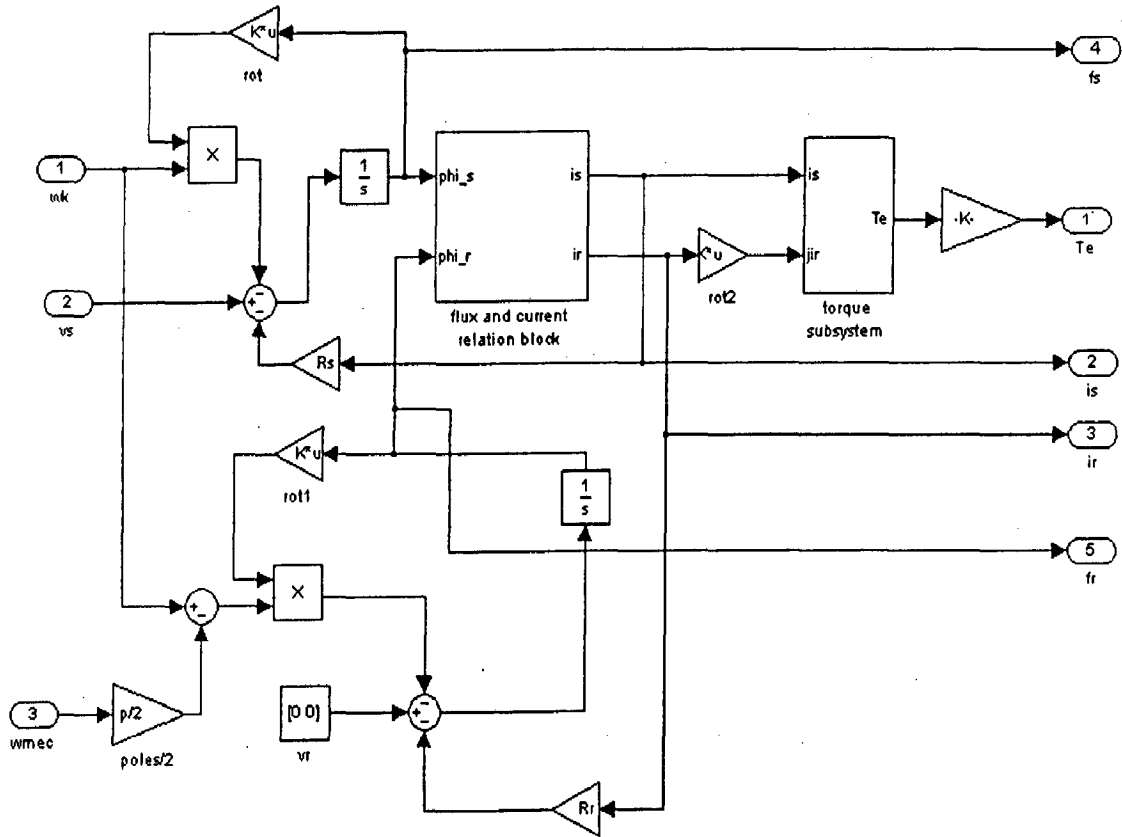


Figure (1.2): Space phasor model of induction motor

Flux and current relation block:

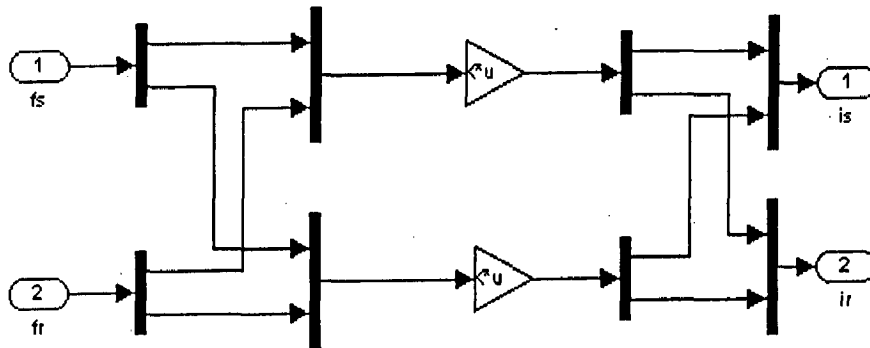


Figure (1.3): Flux and current relation block

1.4 Simulation results.

The induction motor used in drive system is simulated in the MATLAB/SIMULINK with the dynamic space phasor model using nominal parameters given in appendix (1). The behavior of machine has been observed under free acceleration and rated load condition. The voltage is rated rms line-to-line voltage. At the stall the input impedance of the induction motor essentially the stator resistance and leakage reactance in series with the rotor resistance and leakage reactance. Consequently with the rated voltage applied, the starting current is large. A 3-phase 50-hp machine is relatively high-slip machine (4.4%); that is, rated torque is developed at a speed considerably less than synchronous speed. The integration method used is variable step, the “ode23tb (stiff/TRBDF2)”.

1.4.1 Free acceleration characteristics.

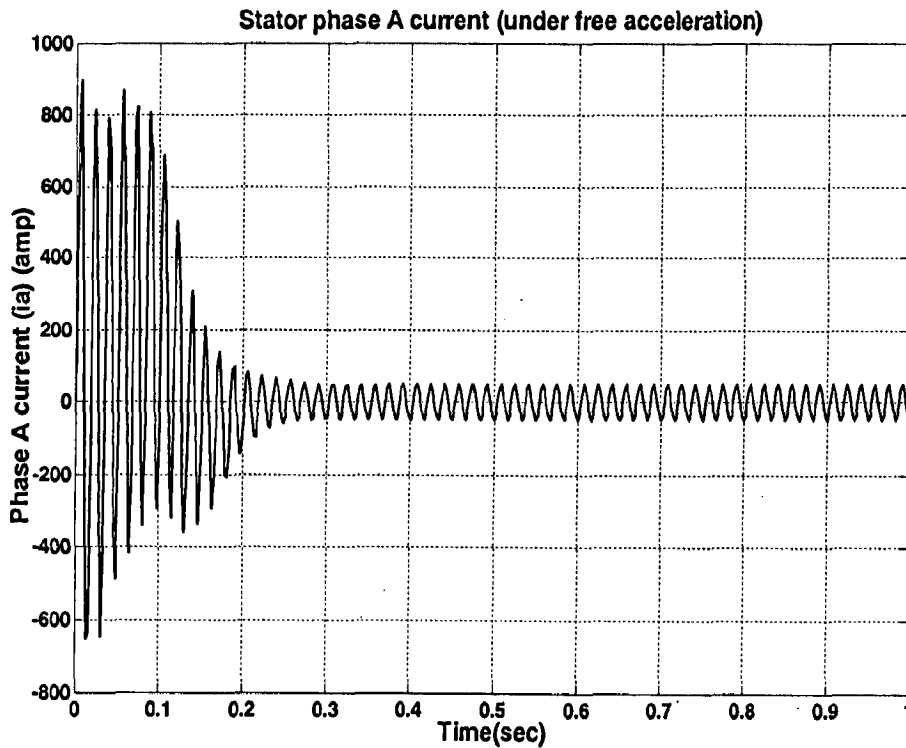


Figure (1.4): stator phase A current under free acceleration

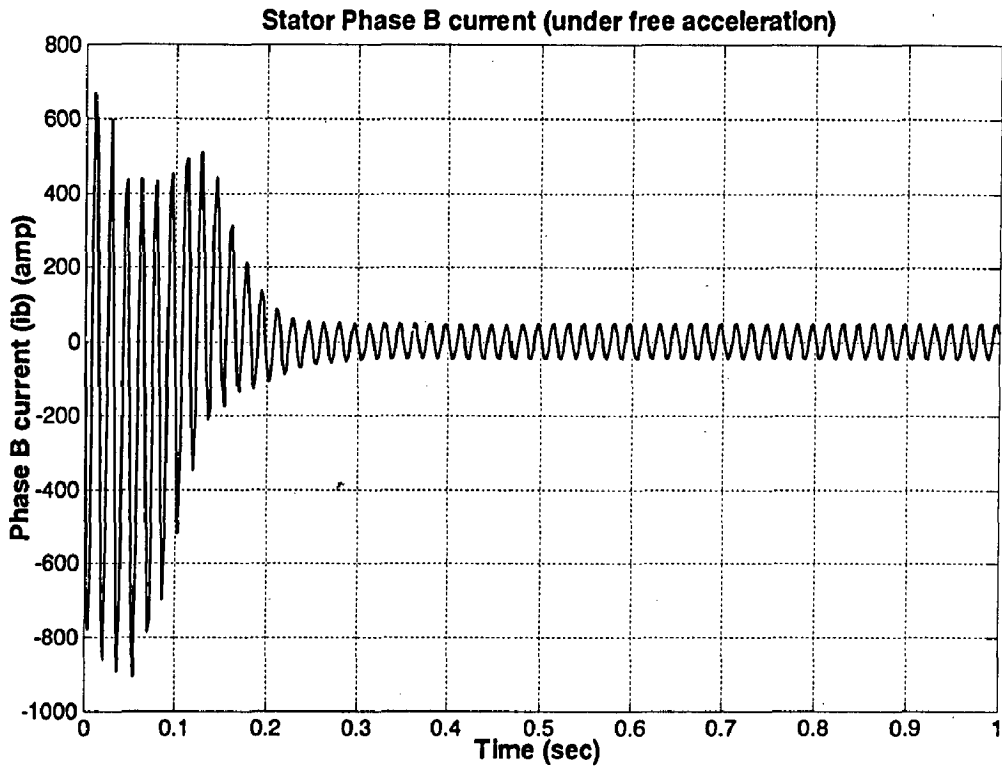


Figure (1.5): stator phase B current under free acceleration

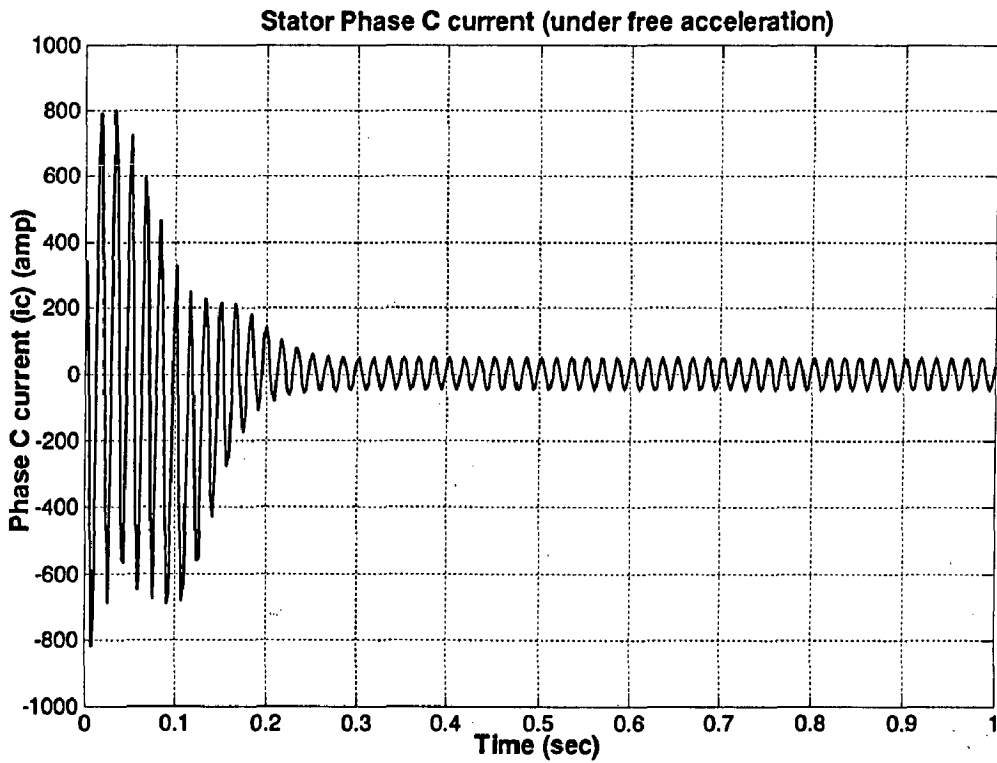


Figure (1.6): stator phase C current under free acceleration

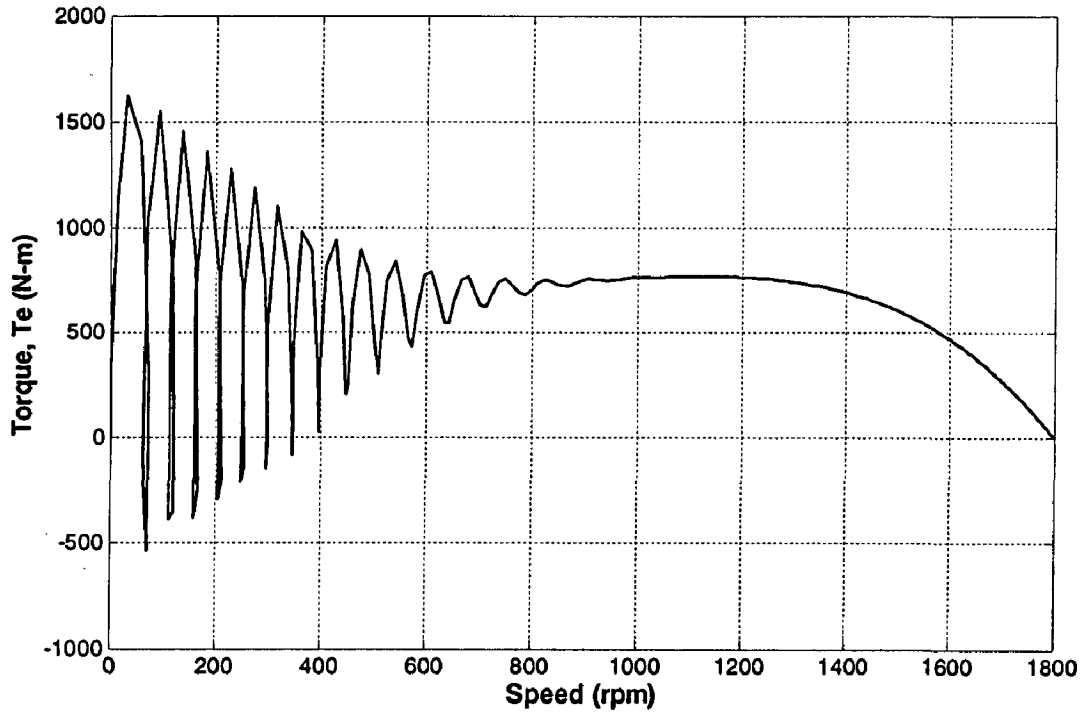


Figure (1.7): Torque-speed characteristic during free acceleration

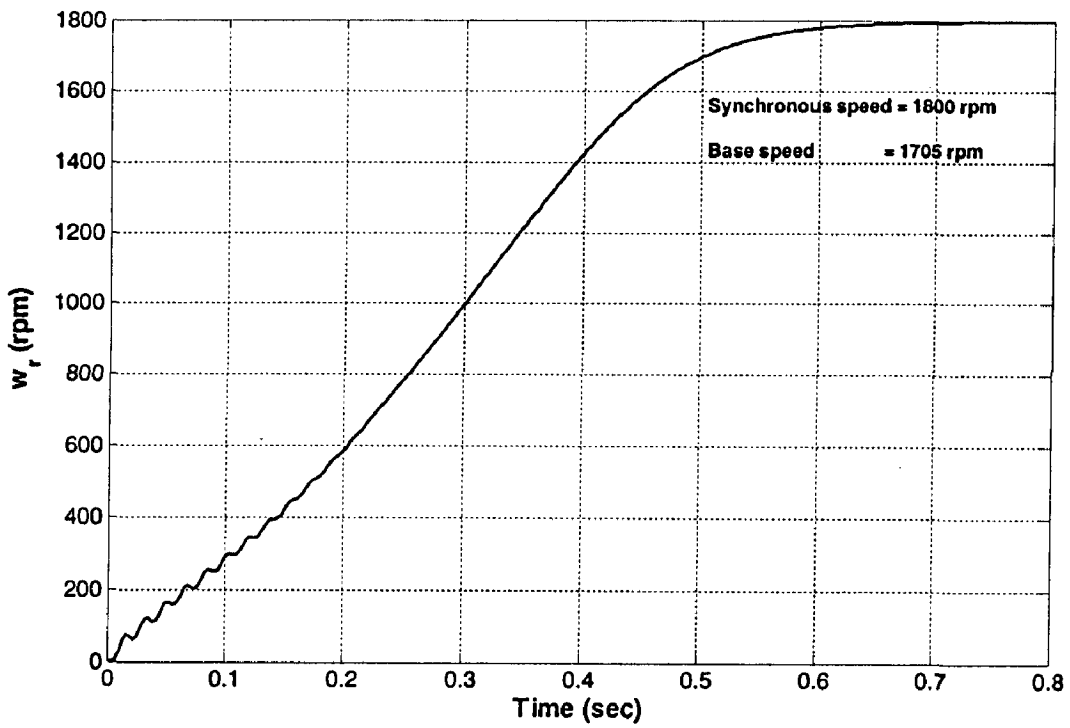


Figure (1.8): Speed response during free acceleration

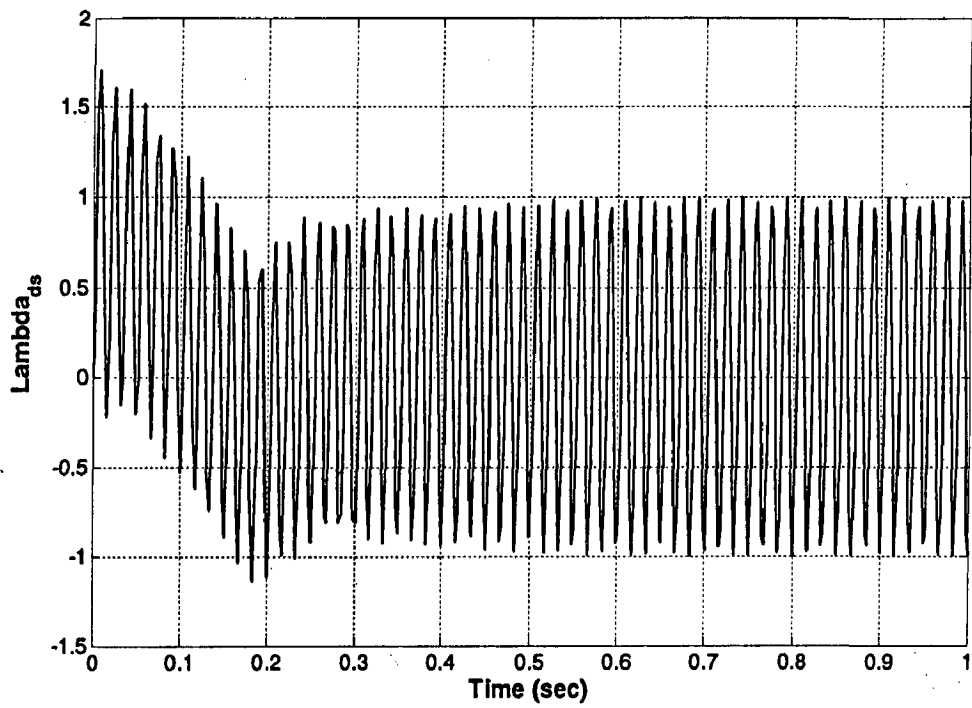


Figure (1.9): Stator d-axis flux response during free acceleration

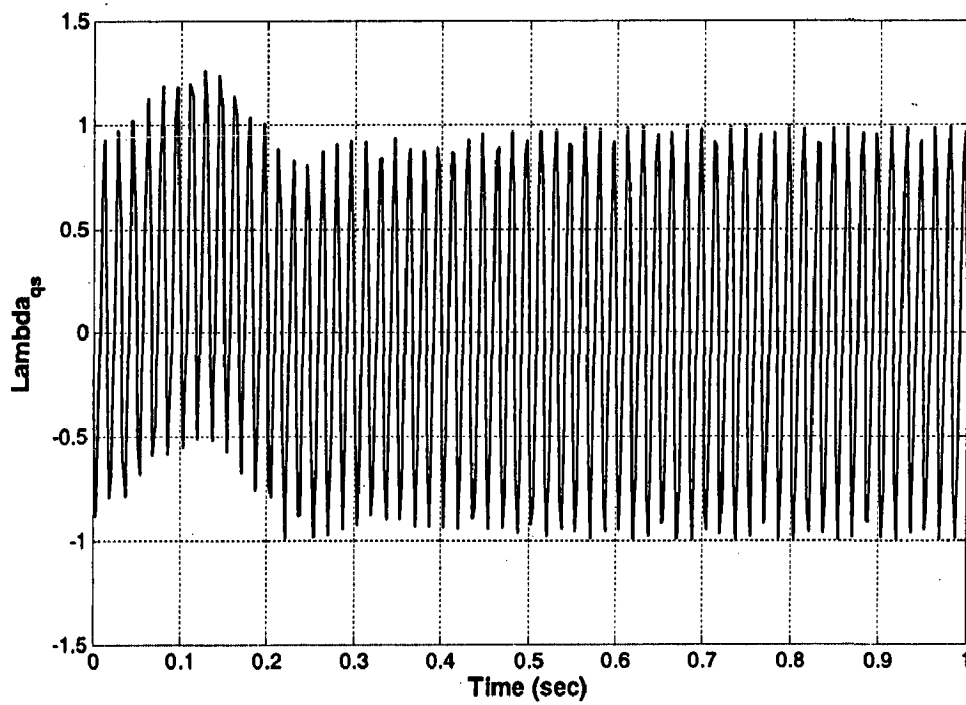


Figure (1.10): Stator q-axis flux response during free acceleration

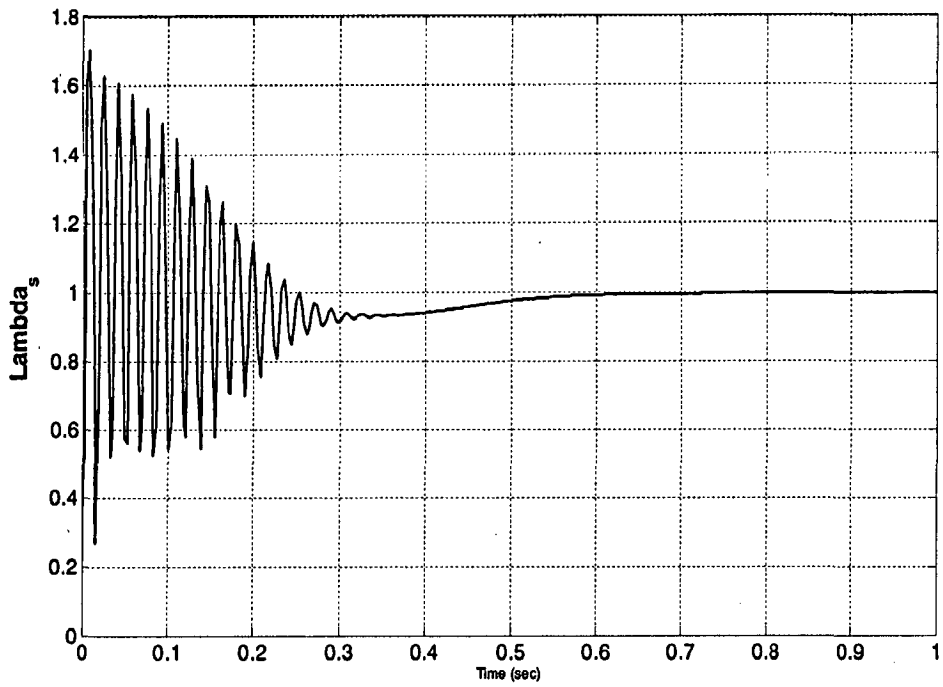


Figure (1.11): Stator flux response during free acceleration

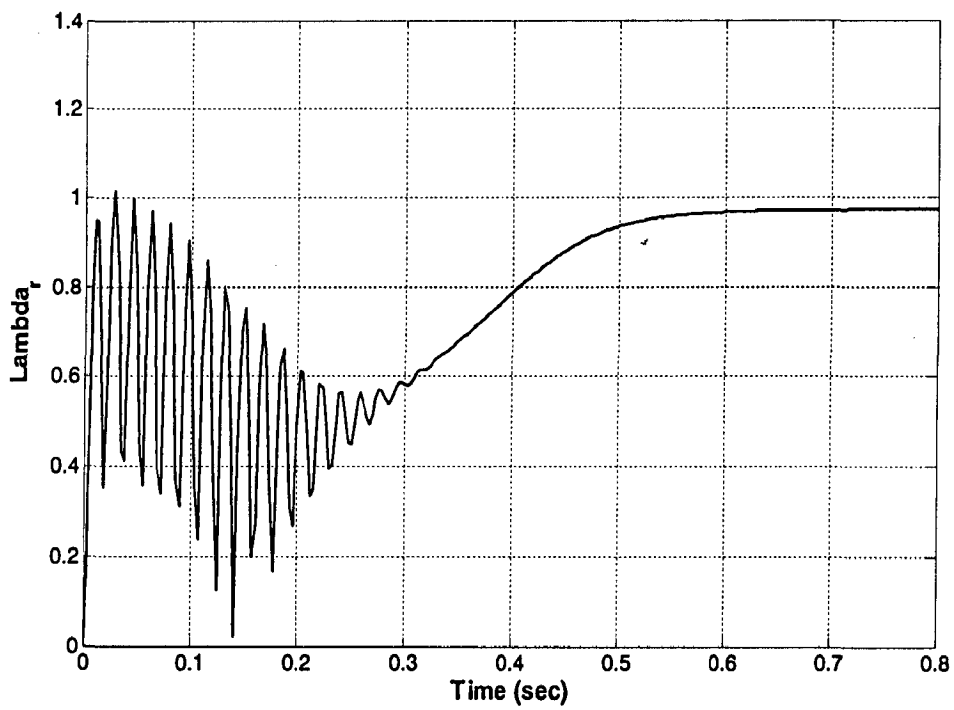


Figure (1.12): Rotor flux response during free acceleration

1.4.2 Rated load characteristics:

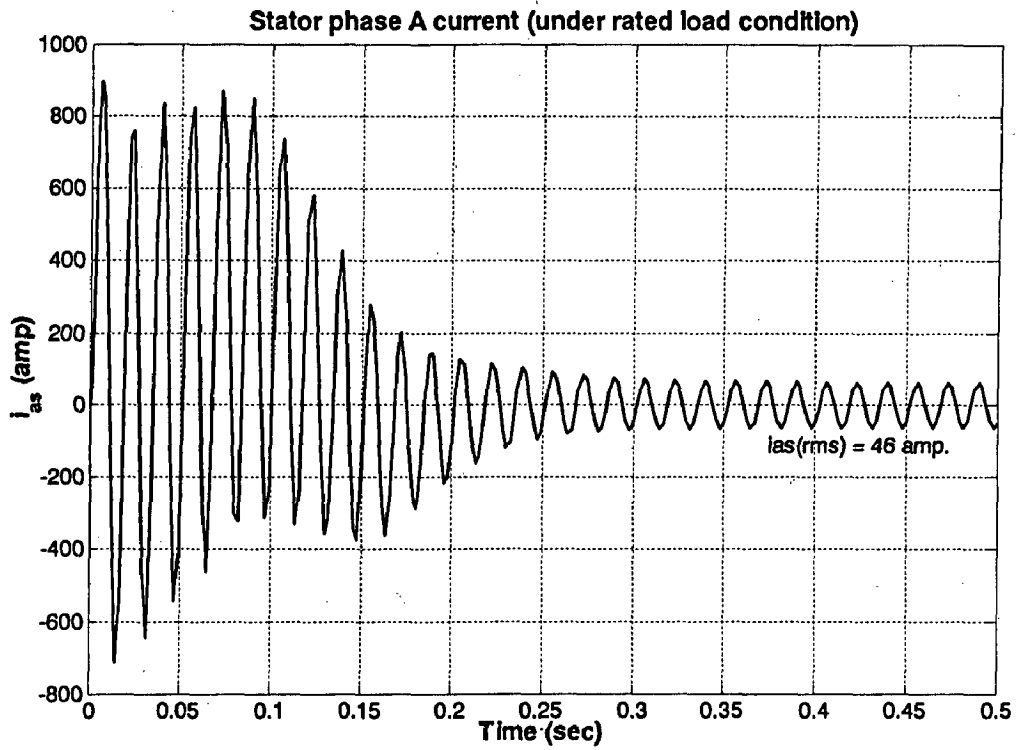


Figure (1.13): stator phase A current under rated load condition

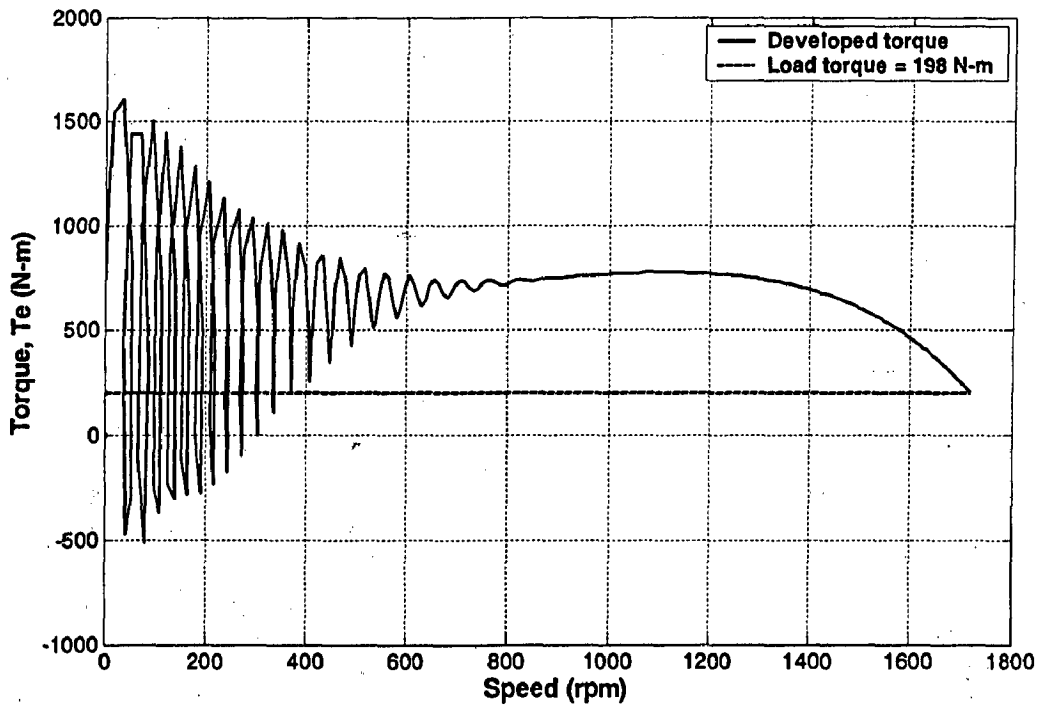


Figure (1.14): Torque-speed characteristic during rated load condition

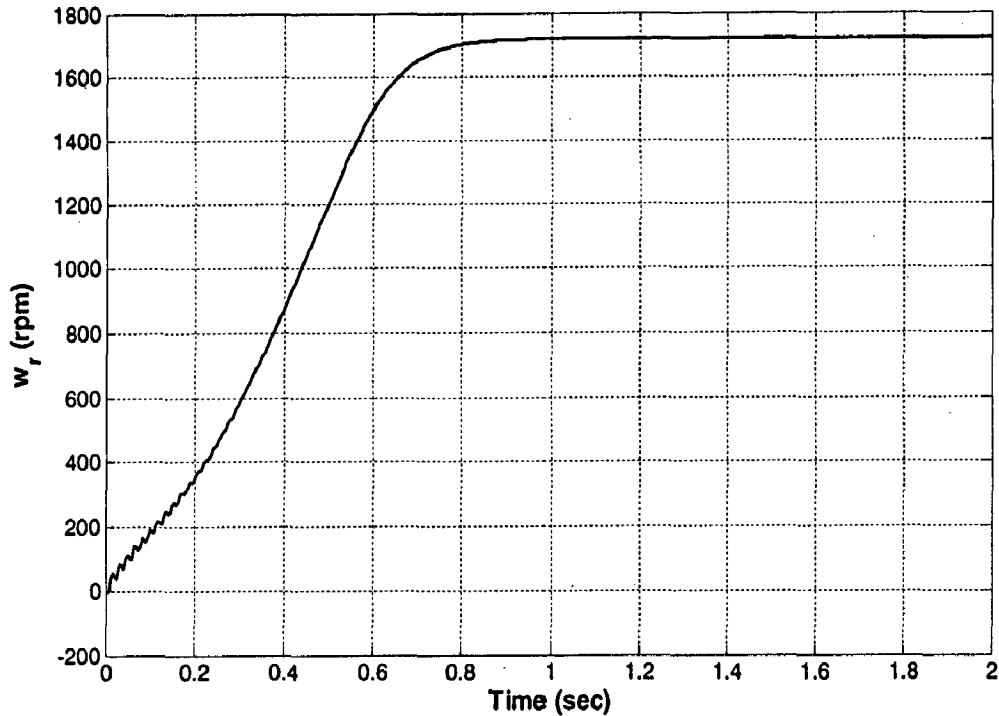


Figure (1.15): Speed response during rated load condition

1.5 Interim conclusions:

The induction motor has been modeled using space phasor model. The space-phasor model simulation has reduced the total number of differential equations from 5 (equations (1.17) and (1.18)) to 3 ((1.45), (1.46) and (1.50)) but the reduction results in introduction of complex variables. Even though there is no distinct advantage in simulating the system in complex variables, the significant has been gained by viewing the phasors rather than dq-components of the key variables. Responses during free acceleration as well as rated load condition have been found according to the rating of motor. Torque oscillation has been found high during transient, because of high power rating of machine.

CHAPTER 2

FIELD ORIENTED CONTROL, PRINCIPLE AND GENERALITIES

2.1 - Principle of Field Oriented Control

The Field Orientated Control (FOC) consists of controlling the stator currents represented by a vector [1] [3]. This control is based on projections which transform a three phase time and speed dependent system into a two coordinate (d and q co-ordinates) time invariant system. These projections lead to a structure similar to that of a DC machine control. Field orientated controlled machines need two constants as input references: the torque component (aligned with the q co-ordinate) and the flux component (aligned with d co-ordinate). As Field Orientated Control is simply based on projections the control structure handles instantaneous electrical quantities. This makes the control accurate in every working operation (steady state and transient) and independent of the limited bandwidth mathematical model. The FOC thus solves the classic scheme problems, in the following ways:

- a) the ease of reaching constant reference (torque component and flux component of the stator current)
- b) the ease of applying direct torque control because in the (d,q) reference frame the expression of the torque is:

$$T_e \propto \lambda_r i_{qs} \quad (2.1)$$

By maintaining the amplitude of the rotor flux (λ_r) at a fixed value we have a linear relationship between torque and torque component (i_{qs}). We can then control the torque by controlling the torque component of stator current vector.

2.2 Phasor diagram of the Vector Controller:

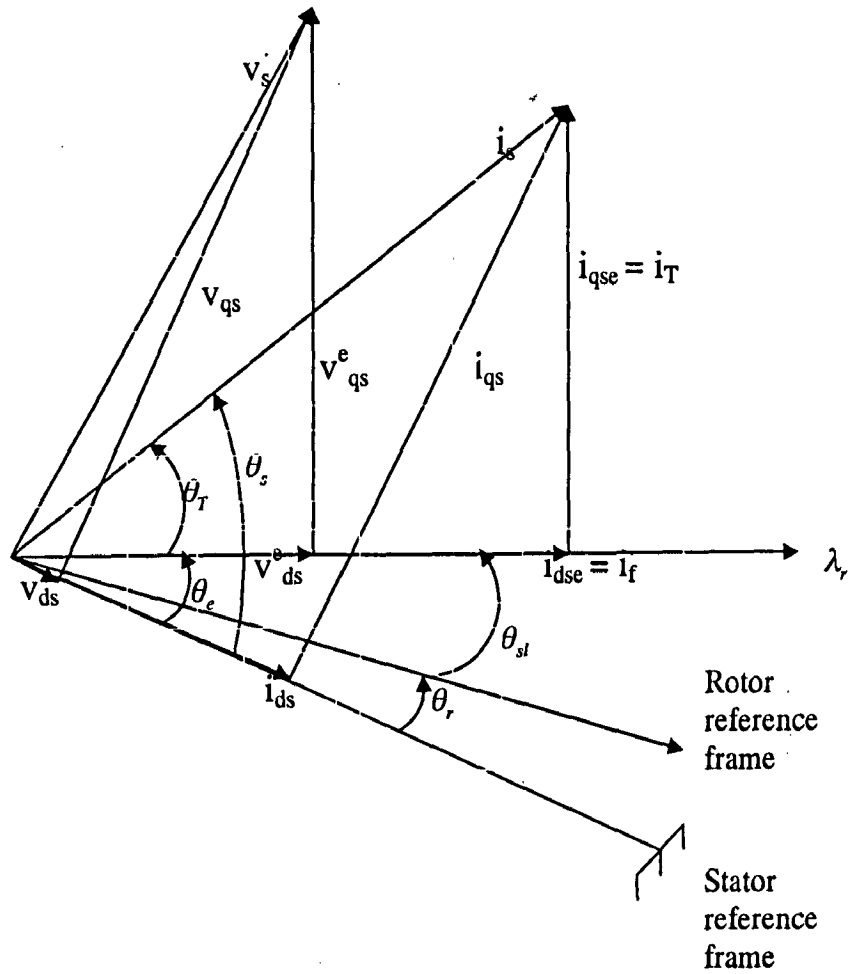


Fig (2.1): Phasor diagram of the vector controller

where $\theta_e = \theta_{sl} + \theta_r$ (2.2)

$$\theta_s = \theta_f + \theta_r \quad (2.3)$$

and,

$$\lambda_r \propto i_f \quad (2.4)$$

$$T_e \propto \lambda_r i_r \propto i_f i_r \quad (2.5)$$

$$\theta_f = \int (\omega_r + \omega_{sl}) dt = \int \omega_s dt \quad (2.6)$$

2.3 Space Vector definition and projection

The three-phase voltages, currents and fluxes of AC-motors can be analyzed in terms of complex space vectors [10] [11]. With regard to the currents, the space vector can be defined as follows. Assuming that i_a , i_b , i_c are the instantaneous currents in the stator phases, then the complex stator current vector \bar{i}_s is defined by:

$$\bar{i}_s = i_a + \alpha i_b + \alpha^2 i_c \quad (2.7)$$

Where $\alpha = e^{j\frac{2\pi}{3}}$ and $\alpha^2 = e^{j\frac{4\pi}{3}}$ represent the spatial operators. The following figure shows the stator current complex space vector:

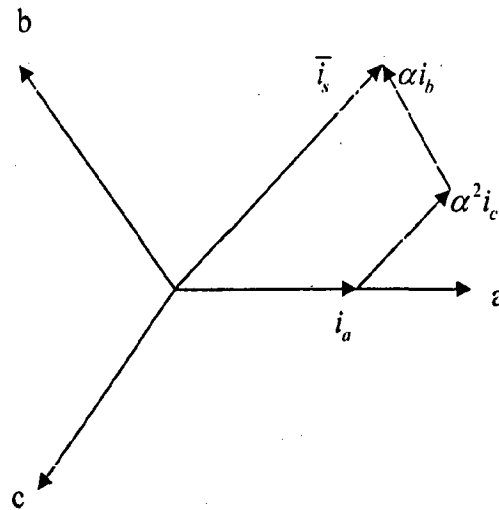


Figure (2.2): Stator current space vector and its component in (a, b, c)

where (a, b, c) are the three phase system axes. This current space vector depicts the three phase sinusoidal system. It still needs to be transformed into a two time invariant co-ordinate system. This transformation can be split into two steps:

- (a, b, c) to (α , β) (the Clarke transformation) which outputs a two co-ordinate time variant system.
- (α , β) to (d, q) (the Park transformation) which outputs a two co-ordinate time invariant system.

2.4 The (a, b, c) → (α, β) projection (Clarke transformation)

The space vector can be reported in another reference frame with only two orthogonal axes called (α, β). Assuming that the axis-a and the axis-α are in the same direction we have the following vector figure (2.3):

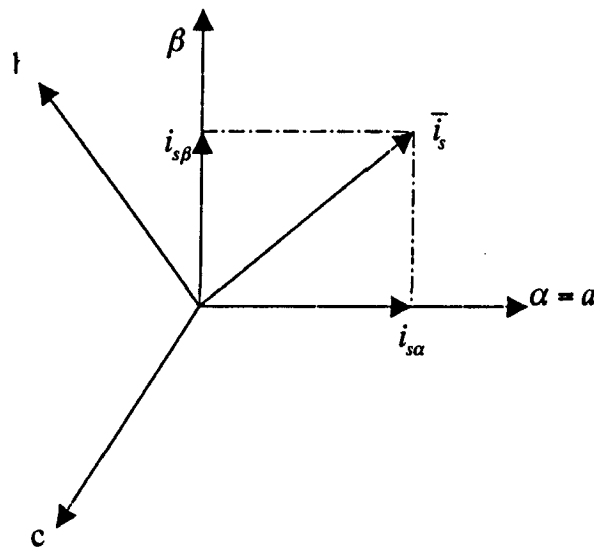


Figure (2.3): Stator current space vector and its components in (α and β)

The projection that modifies the three phase system into the (α, β) two dimension orthogonal system is presented below.

$$i_{s\alpha} = i_a \quad (2.8)$$

$$i_{s\beta} = \frac{1}{\sqrt{3}}i_a + \frac{2}{\sqrt{3}}i_b \quad (2.9)$$

2.5 The (α, β) → (d, q) projection (Park transformation)

This is the most important transformation in the FOC. In fact, this projection modifies a two phase orthogonal system (α, β) in the d, q rotating reference frame. If we consider the d

axis aligned with the rotor flux, the next figure (2.4) shows, for the current vector, the relationship from the two reference frame:

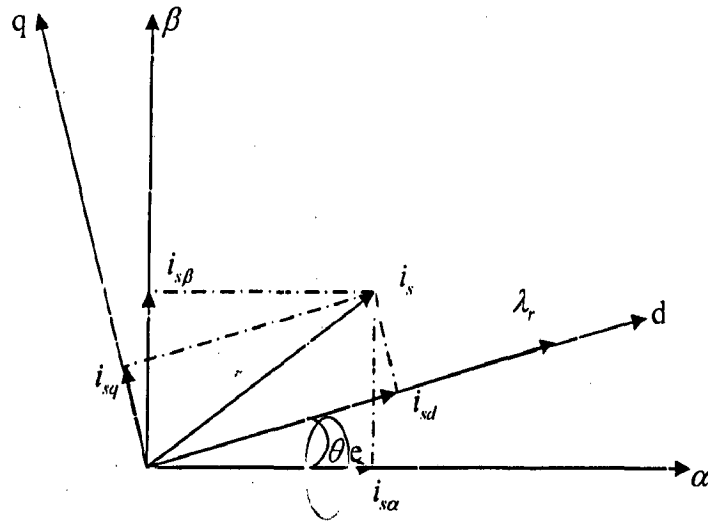


Figure (2.4): Stator current space vector and its component in (α, β) and in the d, q rotating reference frame.

where θ_e is the rotor flux position called field angle. The flux and torque components of the current vector are determined by the following equations:

$$i_{sd} = i_{s\alpha} \cos \theta_e + i_{s\beta} \sin \theta_e \quad (2.10)$$

$$i_{sq} = -i_{s\alpha} \sin \theta_e + i_{s\beta} \cos \theta_e \quad (2.11)$$

These components depend on the current vector (a, b, c) components and on the rotor flux position; if we know the right rotor flux position then, by this projection, the d, q component becomes a constant.

2.6 The (d, q) \rightarrow (α, β) projection (inverse Park transformation)

Here, we introduce from this voltage transformation only the equation that modifies the voltages in d, q rotating reference frame in a two phase orthogonal system:

$$v_{s\alpha ref} = v_{sdref} \cos \theta_e - v_{sqref} \sin \theta_e \quad (2.12)$$

$$v_{s\beta ref} = v_{sdref} \sin \theta_e + v_{sqref} \cos \theta_e \quad (2.13)$$

2.7 The basic scheme for the FOC:

The figure (2.5) summarizes the basic scheme of torque control with FOC. Two motor phase currents are measured. These measurements feed the Clark transformation module. The outputs of this projection are designated $i_{s\alpha}$ and $i_{s\beta}$. These two components of the current are the inputs of the Park transformation that gives the current in the d, q rotating reference frame. The i_{sd} and i_{sq} components are compared to the references i_{sdref} (the flux reference) and i_{sqref} (the torque reference). At this point, this control structure shows an interesting advantage: it can be used to control either synchronous or induction machines by simply changing the flux reference and obtaining rotor flux position. As in synchronous permanent magnet motors, the rotor flux are fixed (determined by the magnets) there is no need to create one. Hence, when controlling a PMSM, i_{sdref} should be set to zero. As induction motors need a rotor flux creation in order to operate, the flux reference must not be zero. This conveniently solves one of the major drawbacks of the "classic" control structures: the portability from asynchronous to synchronous drives. The torque command i_{sqref} could be the output of the speed regulator when we use a speed FOC. The outputs of the current regulators are v_{sdref} and v_{sqref} they are applied to the inverse Park transformation. The outputs of this projection are $v_{s\alpha ref}$ and $v_{s\beta ref}$ which are the components of the stator vector voltage in the α, β stationary orthogonal reference frame. These are the inputs, after converting it to 3 phase, of the 3-phase PWM inverter. Note that both Park and inverse Park transformations need the rotor flux

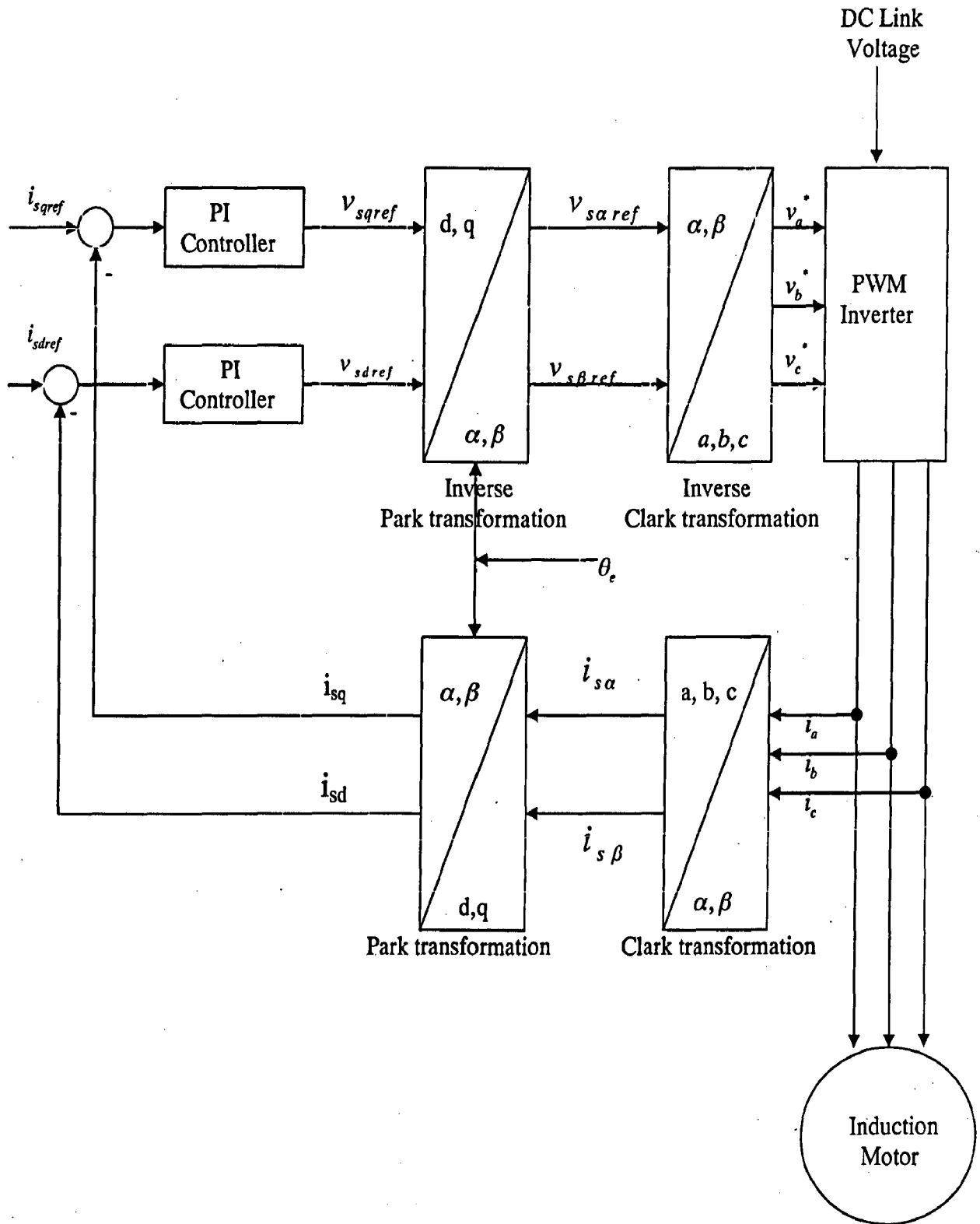


Figure (2.5): Basic scheme of vector control for AC machines

position. Obtaining this rotor flux position depends on the AC machine type (synchronous or asynchronous machine).

2.8 Inputs for FOC:

Fundamental requirements for the FOC are knowledge of three phase currents and the rotor flux position. Knowledge of the rotor flux position is the core of the FOC. In fact if there is an error in this variable, the rotor flux is not aligned with d-axis and $i_{d,s}$ and $i_{q,s}$ are incorrect flux and torque components of the stator current. The figure (2.1) shows the correct position of the rotor flux, the stator current and stator voltage space vector that rotates with d,q reference at synchronous speed. The measure of the rotor flux position is different if we consider synchronous or induction motor.

- a) In the synchronous machine the rotor speed is equal to the rotor flux speed. Then θ_e (rotor flux position, or field angle) is directly measured by position sensor or by integration of rotor speed, ω_r .
- b) In the induction machine the rotor speed ω_r is not equal to the rotor flux speed, (there is a slip speed ω_{sl}), then it needs a particular method to calculate θ_e .

CHAPTER 3

DIRECT VECTOR CONTROL

3.1 Principle of Direct Vector Control.

Vector controlled schemes are classified according to how the field angle (θ_e), shown in figure (2.5), is acquired. If the field is calculated by using terminal voltages and currents or Hall sensors or flux-sensing winding, then it is known as Direct Vector Control [9] [13]. The SIMULINK block diagram for direct vector control for PWM voltage-fed-inverter drive is shown in figure (3.1). The principal vector control parameters, i_{qe}^* and i_{de}^* which are DC values in synchronously rotating frame, are converted to stationary frame (defined as vector rotation (VR) with the help of unit vectors ($\sin\theta_e$ and $\cos\theta_e$) generated from the flux vector signals λ_{dr}^s and λ_{qr}^s . The resulting stationary reference frame signals are then converted to current commands. The current commands are then used to generate voltage commands for the inverter. The flux signals λ_{dr}^s and λ_{qr}^s are generated from the machine terminal voltages and currents with the help of voltage model estimator. The torque and rotor flux references are compared to the torque, T_e , and the rotor flux linkage, λ_r , respectively. These errors are amplified and limited to generate the reference torque and flux-producing components of stator current, $i_{qe}^* = i_T^*$ and $i_{de}^* = i_f^*$ respectively. A flux control loop has been added for precision control of flux. The torque component of the current i_{qe}^* is generated from the speed control loop through a bipolar limiter. The torque, proportional to i_{qs_s} (with constant flux), can be bipolar. It is negative with negative i_{qs_s} and correspondingly the phase position of i_{qs_s} becomes negative. Phasor diagram for DVC is shown in figure (3.2). The scheme has been extended to flux-weakening mode by programming the flux command as a function of speed.

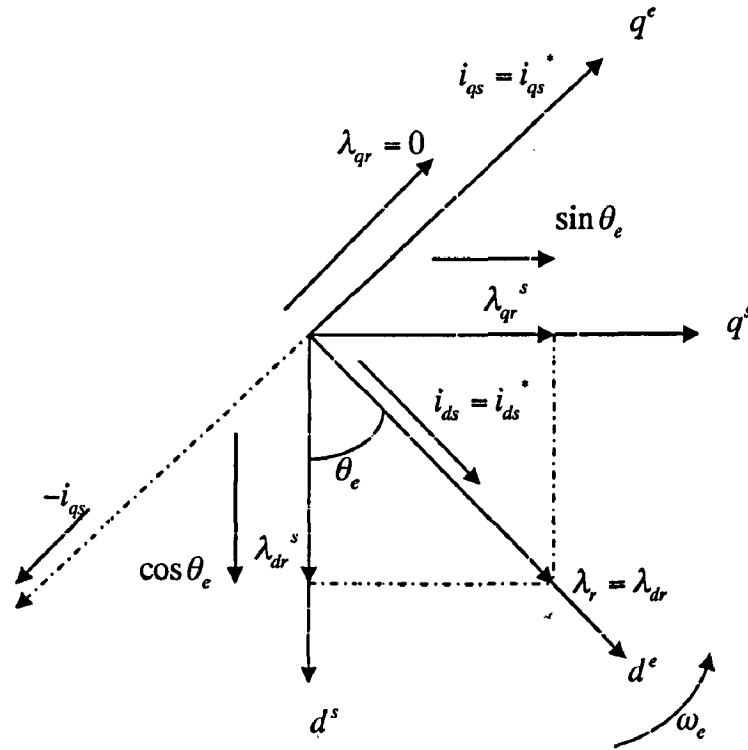


Figure (3.2): $d^s - q^s$ and $d^e - q^e$ phasors showing correct rotor flux orientation

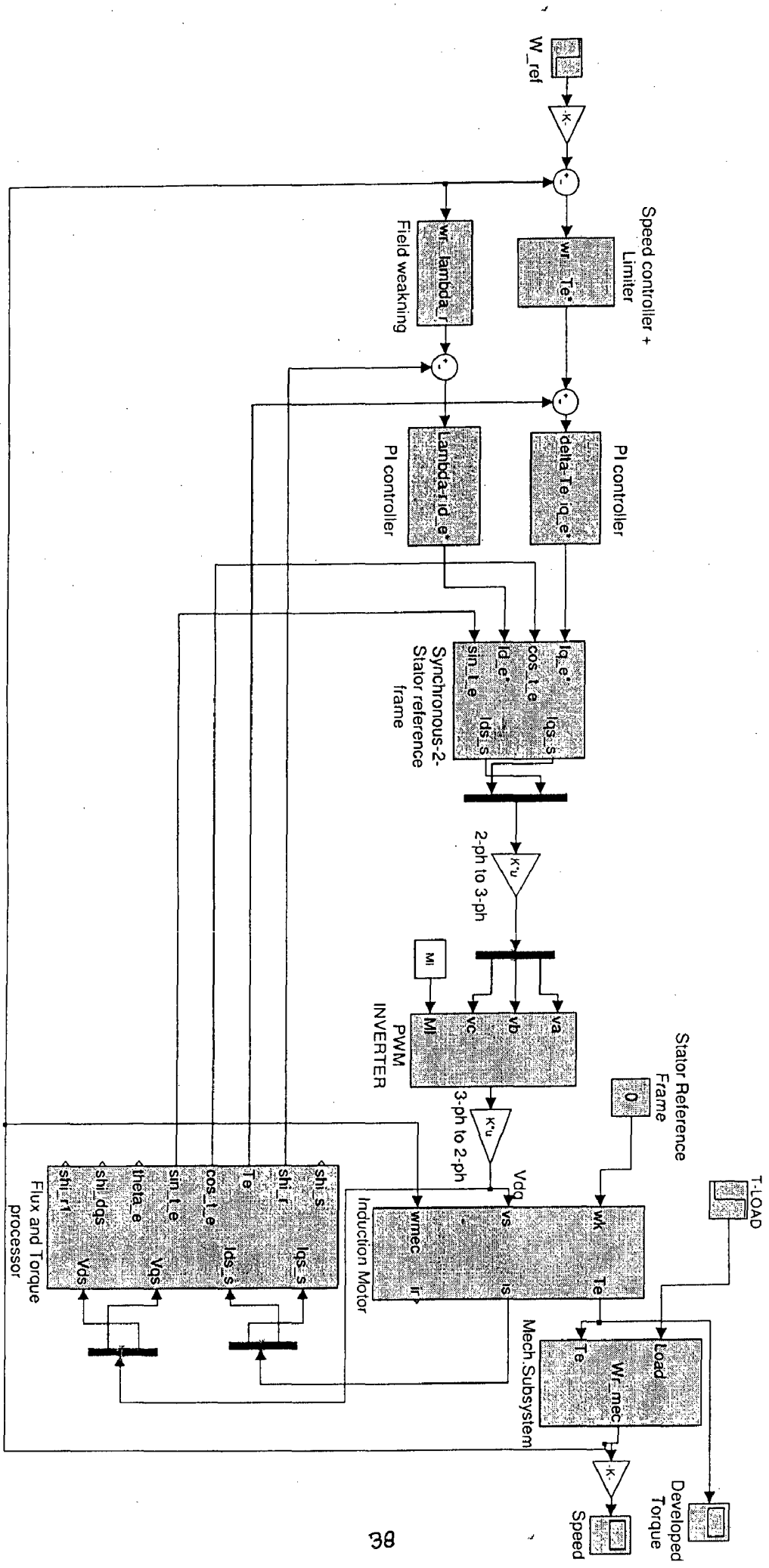
3.2 Rotor Flux Vector Estimation.

In the direct vector control method, it is necessary to estimate the rotor flux components λ_{dr}^s and λ_{qr}^s so that the unit vectors and rotor flux can be calculated. Method used, for the estimation of above parameters, is Voltage Model of induction motor. The determination of field angle θ_e is based on rotor flux calculation [1] [5].

3.2.1 Terminal Voltage Model.

In this method, the machine terminal voltages and currents are sensed and flux are computed from the stationary frame ($d_s - q_s$) model of the machine.

These equations are as follows:



Figure(3.1): SIMULINK DIAGRAM FOR DIRECT VECTOR CONTROL SCHEME

Current equations are:

$$i_{qs}^s = \frac{2}{3}i_a - \frac{1}{3}i_b - \frac{1}{3}i_c = i_a \quad (3.1)$$

$$i_{ds}^s = -\frac{1}{\sqrt{3}}i_b + \frac{1}{\sqrt{3}}i_c = -\frac{1}{\sqrt{3}}(i_a + 2i_b) \quad (3.2)$$

Since $i_c = -(i_a + i_b)$ for isolated neutral system.

Voltage equations are :

$$v_{qs}^s = \frac{2}{3}v_a - \frac{1}{3}v_b - \frac{1}{3}v_c = \frac{1}{3}(v_{ab} + v_{ac}) \quad (3.3)$$

$$v_{ds}^s = -\frac{1}{\sqrt{3}}v_b + \frac{1}{\sqrt{3}}v_c = -\frac{1}{\sqrt{3}}v_{bc} \quad (3.4)$$

Stator flux equations are:

$$\lambda_{ds}^s = \int (v_{ds}^s - R_s i_{ds}^s) dt \quad (3.5)$$

$$\lambda_{qs}^s = \int (v_{qs}^s - R_s i_{qs}^s) dt \quad (3.6)$$

$$\lambda_s = \sqrt{(\lambda_{ds}^s)^2 + (\lambda_{qs}^s)^2} \quad (3.7)$$

$$\lambda_{dm}^s = \lambda_{ds}^s - L_{ls} i_{ds}^s = L_m (i_{ds}^s + i_{dr}^s) \quad (3.8)$$

$$\lambda_{qm}^s = \lambda_{qs}^s - L_{ls} i_{qs}^s = L_m (i_{qs}^s + i_{qr}^s) \quad (3.9)$$

Rotor flux equations are:

$$\lambda_{dr}^s = L_m i_{ds}^s + L_r i_{dr}^s \quad (3.10)$$

$$\lambda_{qr}^s = L_m i_{qs}^s + L_r i_{qr}^s \quad (3.11)$$

$$\lambda_r = \sqrt{(\lambda_{dr}^s)^2 + (\lambda_{qr}^s)^2} \quad (3.12)$$

Torque equation in terms of rotor flux and stator current can be written as:

$$T_e = \frac{3}{2} \frac{p}{2} \frac{L_m}{L_r} (\lambda_{dr}^s i_{qs}^s - \lambda_{qr}^s i_{ds}^s) \quad (3.13)$$

From equations (3.10), (3.11) and (3.12), Unit vectors are derived as:

$$\sin \theta_e = \frac{\lambda_{qr}^s}{\lambda_r} \quad (3.14)$$

$$\cos \theta_e = \frac{\lambda_{dr}^s}{\lambda_r} \quad (3.15)$$

3.3 PWM Voltage Source Inverter.

The objective of PWM is to shape and control the three-phase output voltage, in magnitude and frequency, by utilization of a constant DC voltage. PWM is a process where three phase sinusoidal signals are compared with a repetitive switching frequency triangular waveform. The table (3.1) shown below shows the switching instant of different switching devices.

$$v_{control(phase_a)} > v_{triangle}, T_{a+} \text{ is on}$$

$$v_{control(phase_a)} < v_{triangle}, T_{a-} \text{ is on}$$

$$v_{control(phase_b)} > v_{triangle}, T_{b+} \text{ is on}$$

$$v_{control(phase_b)} < v_{triangle}, T_{b-} \text{ is on}$$

$$v_{control(phase_c)} > v_{triangle}, T_{c+} \text{ is on}$$

$$v_{control(phase_c)} < v_{triangle}, T_{c-} \text{ is on}$$

Table (3.1): switching sequence of PWM inverter

Also,

$$v_{as} = v_{ag} - v_{ng} \quad (3.16)$$

$$v_{bs} = v_{bg} - v_{ng} \quad (3.17)$$

$$v_{cs} = v_{cg} - v_{ng} \quad (3.18)$$

$$v_{ng} = \frac{1}{3}(v_{ag} + v_{bg} + v_{cg}) \quad (3.19)$$

Substituting equation (3.19) in (3.16), (3.17) and (3.18), respectively, we get

$$v_{as} = \frac{2}{3}v_{ag} - \frac{1}{3}v_{bg} - \frac{1}{3}v_{cg} \quad (3.20)$$

$$v_{bs} = -\frac{1}{3}v_{ag} - \frac{2}{3}v_{bg} + \frac{1}{3}v_{cg} \quad (3.21)$$

$$v_{cs} = \frac{1}{3}v_{ag} - \frac{1}{3}v_{bg} + \frac{2}{3}v_{cg} \quad (3.22)$$

In matrix form equations (3.20), (3.21) and (3.22), can be written as

$$\begin{bmatrix} v_{as} \\ v_{bs} \\ v_{cs} \end{bmatrix} = \frac{1}{3} \begin{bmatrix} -2 & -1 & -1 \\ -1 & -2 & -1 \\ -1 & -2 & -1 \end{bmatrix} \begin{bmatrix} v_{ag} \\ v_{bg} \\ v_{cg} \end{bmatrix} \quad (3.23)$$

These are the equations for phase voltages and gains of these equations are used in PWM-transfer function of simulink design of PWM inverter. Relay setting gives the DC link voltage. Basic scheme used for PWM inverter design in SIMULINK is shown in figure (3.3).

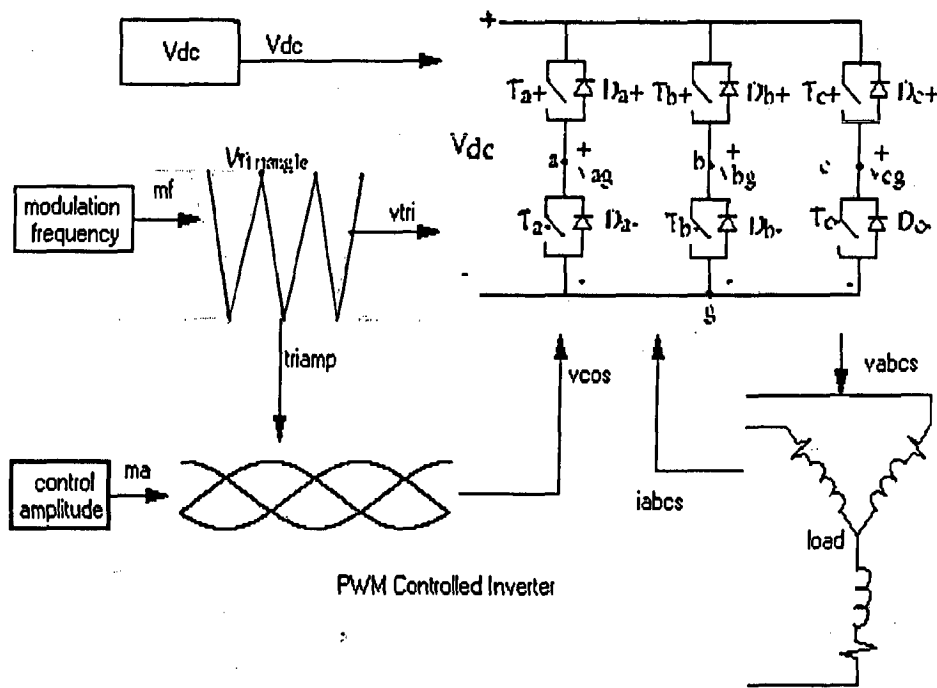


Figure (3.3): Basic scheme of PWM inverter

3.3.1 Simulink design of PWM inverter:

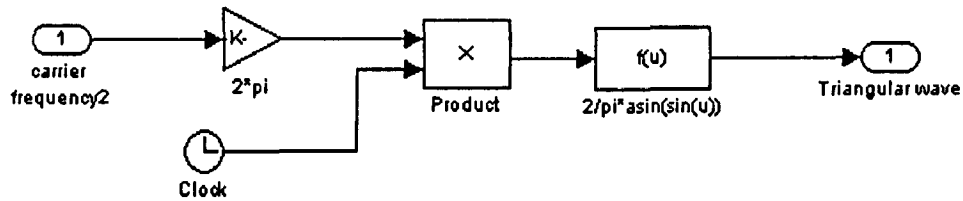


Figure (3.4): Simulink design of triangular wave generation

For transfer function of PWM, matrix gain of equation (3.23) is used. The output of the PWM inverter is the stator phase voltages.

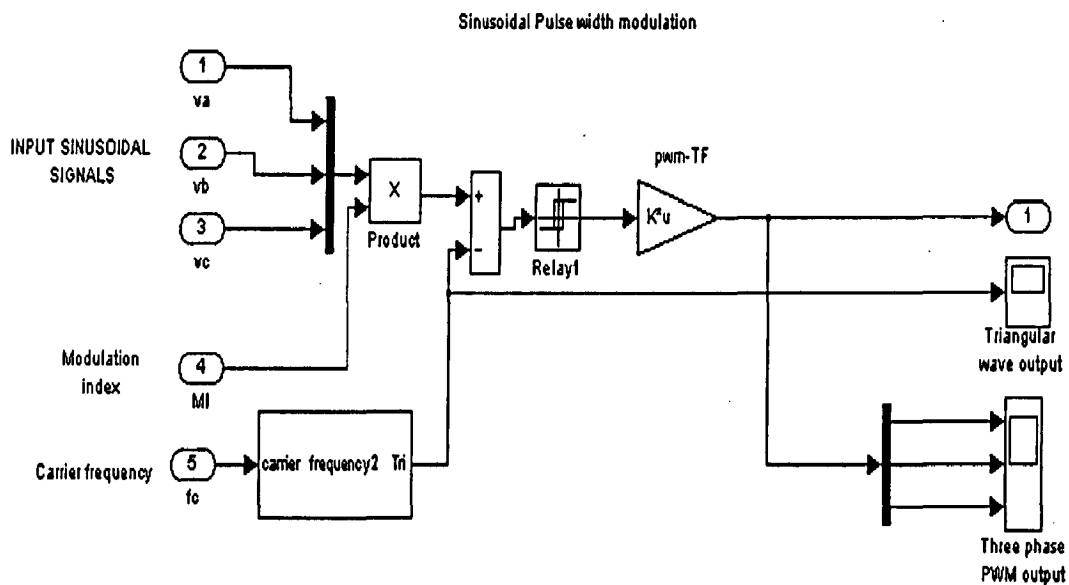


Figure (3.5): Simulink design of sinusoidal PWM inverter

3.4 The PI Controller:

The PI (proportional and integral) controller is an effective means of regulating torque and voltage magnitudes to the desired values. It also improves the steady state error, response time and the error sensibility. This is achieved by providing a gain for the error term with an integral

component correction. K_p is the proportional gain and K_i is the integral gain of the feedback loop. There are three PI controllers used in the design. The first PI controller is called the speed and torque PI controller, as it calculates the electromagnetic torque required by the motor to achieve the set reference speed command. From the other two, one is used to generate torque current command (i_{qe}^*) and other is used for flux current command (i_{de}^*). These PI controllers regulate the voltage into the induction machine by making sure that the induction machine is not drawing too much or too little current.

3.4.1 Simulink Design of PI Controllers.

3.4.1.1 Torque and Speed PI controller.

This PI controller figure (3.6) processes the speed error and according to which torque command is generated. It has a bipolar torque limiter which is set at ± 198 N-m. Value of gains used are $K_p = 100$ and $K_i = 5200$. These values are chosen on the basis of speed of response and limit of torque oscillation. Because of large integral gain in the speed controller, its output will saturate in time. An anti-windup with a gain of 200 is added to overcome this saturation in the controller and to keep the speed controller responsive.

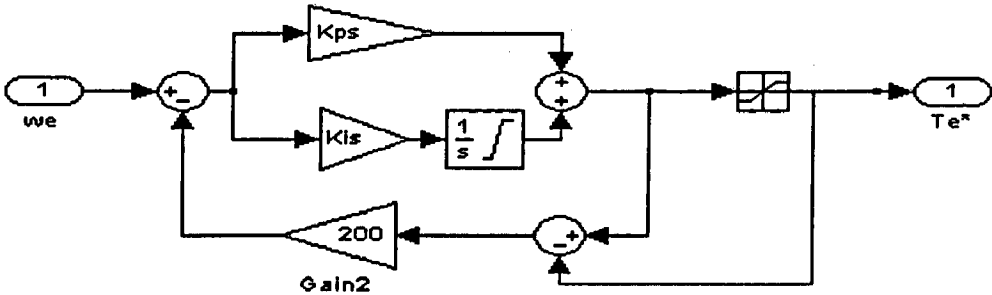


Figure (3.6): Simulink design of speed PI controller for torque command

3.4.1.2 Torque current PI controller:

This PI controller figure (3.7) utilizes the torque error and generates the commanded torque current i_{qe}^* in synchronous reference frame. The values of proportional gain (K_{p1}) is 12.55 and that of integral gain (K_{i1}) is 66. The bipolar current limiter is set at ± 30 .

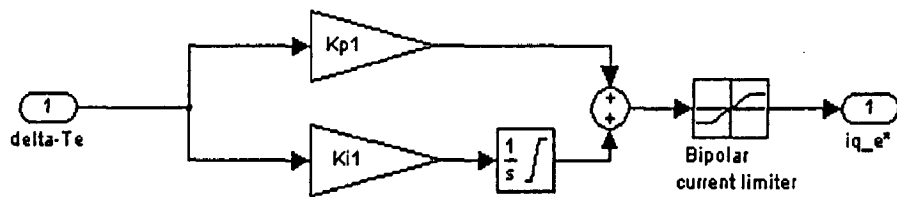


Figure (3.7): Simulink design of current PI controller for i_{qe}^* component

3.4.1.3 Flux current PI controller:

This PI controller figure (3.8) processes the rotor flux error. One flux comes from the generated speed and other one is the actual value of rotor flux. The flux error generates the desired flux command current i_{de}^* . The value of proportional gain K_{p2} is 12.55 and that of proportional gain K_{i2} is 66. The bipolar current limiter is set at ± 10 .

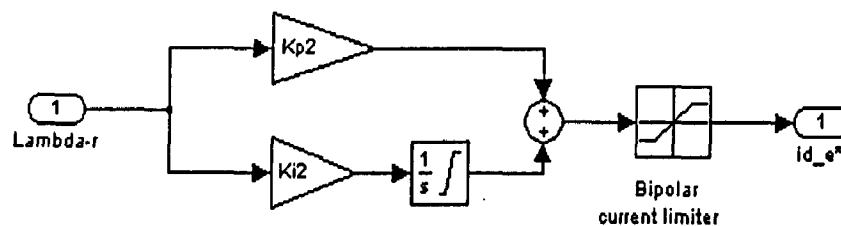


Figure (3.8): Simulink design of current PI controller for i_{de}^* component

3.5 Simulation results:

Simulation of the proposed MATLAB design is shown in the figure (3.1). While simulation gives desired performance, it also shows how the subsystems within FO control work together to produce the desired outputs. Hence it helps in deeper understanding of Field Oriented Control system of an induction motor. This knowledge is mainly obtained through the use of “Scopes”. A scope is a SIMULINK block that displays signals at nodes during simulation. The simulation studied occurred over 1 second. The integration method used is variable step, the “ode23tb (stiff/TR-BDF2)”.

3.5.1 Speed response analysis.

The speed response of designed control system is the outcome that is of utmost significance to this work. By feeding an input speed command (w_{ref}) into the system, we are going to observe the speed developed by the rotor of the induction motor over time. The two major criterions that we are going to fulfill are:

- a) That the system develops a speed response that is closely resembles the input speed command.
- b) That the system is stable (stability is the most important design specification of any control system).

Other criterion that we are looking to achieve are a quick transient response (quick acceleration) and a response that is “smooth”.

No Load Condition:

For the simulation conducted, the speed input fed into the system (in figure 3.1) remains at 800 rpm for initial 0.5sec and then goes to 400 rpm for remaining 0.5sec. This is a step speed command. In the figure (3.9) one curve shows the actual speed developed by the motor and other is the reference speed signal that is set by the observer. It shows that actual speed i.e. speed of rotor, is closely following the reference speed signal in the steady state. Inspections of the figure suggest that there is a room to speed up the transient response. To do

this, we have to add more proportional gain to the torquecontroller (the PI controller for the speed error signal). But addition of proportional gain increases the torque oscillation. Machine is running under no load condition. This figure also shows the fast response of the system.

$$\omega_{ref} = 800 \text{ rpm to } 400 \text{ rpm at } 0.5 \text{ sec.}$$

$$T_L = 0 \text{ N-m}$$

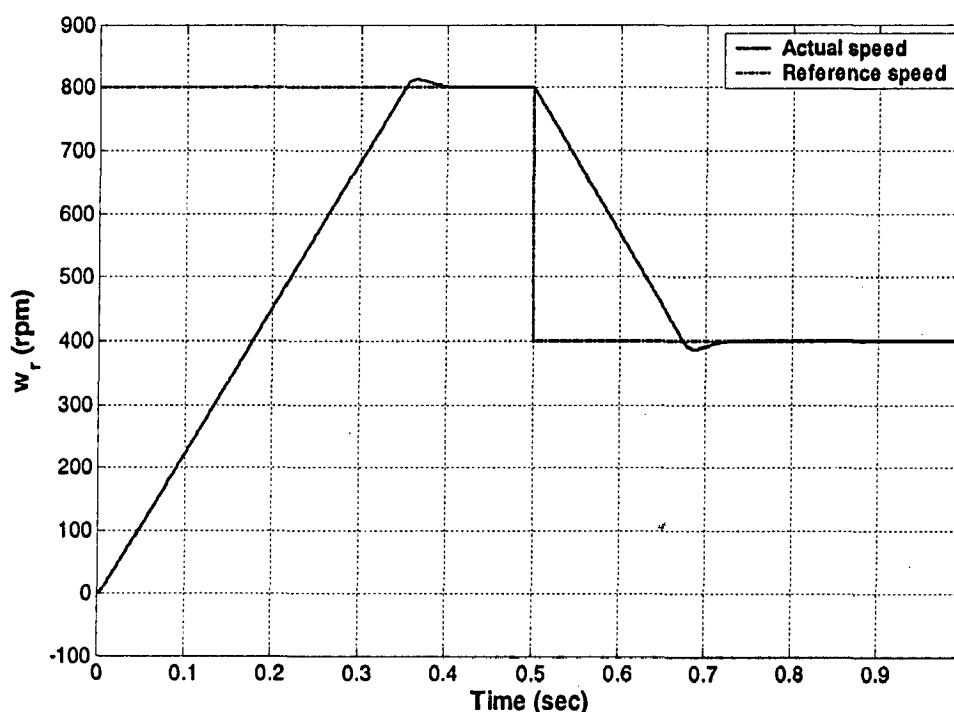


Figure (3.9) Speed response under no load condition

The unit vectors ($\cos\theta_e$ and $\sin\theta_e$) are also called Vector Rotator. The vector rotates the stator current according to the torque signal and keeps the flux current component of the stator current i.e. i_{ds} in the direction of rotor flux in all operating conditions of machine. The correct alignment of current i_{ds} in the direction of flux λ_r and the current i_{qs} perpendicular to it is shown with the help of unit vectors.

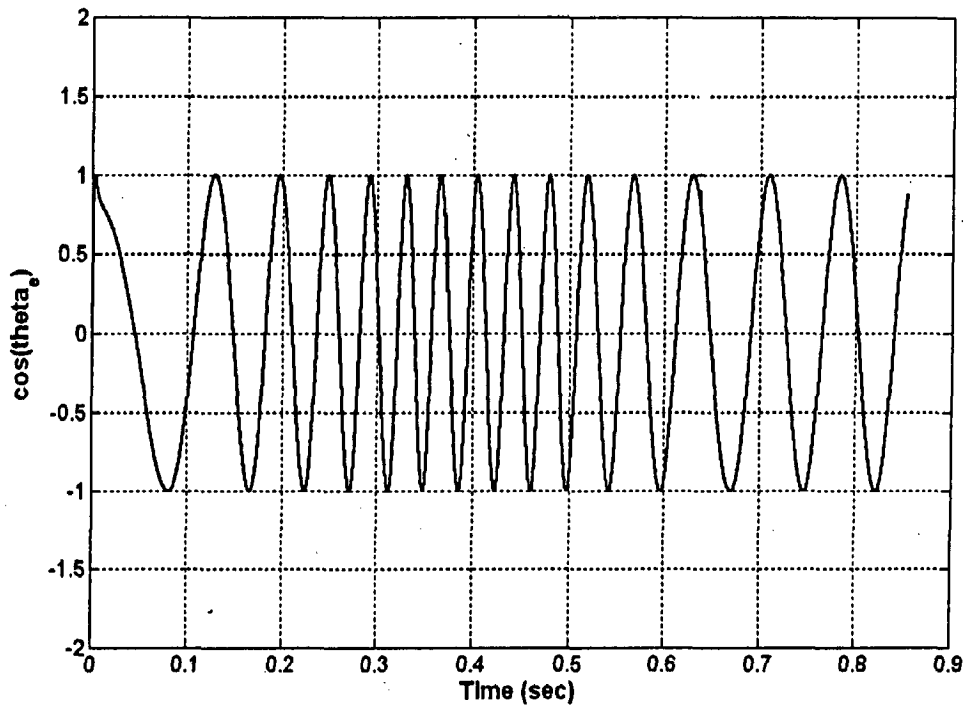


Figure (3.10): Unit vector $\cos\theta_e$

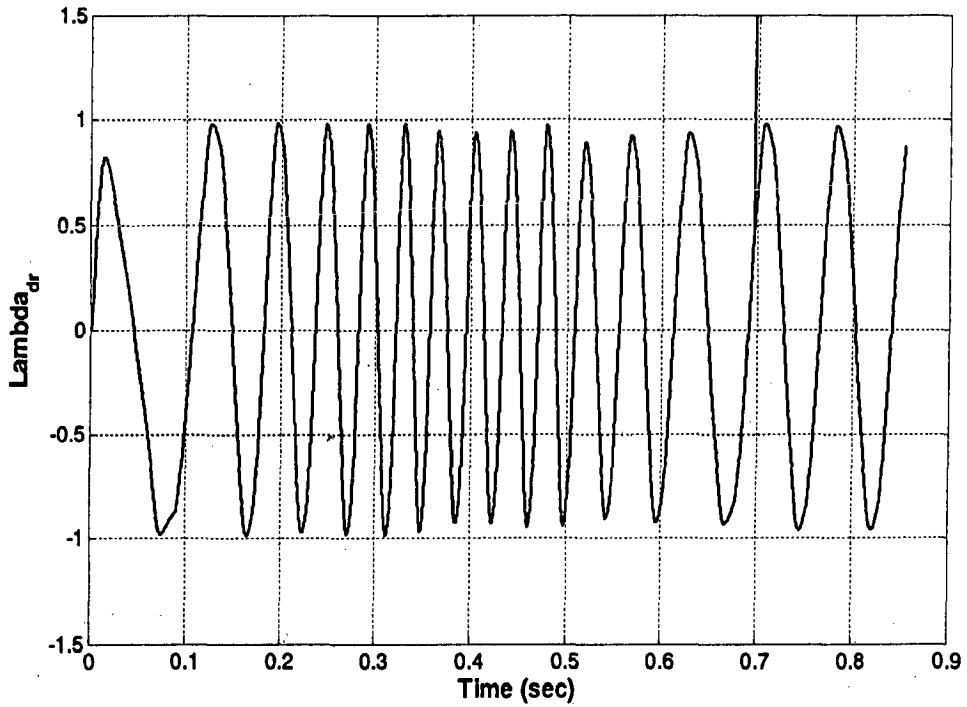


Figure (3.11): d-axis rotor flux

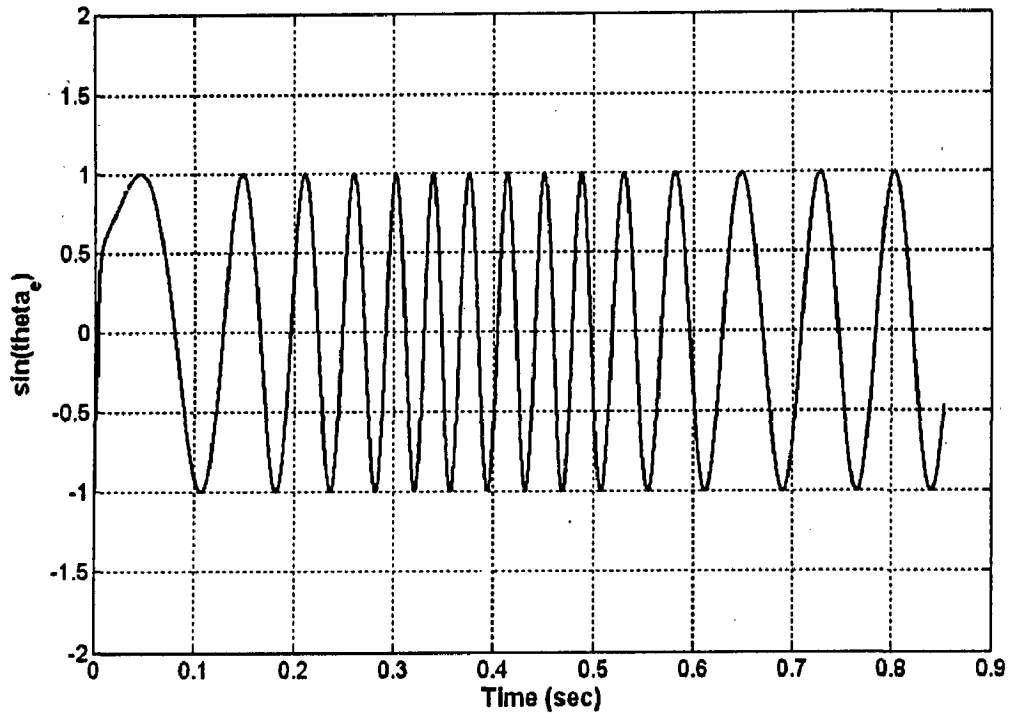


Figure (3.12): Unit vector $\sin\theta_e$

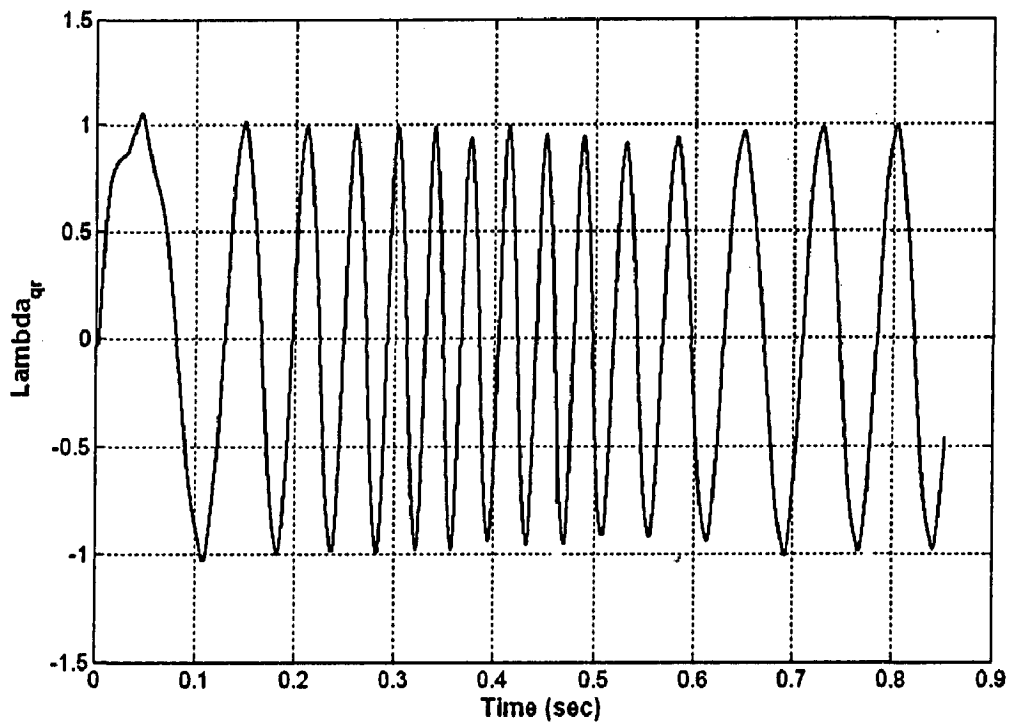


Figure (3.13): q-axis rotor flux

Figure (3.11) and (3.12) shows that unit vector, $\cos\theta_e$ and d-axis rotor flux is in correct phase position. Also figure (3.13) and (3.14) shows that unit vector $\sin\theta_e$ and rotor q-axis flux, λ_{qr} is in phase. Inphase behavior of unit vectors and rotor flux is the key of vector control scheme.

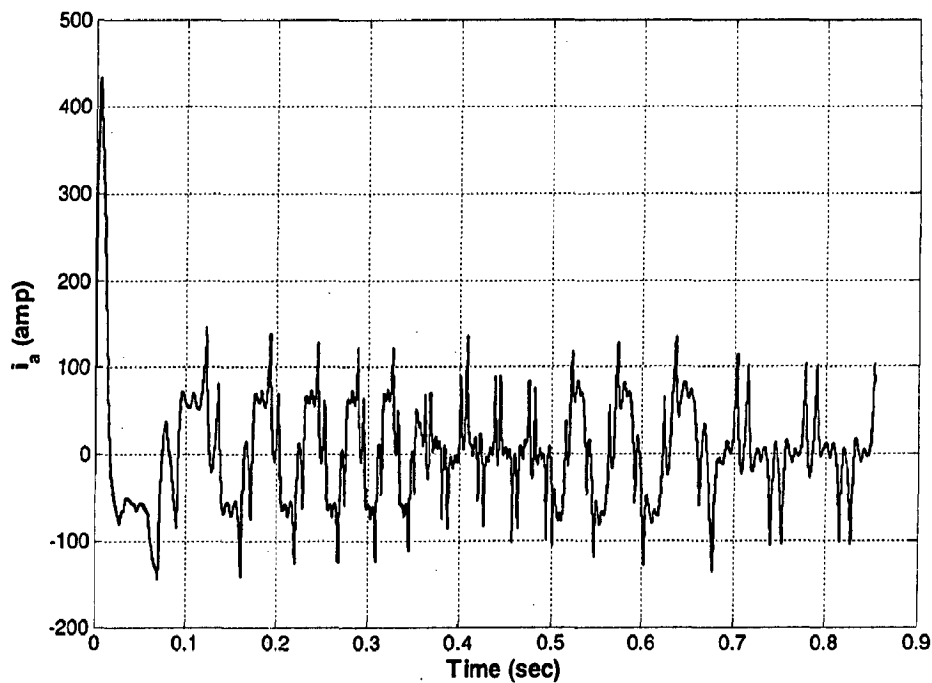


Figure (3.14) Stator phase A current response

Figure (3.14), (3.15) and (3.16) shows the stator phase current response under no load condition of machine. At the starting current shoots to a very high value, upto 10 times its rated value. Figure (3.17) and (3.18) shows the stator and rotor flux response. The rated value of rotor flux is 0.96 weber.

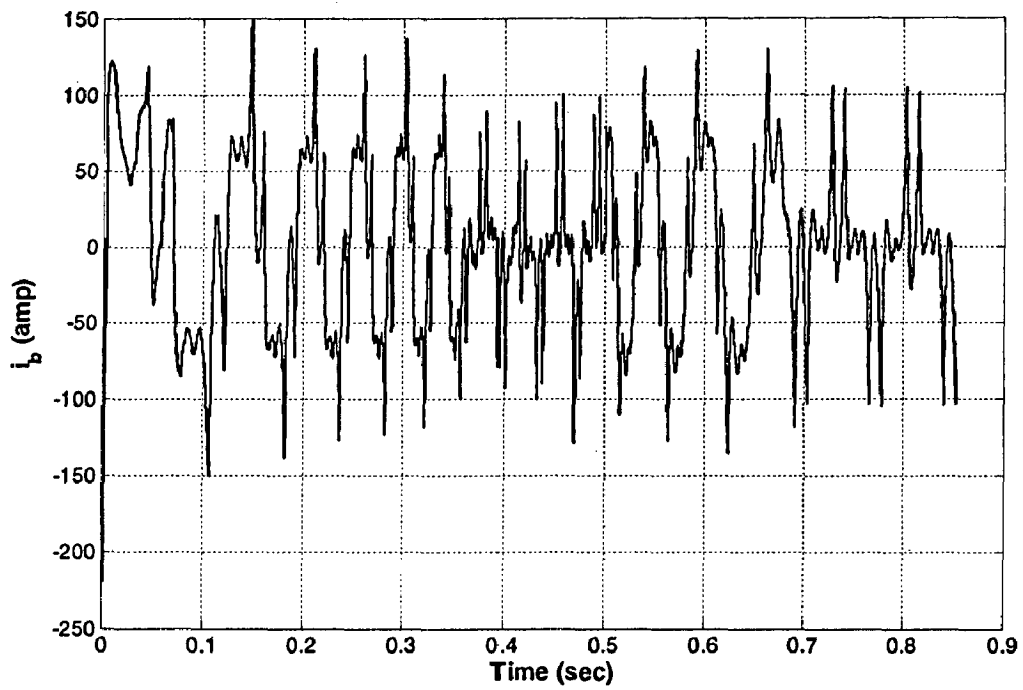


Figure (3.15) Stator phase B current response

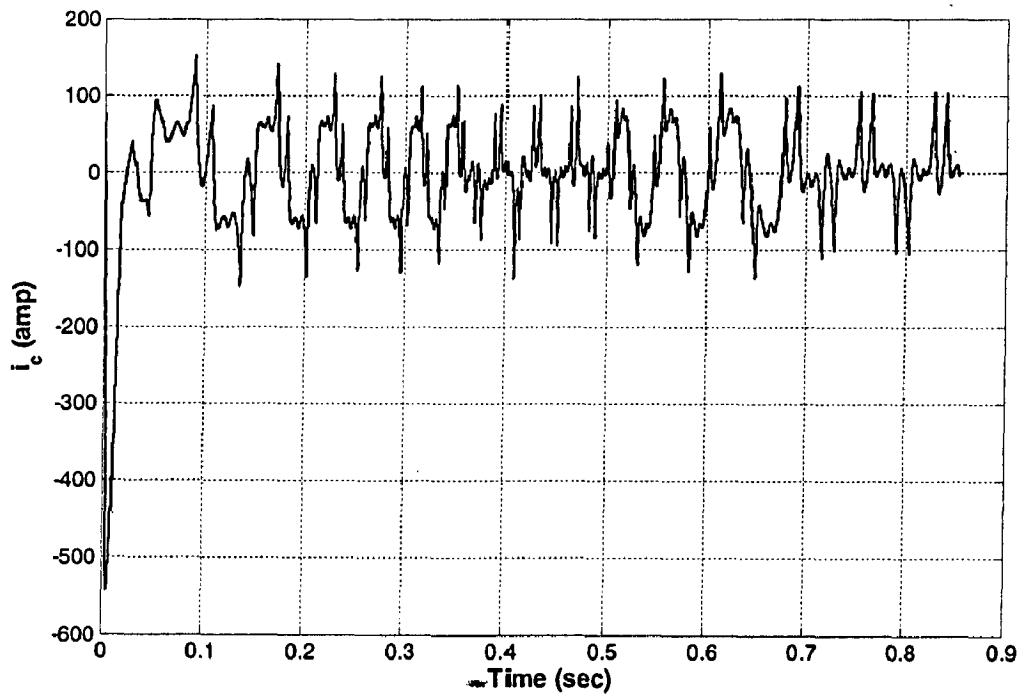
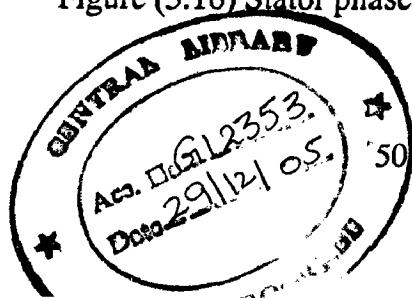


Figure (3.16) Stator phase C current response



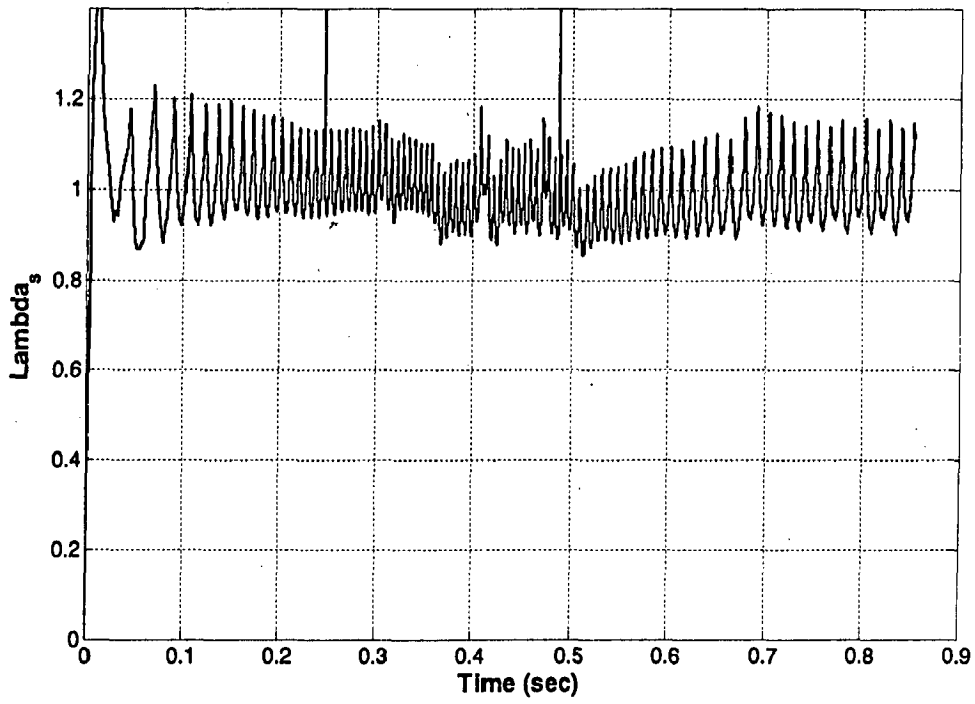


Figure (3.17) Stator flux response (no load condition)

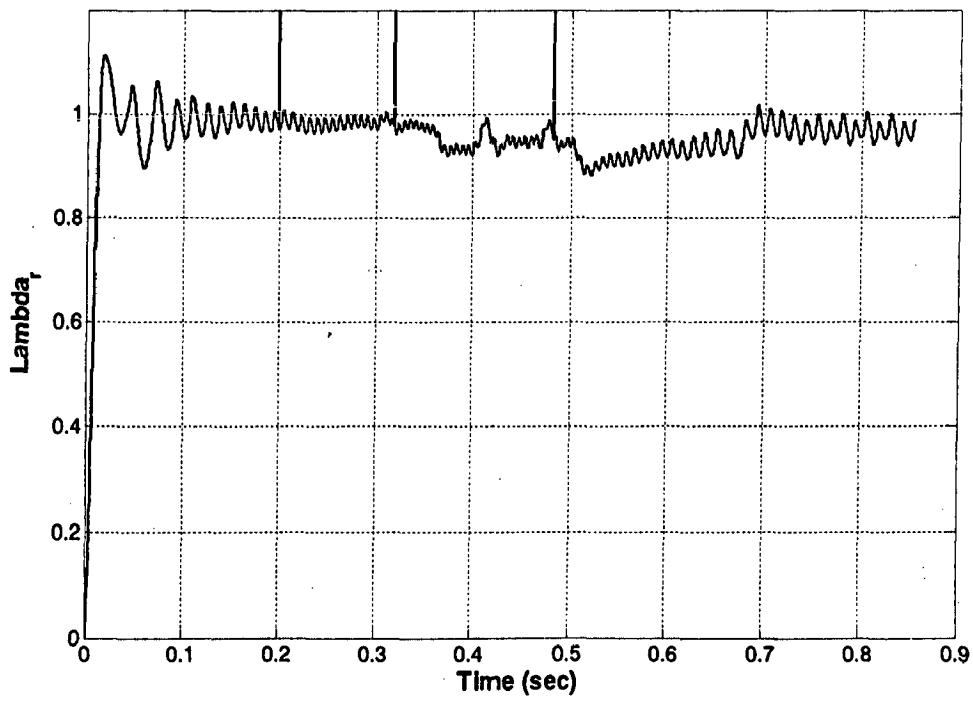


Figure (3.18) Rotor flux response (no load condition)

3.5.2 Torque response analysis under no load condition ($T_l = 0$):

The torque response is almost instantaneous and is shown in figure (3.19). This figure shows that the developed torque remains at zero value equal to load torque, except when the motor is accelerating and decelerating. The developed torque initially rises to rated value of 198 N-m. When rotor speed reaches the reference speed command, then developed torque again traces the applied load torque. The system is in overdamped condition. There is no oscillation in torque behavior and the system is stable.

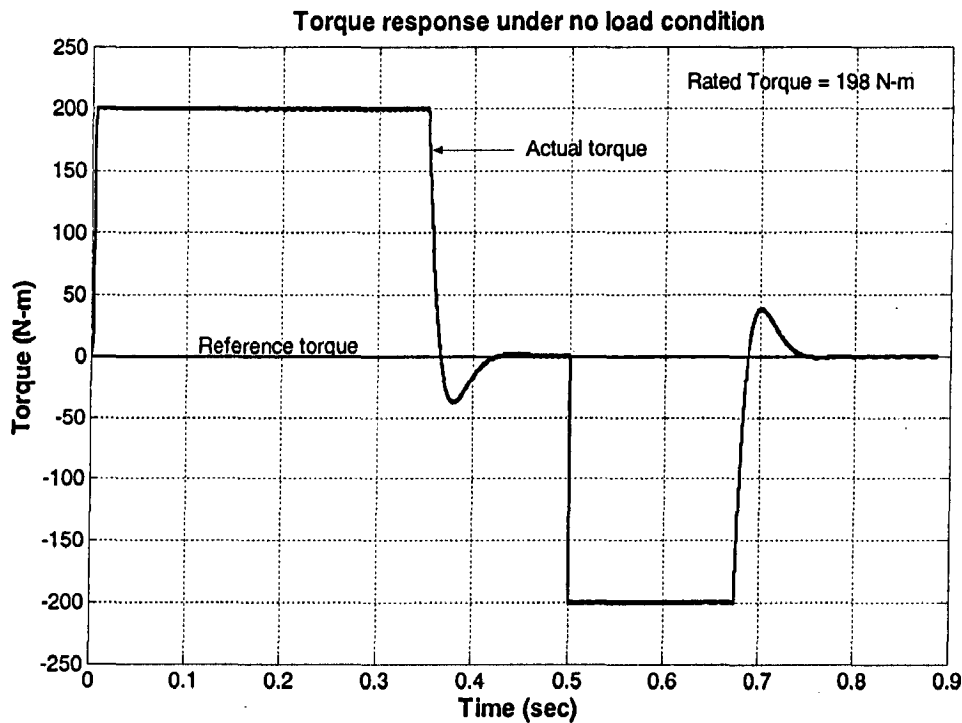


Figure (3.19) Torque response under no load condition

3.5.3 Response under speed reversal ($T_l = 0$):

For reverse motoring operation a step signal of 600 rpm to -300 rpm is applied as reference signal. The applied load torque is zero. Figure (3.20) and (3.21) shows that during acceleration and deceleration only, the generated rotor torque is maintained at 198 N-m and -198 N-m respectively and acceleration and deceleration profiles are smooth as shown. Speed profile shown in figure (3.20) closely follows the commanded speed signal. As shown in figure (3.22) and (3.23), when the rotor speed crosses the zero, the unit vector changes their phase sequence. As shown in figure (3.24), the phase A current of motor changes its phase sequence when the motor starts to operate in reverse mode. Simulation inputs are:

$$\omega_{ref} = +600 \text{ rpm to } -300 \text{ rpm at } 0.5 \text{ sec}$$

$$T_L = 0 \text{ N-m}$$

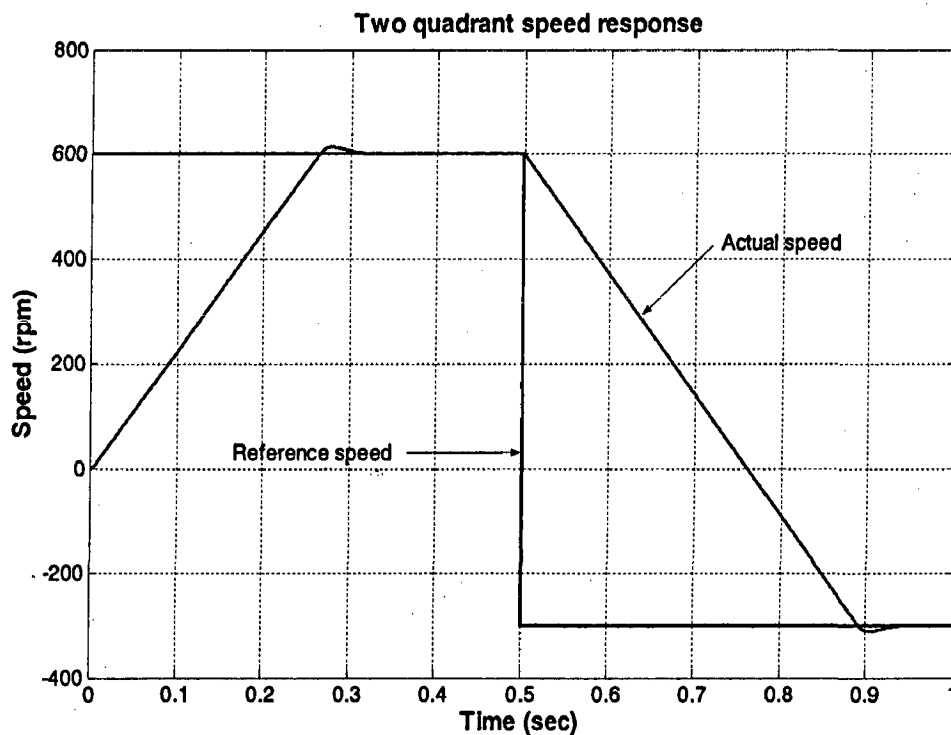


Figure (3.20) Speed response during reverse motoring (no load condition)

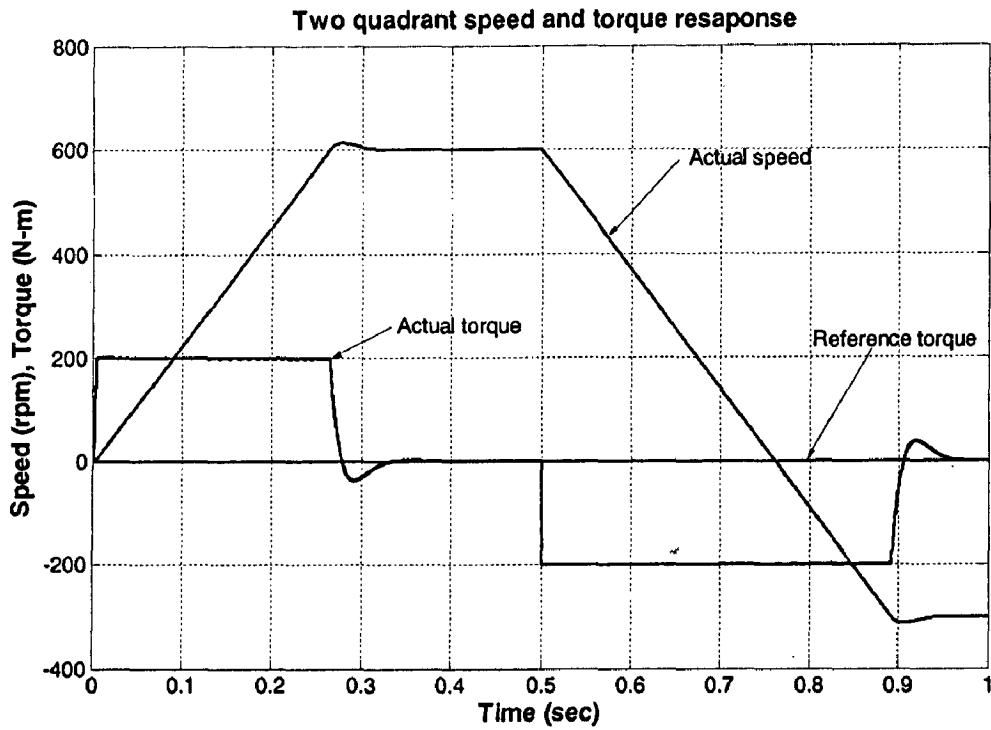


Figure (3.21) Speed and torque response during reverse motoring operation

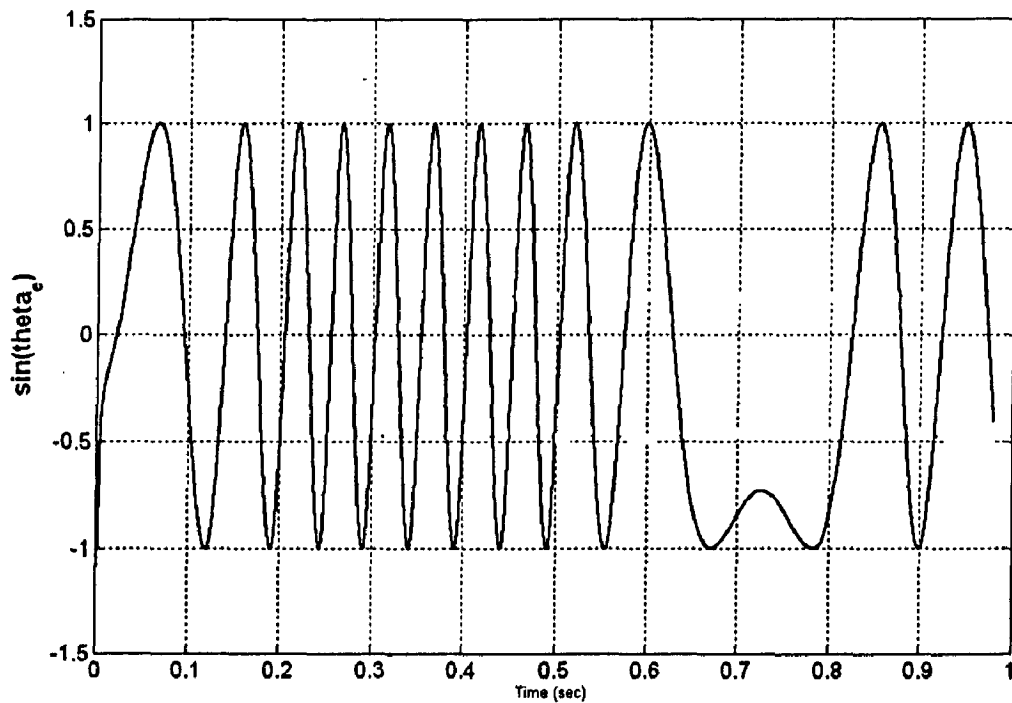


Figure (3.22): Unit vector signal $\sin\theta_e$ during reverse motoring operation

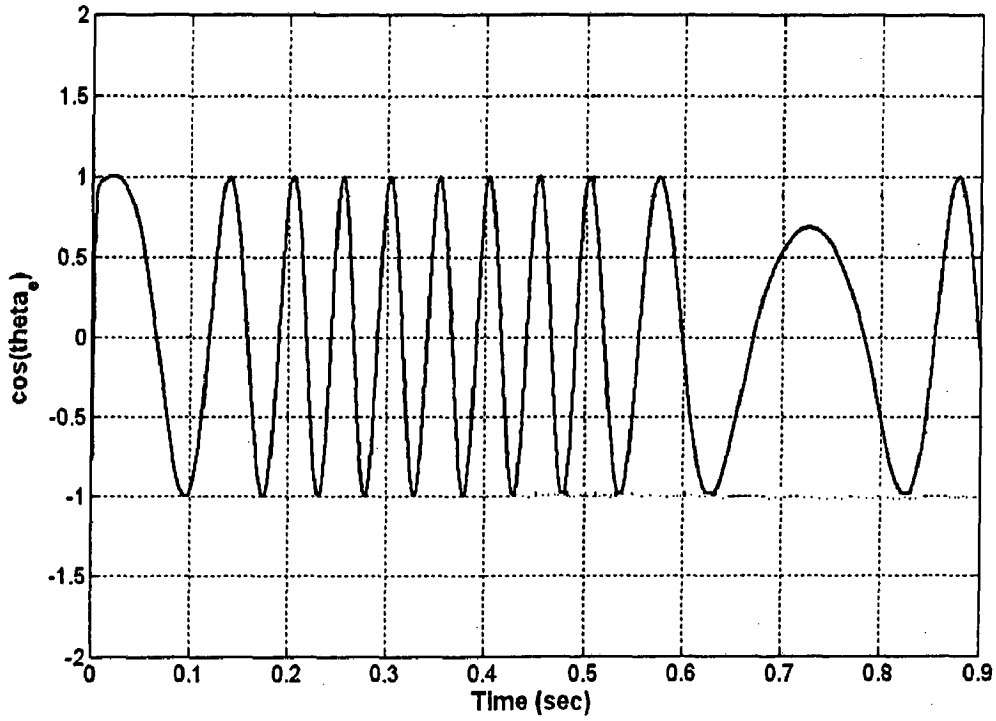


Figure (3.23): Unit vector signal $\cos\theta_e$ during reverse motoring operation

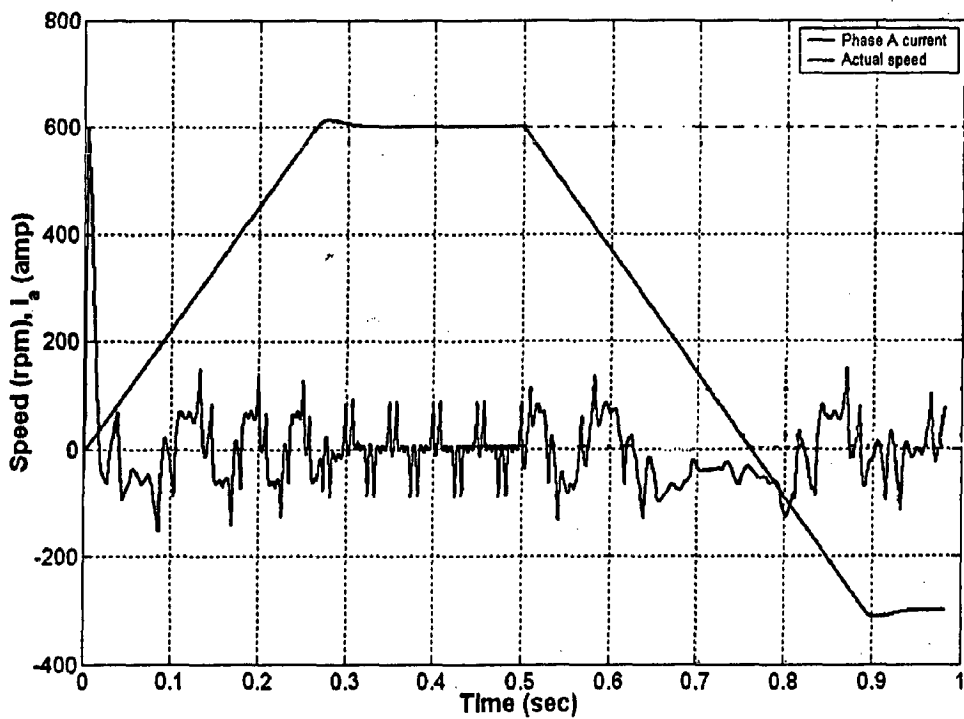


Figure (3.24): Stator phase A current during reverse motoring operation

3.5.4 Response under load condition:

For the analysis of torque response under load condition, a load torque of 100 N-m is applied at 0.6 sec and reference speed has changed from 800 rpm to 500 rpm at 0.5 sec. The response of the system shows that under steady state condition developed torque follows the load torque, independent of the speed command. If speed reference is changed to a new value, then also the electromagnetic torque follows the load torque. Behavior of the motor under load condition is shown in figure (3.25) and (3.26).

Simulation inputs are:

$$\omega_{ref} = 800 \text{ rpm to } 500 \text{ rpm at } 0.5 \text{ sec.}$$

$$T_L = 100 \text{ N-m. at } 0.6 \text{ sec}$$

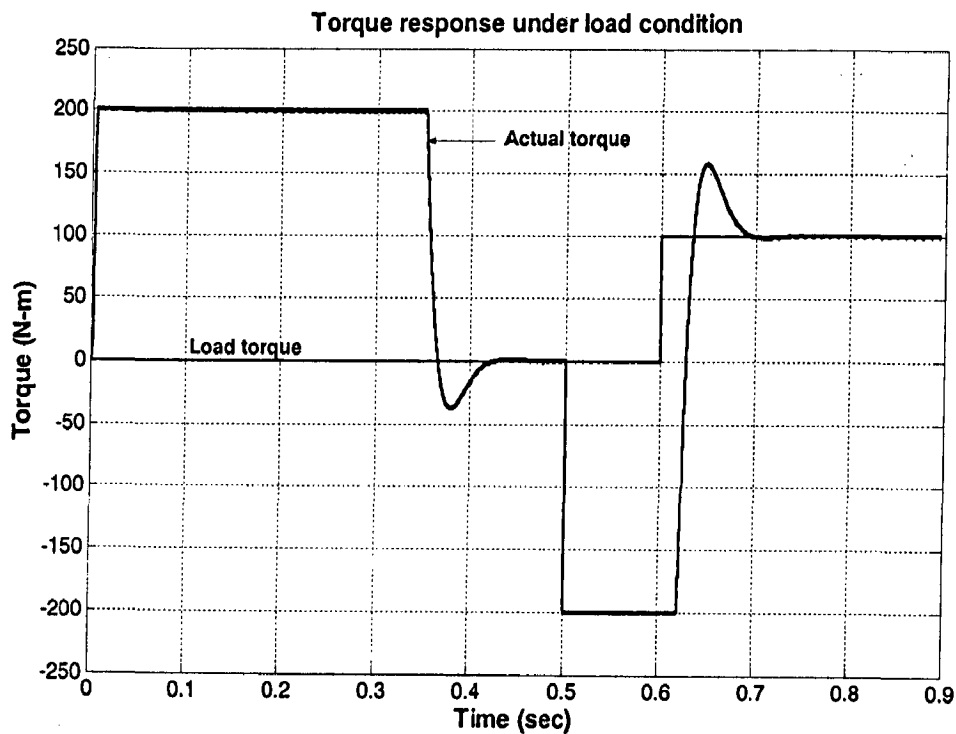


Figure (3.25) Torque response under load condition

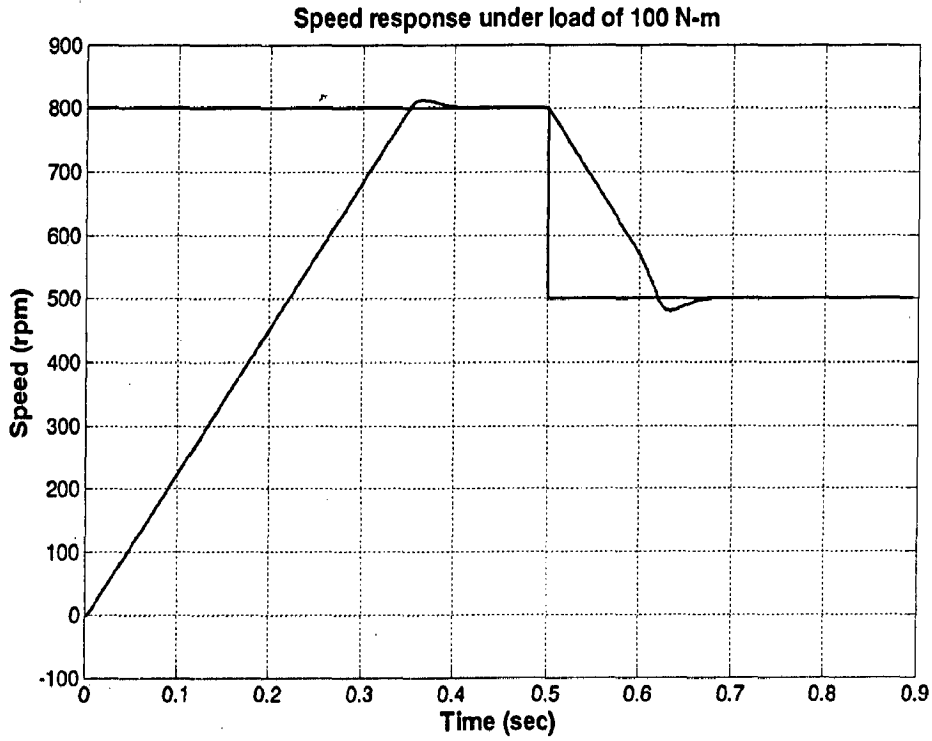


Figure (3.26) Speed response under load condition

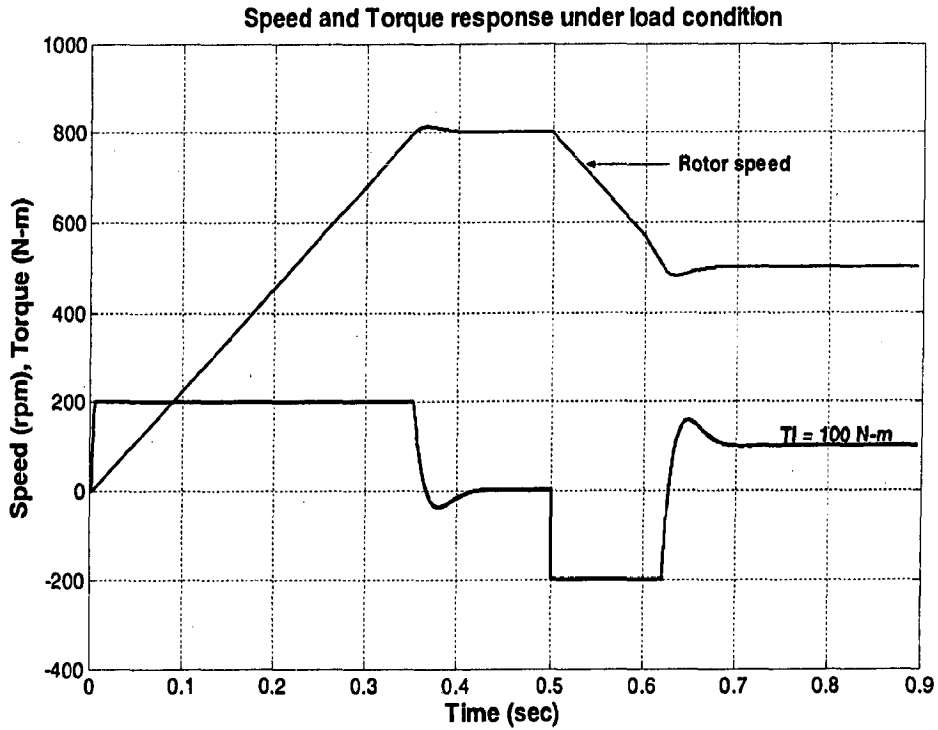


Figure (3.27) Speed and torque response under load condition

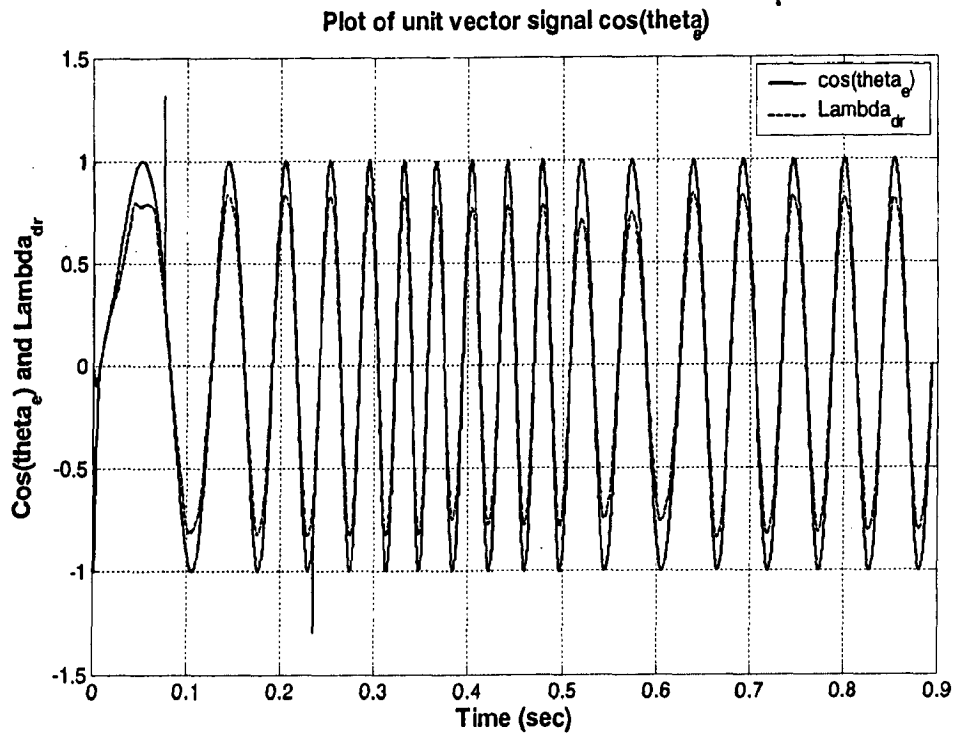


Figure (3.28) Unit vector signal $\cos\theta_e$ and λ_{dr} under load condition

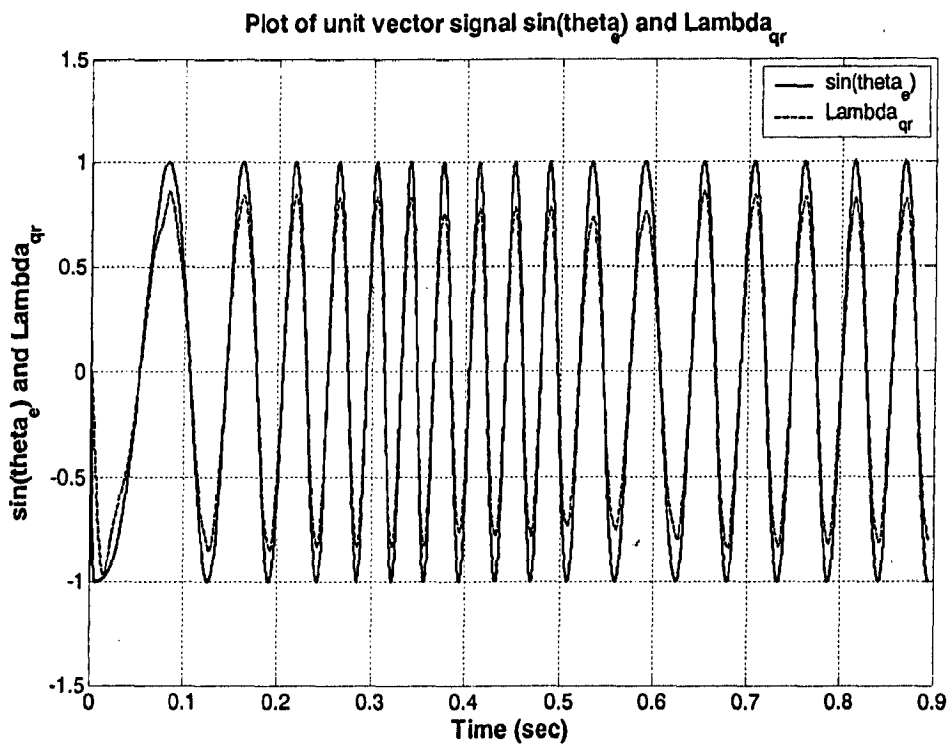


Figure (3.29) Unit vector signal $\sin\theta_e$ and λ_{qr} under load condition

Fig (3.28) and (3.29) shows the unit vectors that are in correct phase position with the rotor flux that proves the decoupled control of drive system. Rotor flux response when motor is under load condition is shown in figure (3.30).

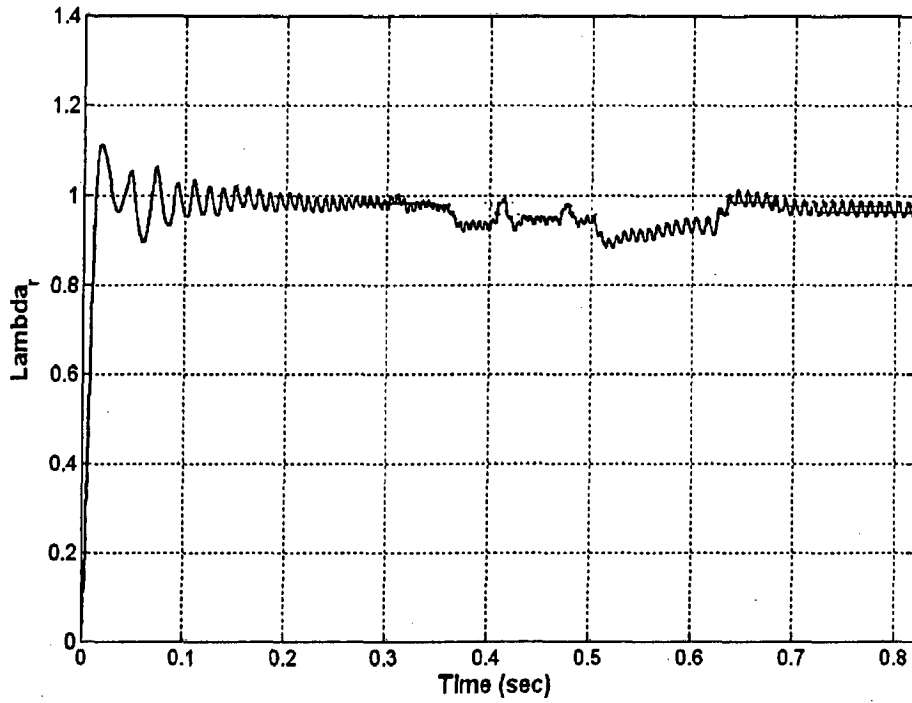


Figure (3.30): Rotor flux (λ_r) response under load condition

3.6 Interim conclusions:

From the above simulation results, it has been concluded that the drive system operates stably in direct vector control mode, both under load as well as no load condition. The unit vector response shown in figures (3.28) and (3.29) closely follows the rotor flux orientation in all conditions. These unit vectors rotate the stator dqcurrent components in the direction of rotor flux achieving the decoupled control. A speed response has been less oscillatory and is stable. The stable operation of drive in DVC mode depends on the accuracy of motor terminal currents (i_{ds} and i_{qs}) and voltages (v_{ds} and v_{qs}) measurements. At very low speed, sensing of these parameters (i.e. voltage and current) becomes difficult due to offset voltage and hence drive performance deteriorates. Rotor flux can also be calculated using stator flux linkage to reduce the computational steps and dependence on motor parameters. But this method also depends on stator resistance as in rotor flux based calculation, used in the above drive system. The dynamic response of the system is shown in figure (3.27). From this response, it has been seen that when the motor is running, a sudden application of load doesn't affect the speed profile and drive system operates maintaining its stability..One important point that should be reinforced is that, MATLAB is a program that models all the physical processes involved with this motor controller mathematically. It does not consider variables such as heat, magnetic saturation etc.

CHAPTER 4

INDIRECT VECTOR CONTROL

4.1 Principle of Indirect Vector Control.

The indirect vector control method is essentially the same as direct vector control method, except the unit vector signals ($\cos\theta_e$ and $\sin\theta_e$) are generated in feed forward manner. Figure (4.1) explains the fundamental principal of indirect vector control with the help of phasor diagram [1] [9] [13]. The d^s and q^s axes are fixed on the stator, but the d^r and q^r axes, which are fixed on the rotor, are moving at a speed ω_r as shown. Synchronously rotating axes d^e and q^e are rotating ahead of the d^r - q^r by the positive slip angle θ_{sl} corresponding to slip frequency ω_{sl} . Since the rotor pole is directed on the d^e axis and $\omega_e = \omega_r + \omega_{sl}$, we can write

$$\theta_e = \int \omega_e dt = \int (\omega_r + \omega_{sl}) dt = \theta_r + \theta_{sl} \quad (4.1)$$

The phasor diagram suggests that for decouple control, the stator flux component of current i_{ds} should be aligned on the d^e axis, and the torque component of the current i_{qs} should be on the q^e axis. Then only the i_{ds} becomes the magnetizing of flux component and i_{qs} becomes torque component

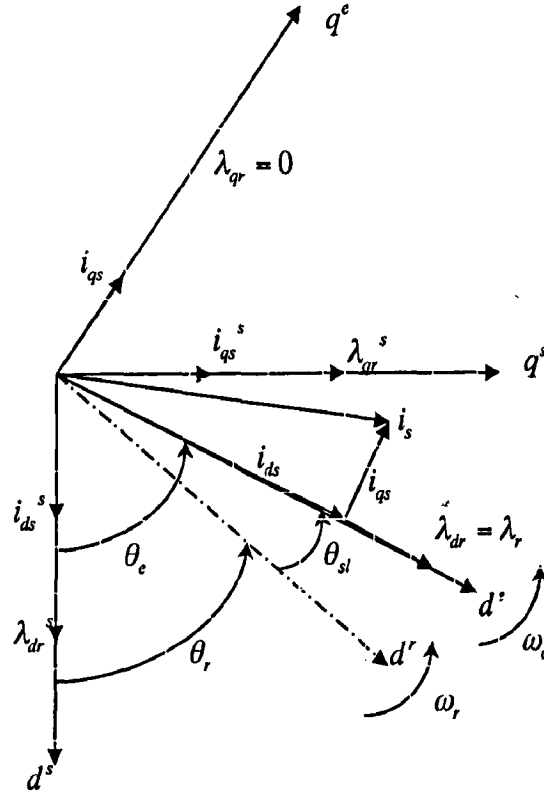


Figure (4.1): Phasor diagram of indirect vector control

4.2 Indirect Vector Control Scheme.

A vector controller accepts the torque and the flux requests and generates the torque and flux producing components of the stator current phasor and the slip angle θ_{sl} commands. The request/command values and the controller instrumented parameters are denoted as asterisk (*).

The mathematical equations for the command values of i_T^* , i_f^* and ω_{sl}^* are

$$i_T^* = \frac{T_e}{K_r \cdot T_{rc}} = \frac{T_{ec}}{T_{rc}} \cdot \frac{L_{rc}}{L_{mc}} \cdot \frac{2}{3} \cdot \frac{2}{P} = K_r \cdot \left[\frac{T_{ec}}{T_{rc}} \right] \left[\frac{L_{rc}}{L_{mc}} \right] \quad (4.2)$$

$$i_f^* = (1 + T_{rc} \cdot p) \frac{i_{rc}}{L_{mc}} \quad (4.3)$$

$$\omega_{sl}^* = K_r \left[\frac{L_{rc}}{T_{rc}} \right] \left[\frac{T_{ec}}{(T_{rc})^2} \right] = K_r \cdot R_{rc} \frac{T_{ec}}{(T_{rc})^2} = \frac{L_{mc}}{T_{rc}} \cdot \frac{i_T^*}{T_{rc}} \quad (4.4)$$

Where

$$K_t = \frac{3}{2} \cdot \frac{p}{2} \cdot \frac{L_{me}}{L_{lc}} \quad \text{and} \quad K_r = \frac{2}{3} \cdot \frac{2}{P}$$

The design employed here is referred to as “Indirect Field Oriented”. This is because this method uses a speed sensor in the feed back loop to calculate the rotor flux, instead of a Hall sensor that the direct method uses. ω_{ref} is the input applied by the user. This is compared with the attained speed of the rotor that is obtained from the speed sensor. This is then converted into the electromagnetic torque signal T_{em}^* via the speed controller (this is a PI controller).

The obtained speed of the rotor is also used to set the required rotor flux λ_r^* . The field weakening block compares the incoming speed value and output a desired rotor flux value. For most of the part, induction motor requires a constant rotor flux, however, at high positive and negative speeds, the Field weakening block have to decrease the output flux in a nonlinear fashion. The T_{em}^* and λ_r^* are then converted into i_{sd}^* and i_{sq}^* signals using equation (4.2) and (4.3).

These values that are in synchronous reference frame are then compared with the stator dq-currents that are also in synchronous reference frame. Errors are processed through PI controller blocks (these blocks convert current signal into voltage signal and also limit the amount of voltage that can be applied to the next stage) and then required dqvoltage commands are generated. By using transformation matrix, the two axis voltage commands are converted into three-phase voltage commands. These sinusoidal voltage signals are converted to PWM signals and are amplified by the inverter using any switching techniques. The output voltage of the inverter is then converted into stationary reference frame and fed into the stator winding of the induction motor.

4.3 SIMULINK design of Indirect Vector Control scheme.

There are two inputs into this system, ω_{ref} and T_{load} . The fundamental intention of this SIMULINK design, is that the FO control portion of the design that causes the rotor to generate a speed profile that follows the commanded speed input ω_{ref} . To do this the commanded speed is fed into the FO section of the design where it is compared with the measured speed of the rotor. The generated speed error is then fed into a torque controller block. The torque controller block is a PI controller that generates a torque command T_{em}^* . This torque command is used to set the electromagnetic torque induced within the induction motor by calculating an appropriate i_{qs}^* command based on equation (4.2). Also by using equation (4.3) and field weakening block, i_{ds}^* command is set. Rotor flux angle θ_e with respect to stator reference frame is calculated in the "Theta Calculator" block. Equation for converting three phase stator current into two phase synchronous reference current is:

$$\begin{bmatrix} i_d \\ i_q \end{bmatrix} = \frac{2}{3} \begin{bmatrix} \cos\theta_e & \cos(\theta_e - \frac{2\pi}{3}) & \cos(\theta_e + \frac{2\pi}{3}) \\ \sin\theta_e & -\sin(\theta_e - \frac{2\pi}{3}) & -\sin(\theta_e + \frac{2\pi}{3}) \end{bmatrix} \begin{bmatrix} i_a \\ i_b \\ i_c \end{bmatrix} \quad (4.5)$$

And equation for converting two phase synchronous reference voltages into three phase stator reference voltage is:

$$\begin{bmatrix} v_a \\ v_b \\ v_c \end{bmatrix} = \begin{bmatrix} \cos\theta_e & \sin\theta_e \\ \cos(\theta_e - \frac{2\pi}{3}) & \sin(\theta_e - \frac{2\pi}{3}) \\ \cos(\theta_e + \frac{2\pi}{3}) & \sin(\theta_e + \frac{2\pi}{3}) \end{bmatrix} \begin{bmatrix} v_d \\ v_q \end{bmatrix} \quad (4.6)$$

Simulation diagram of the proposed MATLAB design is shown in the figure (4.2). While simulation gives desired performance, it also shows how the subsystems within FO control work together to produce the desired outputs. Hence it helps in deeper understanding of Field Oriented Control system of an induction motor. This knowledge is mainly obtained through the use of “Scopes”. A scope is a SIMULINK block that displays signals at nodes during simulation. The simulation studied occurred over 1.5 seconds. The integration method used is variable step, the “ode23tb (stiff/TR-BDF2)”. One important point that should be reinforced is that, MATLAB is a program that models all the physical processes involved with this motor controller mathematically. It does not consider variables such as heat, magnetic saturation etc.

4.4 Response under No load condition.

4.4.1 Speed response analysis.

The simulation is conducted with a reference speed signal of 400 rpm that changes to 200 rpm at 0.6 sec. It is a step speed signal. The applied load torque is kept at zero ($T_l = 0$). The response shown in the figure (4.3) shows that generated rotor speed closely follows the reference speed with minimum oscillation both under acceleration and deceleration. The proportional and integral gain of the speed PI controller is set at 100 and 5200 respectively. From the figure (4.3) it is clear that under steady state rotor speed is relatively constant and follows the reference speed. If the proportional gain of the torque PI controller is increased, then there is oscillation in torque response and speed reaches to constant value in a smaller time.

Simulation inputs are:

$$\omega_{ref} = 400 \text{ rpm to } 200 \text{ rpm at } 0.6 \text{ sec.}$$

$$T_l = 0 \text{ N-m.}$$

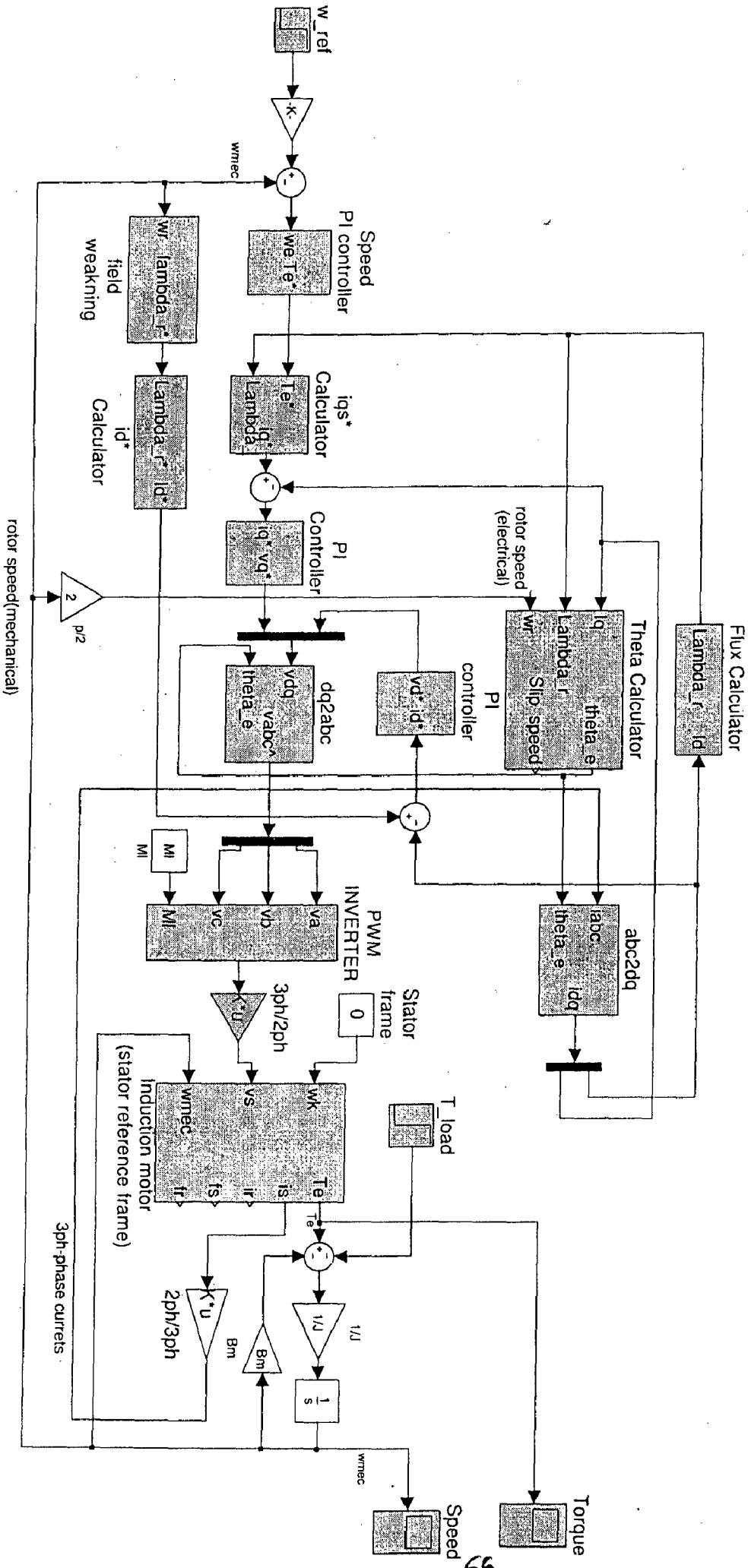


Figure (4.2): SIMULINK DIAGRAM FOR INDIRECT VECTOR CONTROL SCHEME

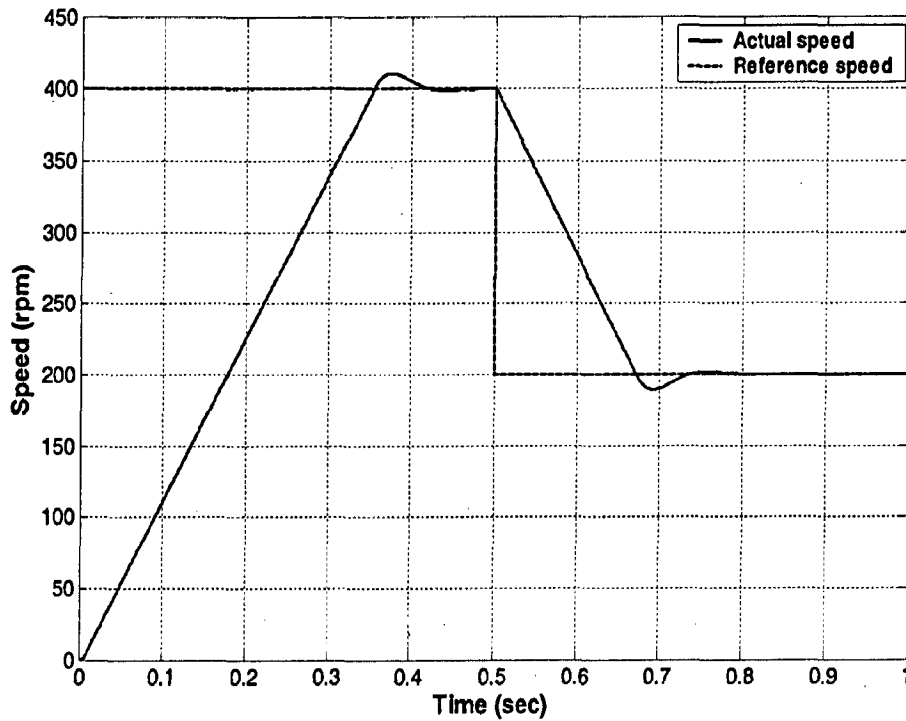


Figure (4.3): Speed response during no load condition

4.4.2 Torque response analysis.

As shown in figure (4.4), the torque response is almost instantaneous. For simulation purpose first machine is run at no load condition. Torque response shows that developed torque remains at zero value except when the motor is accelerating and decelerating. The developed torque initially remains at rated value of 198 N-m (rated torque) when motor is accelerating and at -198 N-m, when it is decelerating. When rotor speed reaches the reference speed command, then developed torque again traces the applied load torque. There is minimum oscillation in torque behavior and the system is stable.

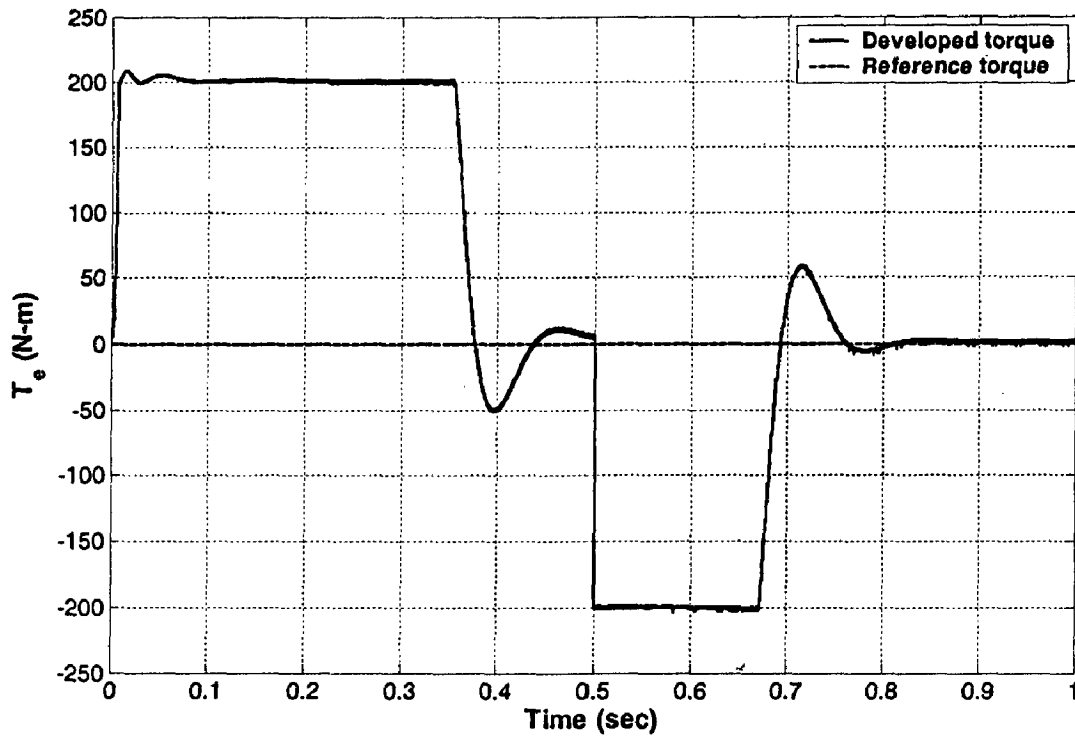


Figure (4.4): Torque response during no load condition

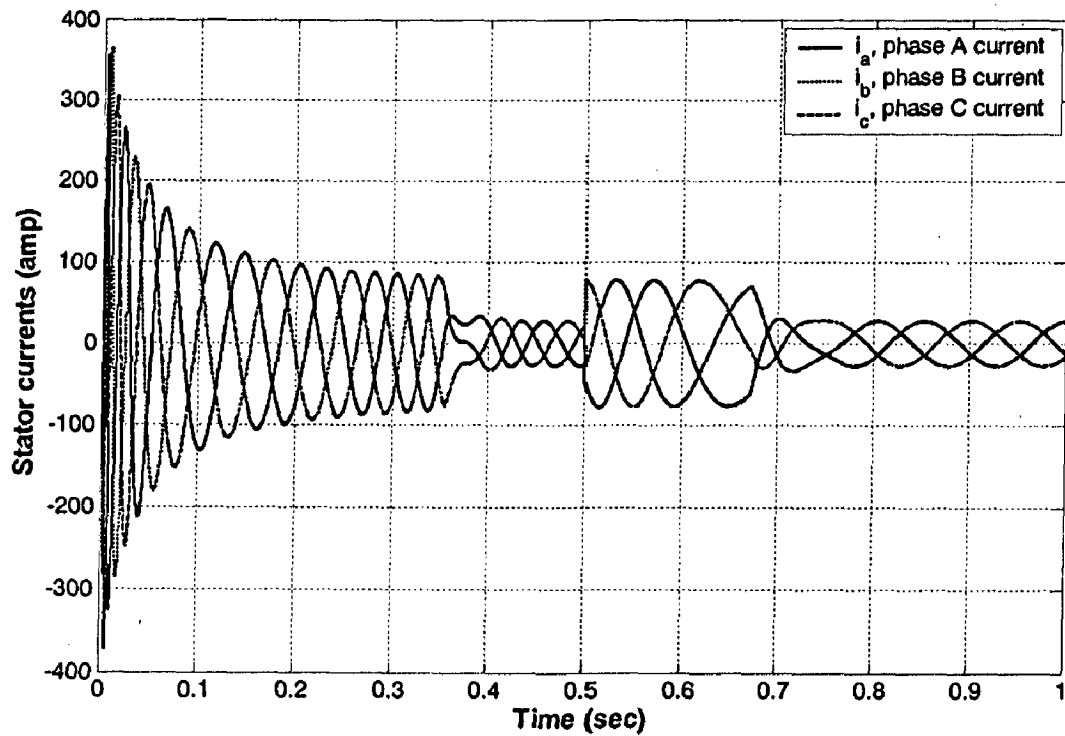


Figure (4.5): stator phase currents response during no load condition

Figure (4.5) shows the stator current response, when the machine is running in free acceleration mode. Transient starting current of motor rises to 8 to 10 times its rated value (base current of machine is 46 amps). Machine is drawing a current of 21 amps in steady state, under no load condition.

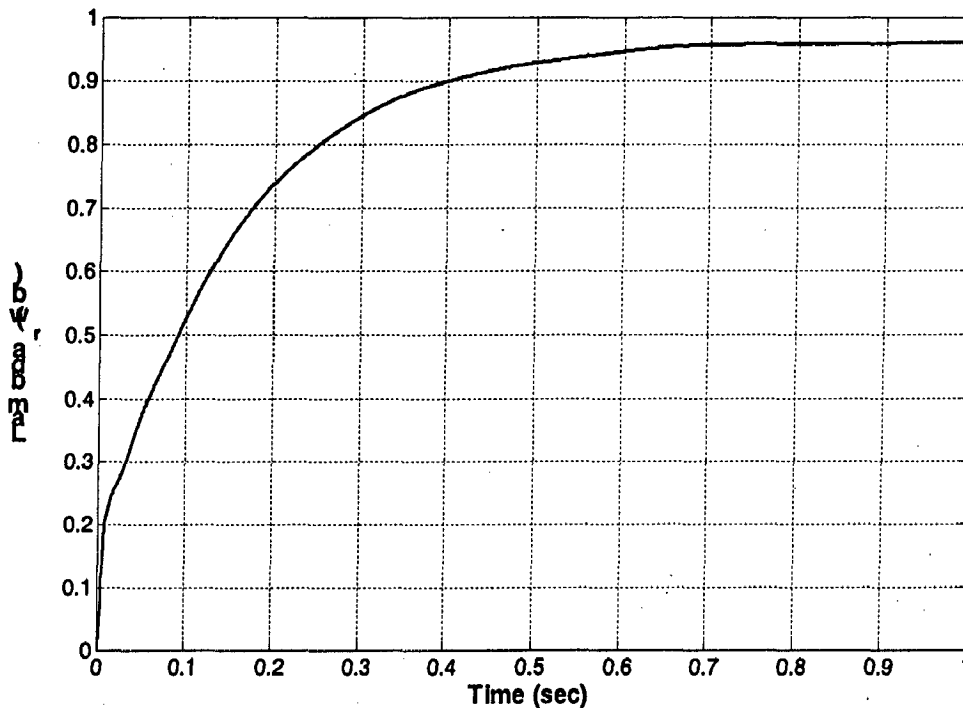


Figure (4.6): Rotor flux response

Figure (4.6) shows the response of rotor flux λ_r . The rated flux of the machine is 0.96 Weber.

As shown in figure (4.1), flux component of the stator current i_{ds} is aligned along rotor flux direction and torque producing component i_{qs} is aligned perpendicular to it. This correct alignment of stator current components which is necessary for decoupled control scheme is shown in the figure (4.7) and figure (4.8) with the help of unit vectors. Unit vectors assure the correct alignment of i_{ds} current with the rotor flux vector λ_r and i_{qs} perpendicular to it.

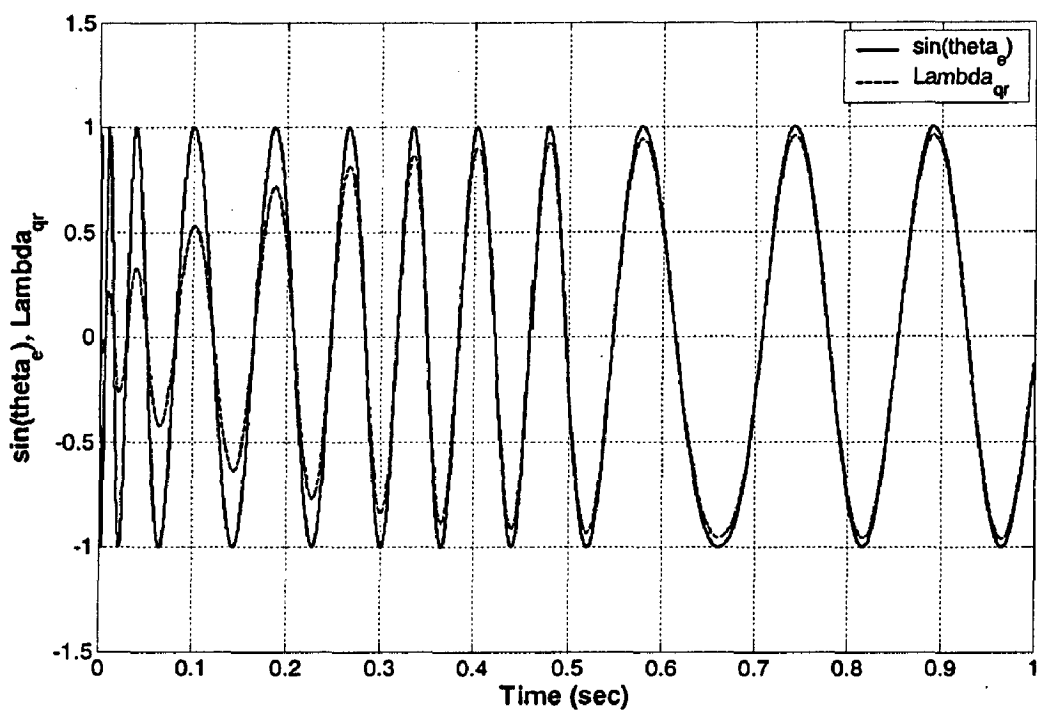


Figure (4.7): Unit vector $\sin\theta_e$ and λ_{qr} during no load condition

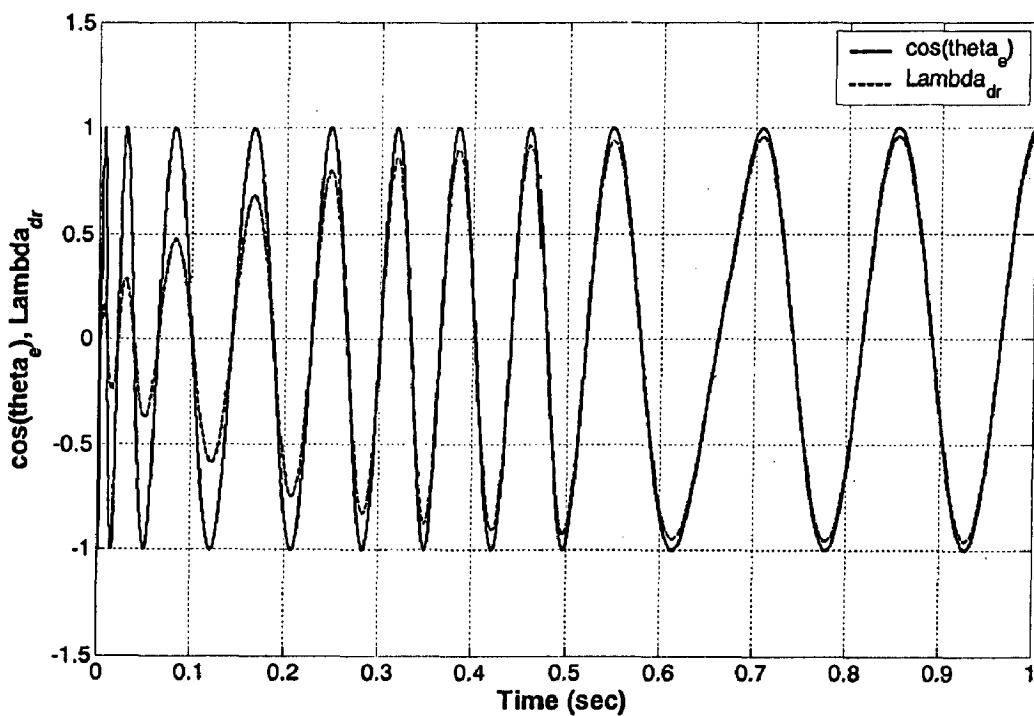


Figure (4.8): Unit vector $\cos\theta_e$ and λ_{dr} during no load condition

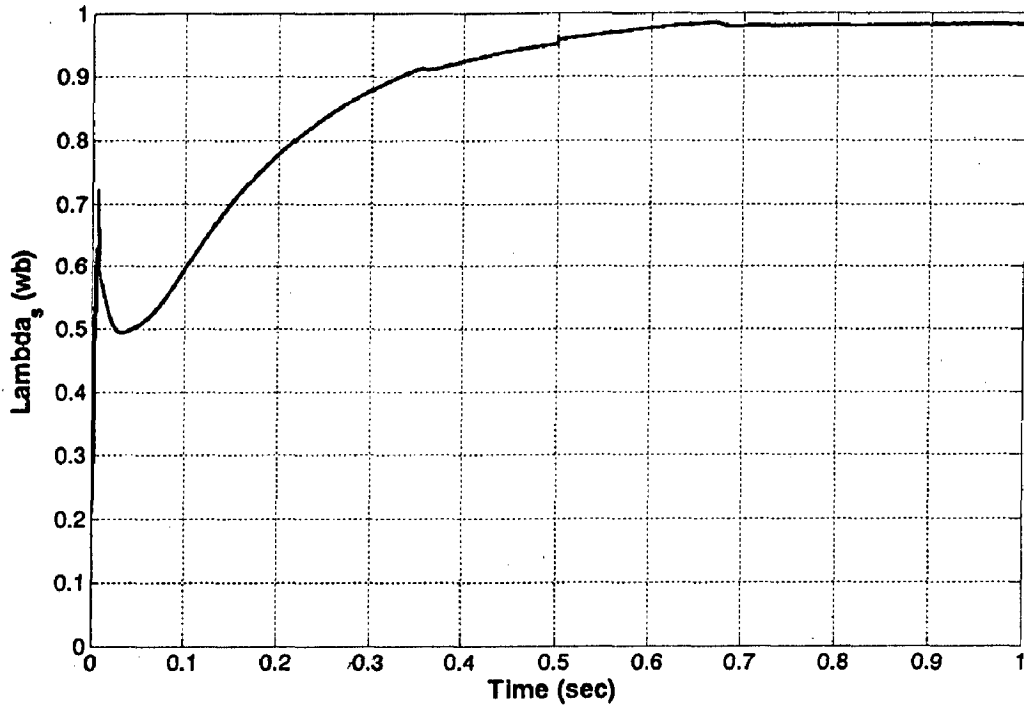


Figure (4.9): Stator flux response during no load condition

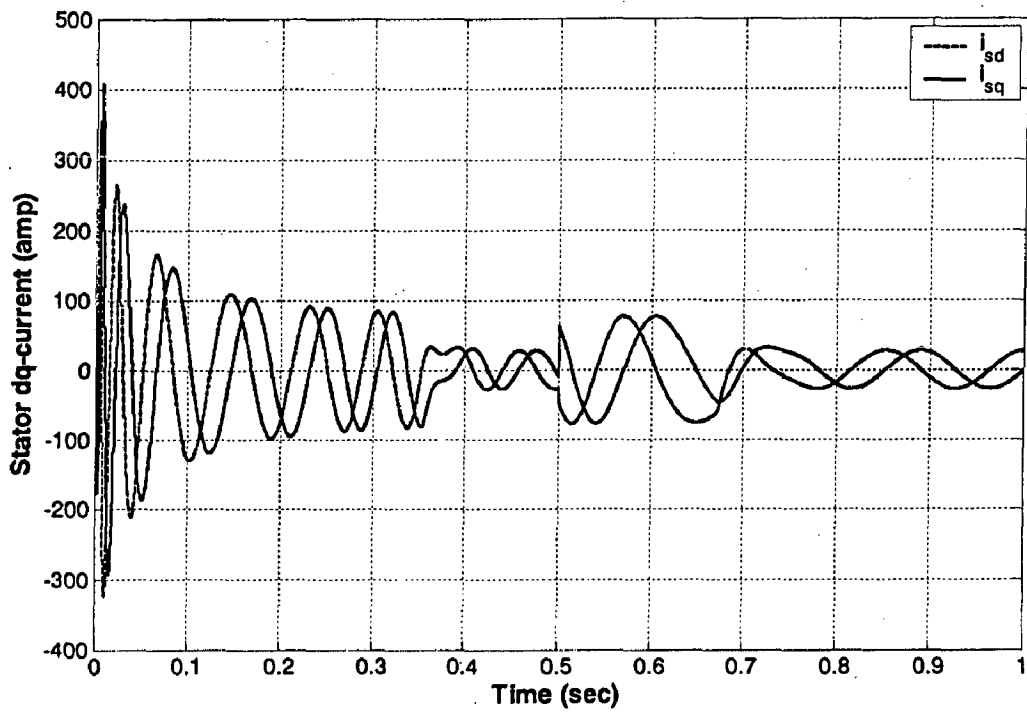


Figure (4.10): Stator dq-current response during no load condition

Stator voltage response (VSI output)

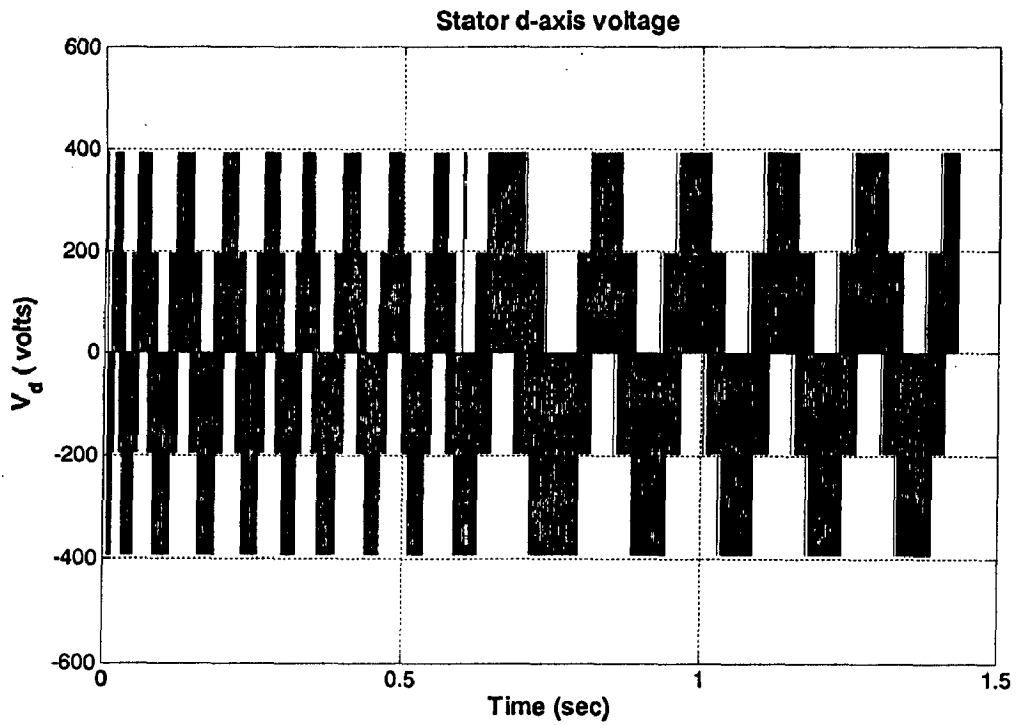


Figure (4.11): Stator d-axis voltage

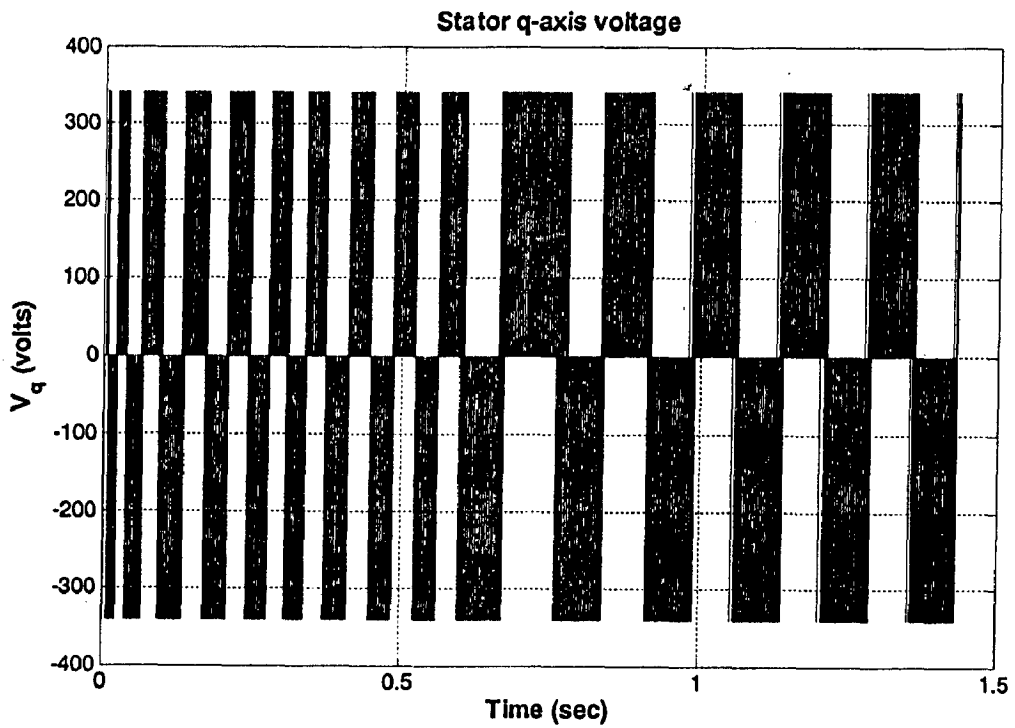


Figure (4.12): Stator q-axis voltage

4.5 Response Under Reverse Motoring Operation.

For simulation in reverse motoring operation, a step speed command of +200 rpm to -200 rpm is set as reference speed command. There is a step change in speed at 0.6 sec. Load torque is set to zero. Speed response shown in figure (4.13) shows that actual rotor speed closely follows the reference speed with minimum oscillation under all conditions i.e. during acceleration, deceleration and steady state. Figure (4.14) shows the torque response when speed direction is changed from positive to negative. When motor accelerates and decelerates, torque developed is 198 N-m and -198 N-m respectively. In the steady state condition, developed torque follows the load torque T_L that is zero in this condition. Unit vectors response shown in figure (4.15) and figure (4.16) shows the correct phase alignment of stator d and q -axis current in rotor flux direction.

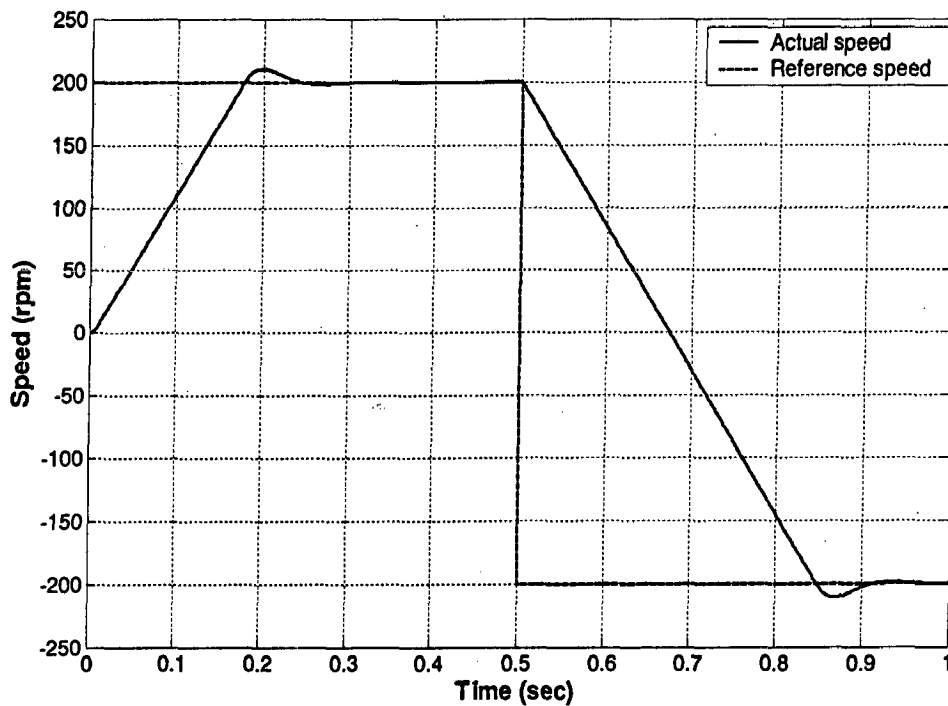


Figure (4.13): Speed response during reverse motoring operation

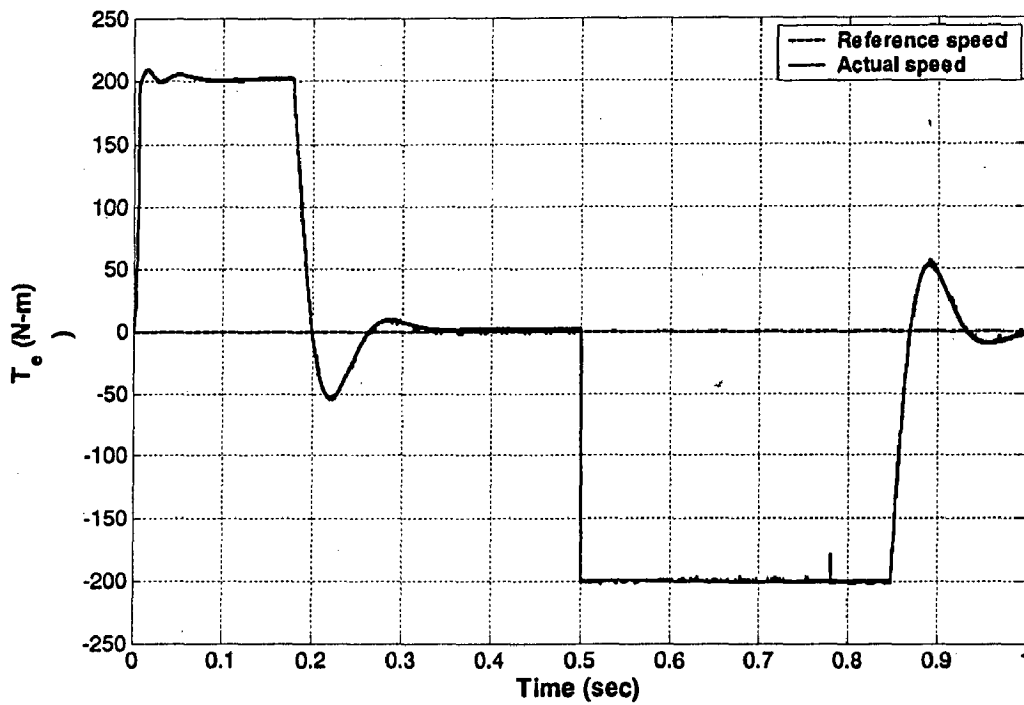


Figure (4.14): Torque response during reverse motoring operation

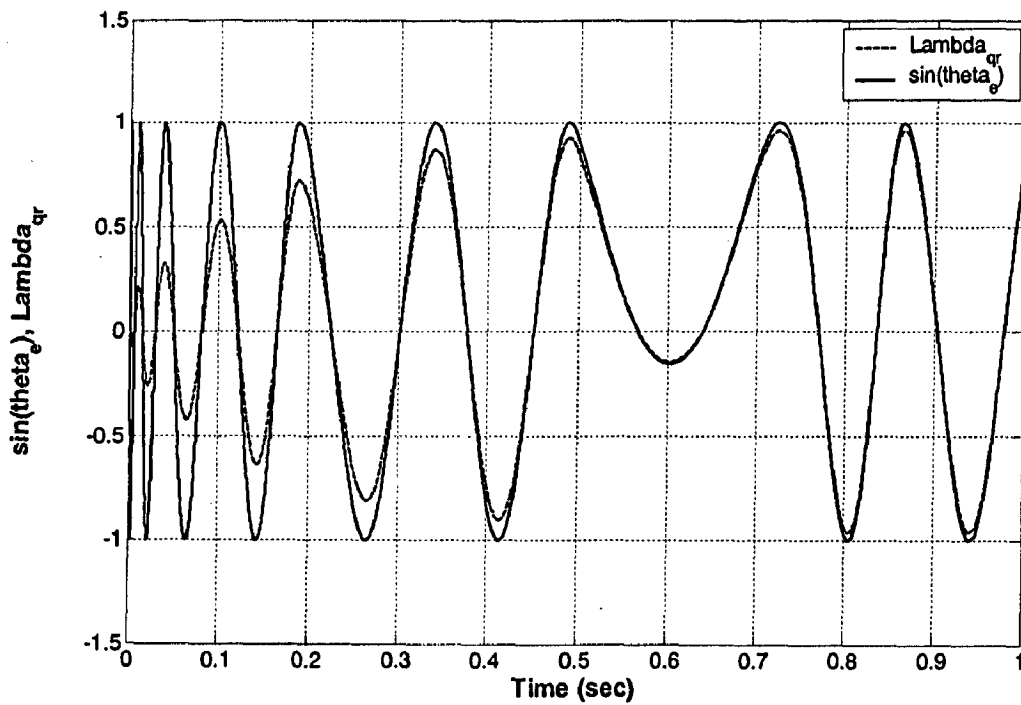


Figure (4.15): Response of unit vector $\sin\theta_e$ and λ_{gr} during reverse motoring operation

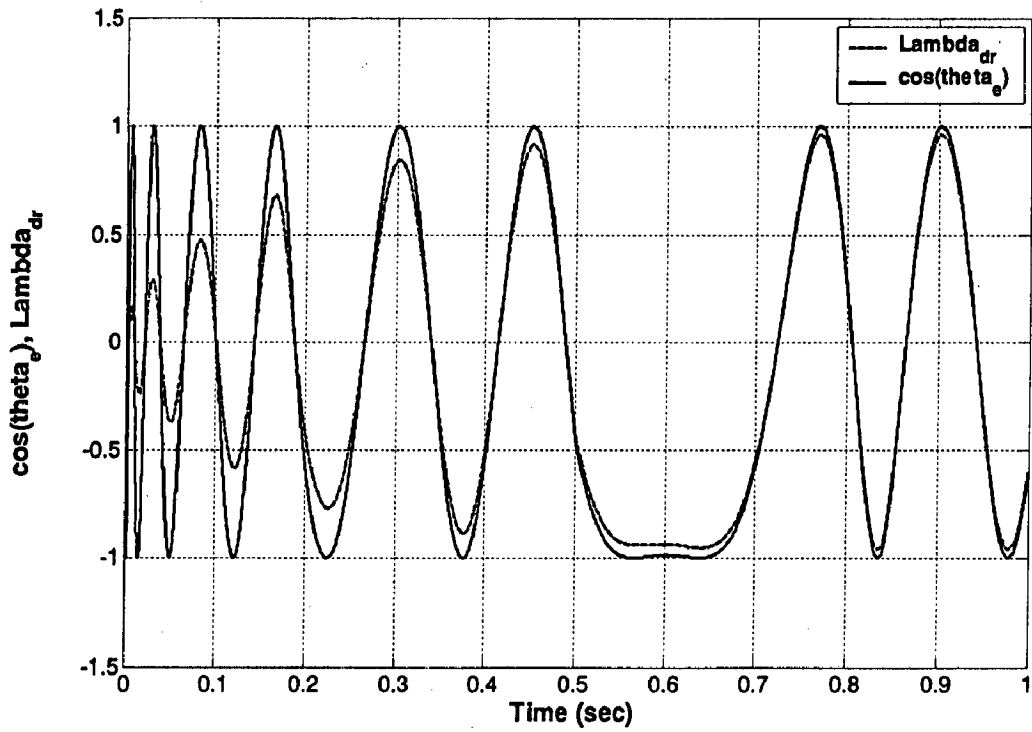


Figure (4.16): Response of unit vector $\cos\theta_e$ and λ_{dr} during reverse motoring operation

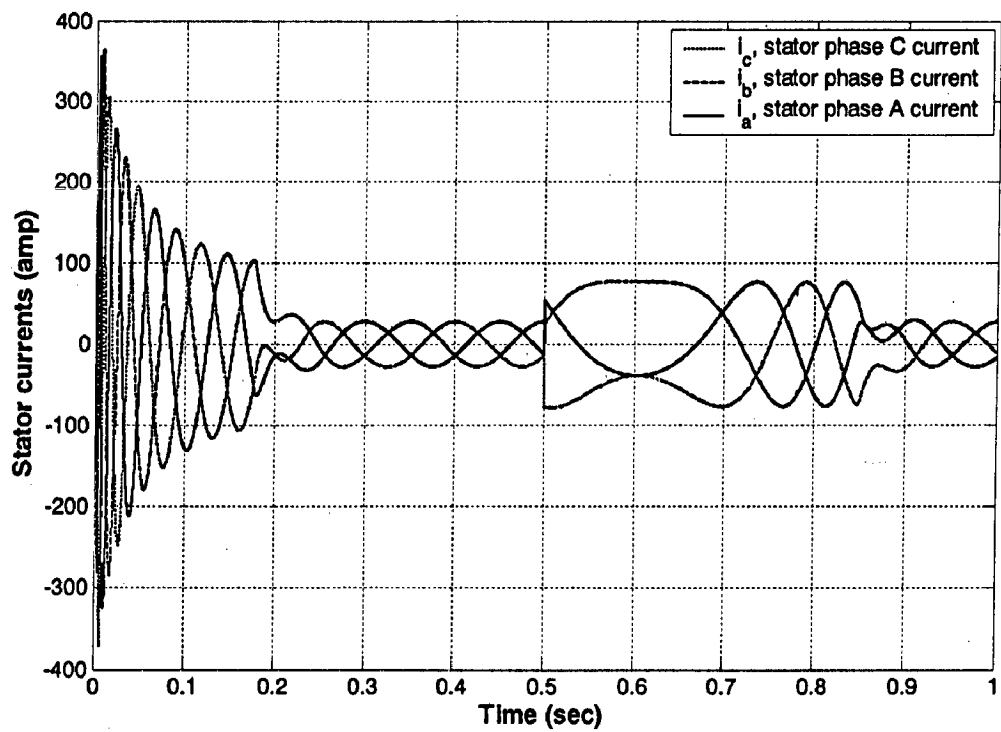


Figure (4.17): Stator phase current response during reverse motoring operation

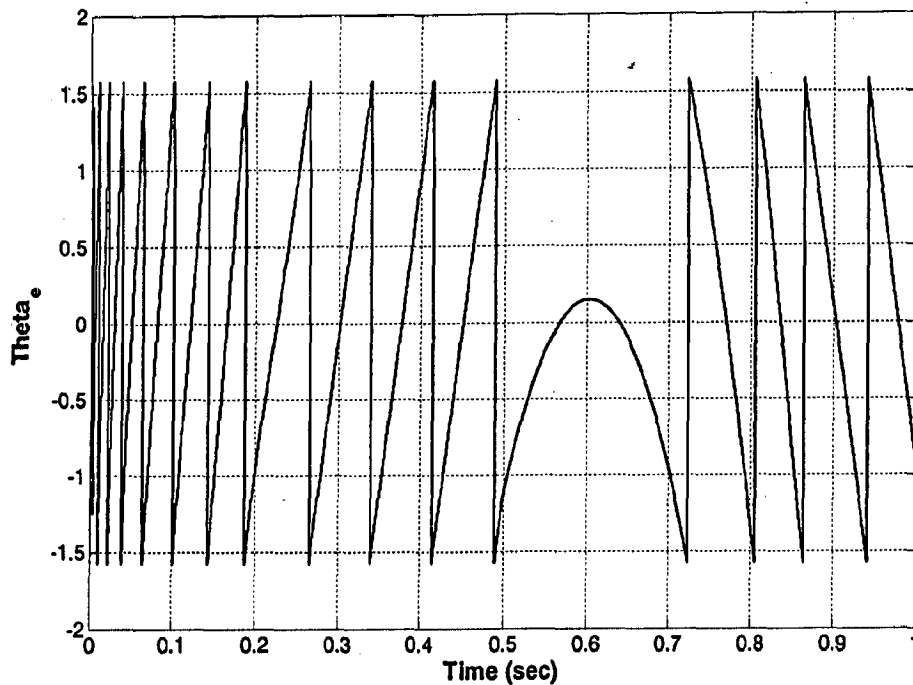


Figure (4.18): Field angle (θ_e) variation during reverse motoring operation

4.6 Response under load condition.

For analysis under load condition, a step speed command of 200 rpm is applied as reference signal. The speed response of the motor is shown in figure (4.19). It clearly shows that drive system is stable and the generated speed signal follows the reference speed signal. There is minimum oscillation and the response is fast. The proportional gain of the speed PI controller is set at 100 and integral gain is set at 5200 to achieve quick and fast transient response. The applied load torque is a pulse signal of magnitude 100 N-m and duration of 0.5 sec. There is slight dip in the speed response when the load torque is applied at 0.2 sec, but again under steady state, rotor speed follows the reference speed signal. This shows that speed of the motor is behaving independent of the torque variation figure (4.19) and (4.20). Torque response of the motor is shown in figure (4.19). When machine accelerates and decelerates, the developed torque goes to rated value of +198 N-m and -198 N-m respectively. The torque response follows closely the applied load torque. With the value of gains in the torque PI

controller, there is little oscillation in the torque response. The band of the torque oscillation is controlled by integral gain of current PI controller. Figure (4.21) and (4.22) shows the correct phase orientation of the unit vectors in the rotor flux direction. The unit vectors controls the behavior of stator dq-currents according to speed and torque variation. Figure (4.23) shows the stator current behavior. Phase sequence of current changes as the machine goes into breaking mode. Figure (4.24) shows the response of system during dynamic load and speed condition.

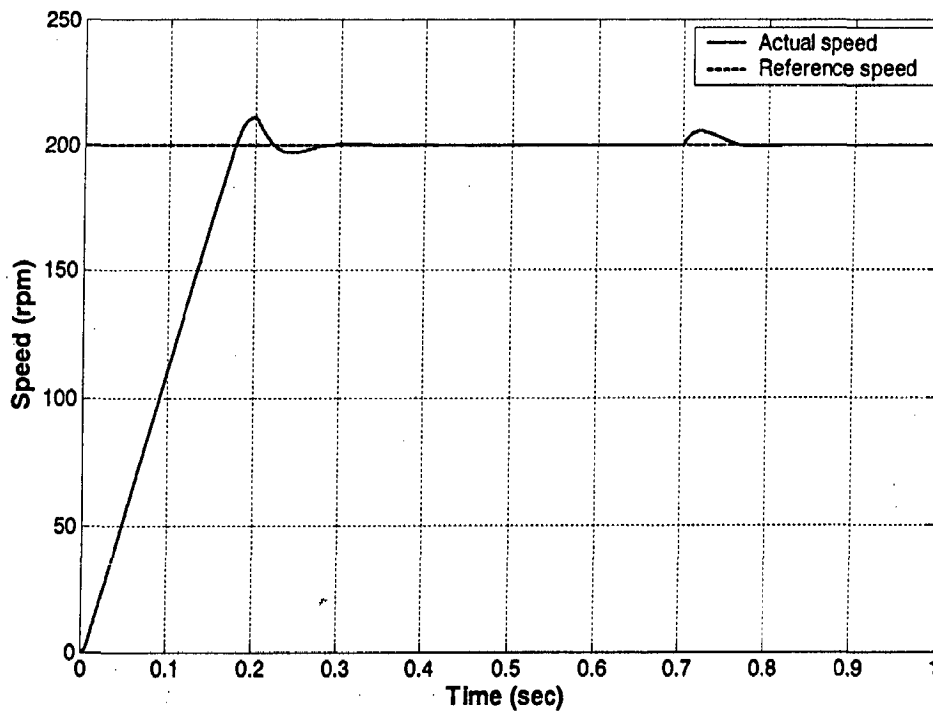


Figure (4.19): Response of rotor speed under load condition

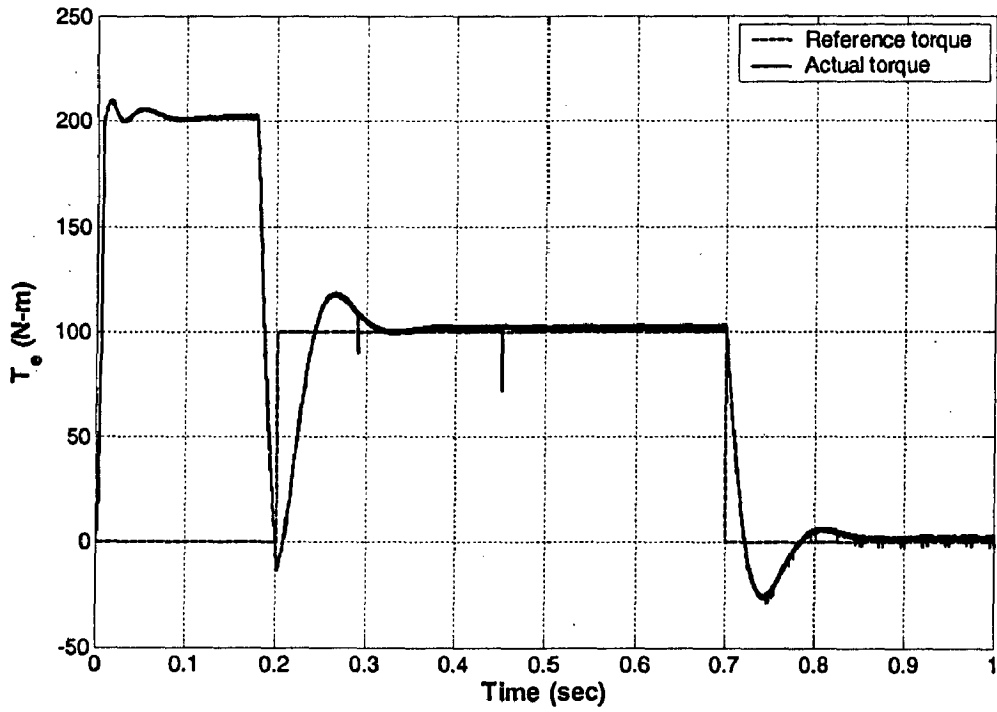


Figure (4.20): Torque response under load torque of 100 N-m

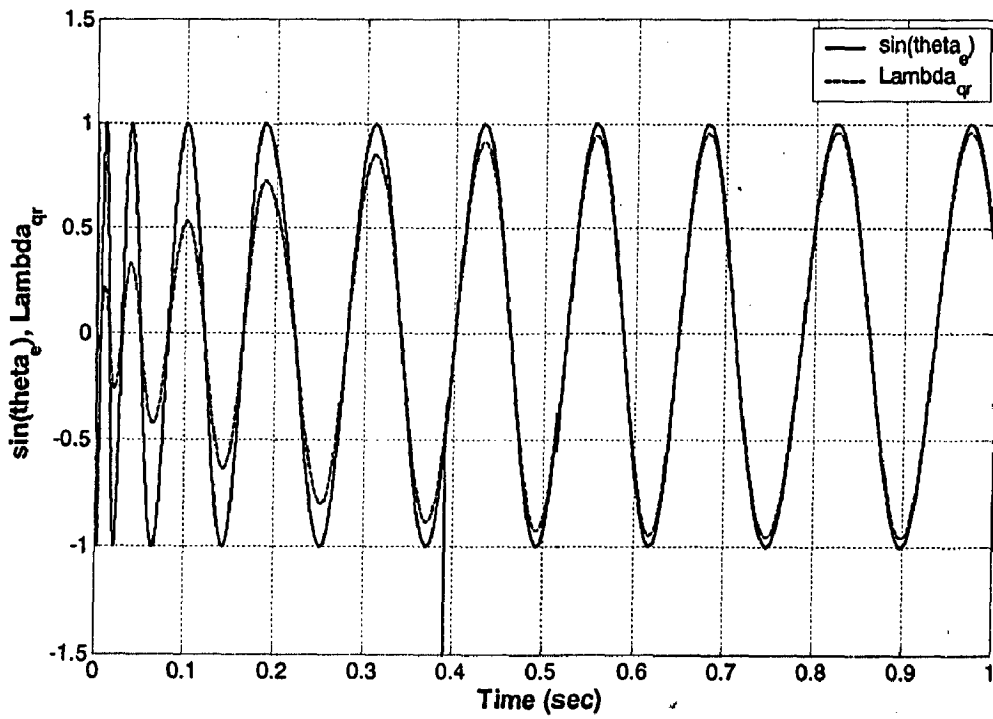


Figure (4.21): Response of $\sin \theta_e$ and λ_{qr}

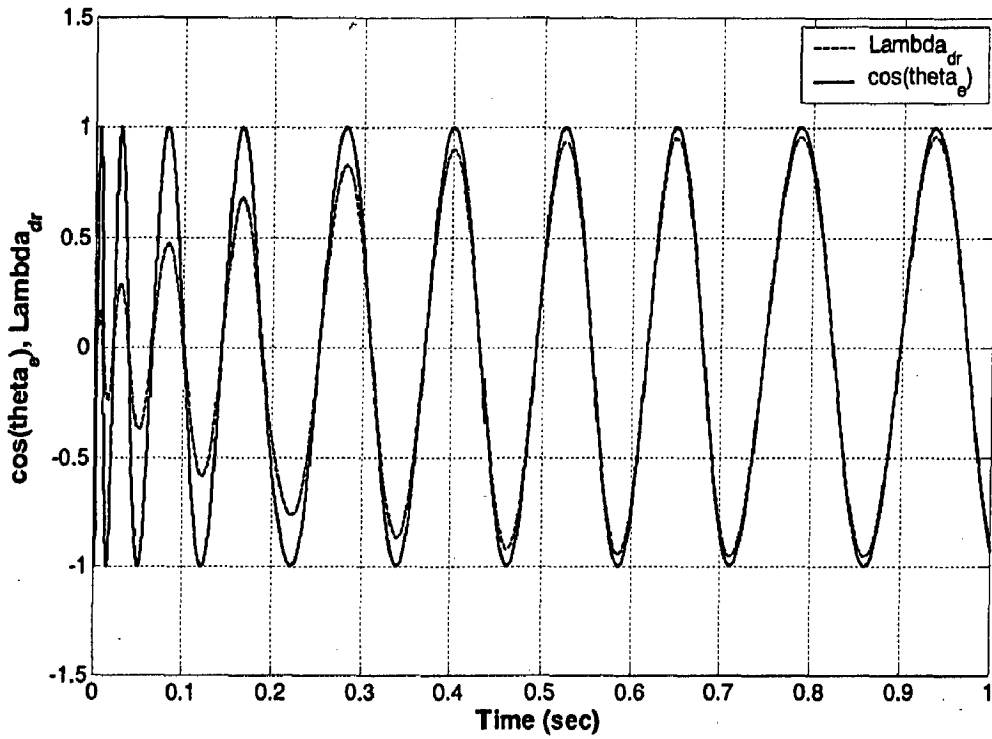


Figure (4.22): Response of $\cos\theta_e$ and λ_{dr}

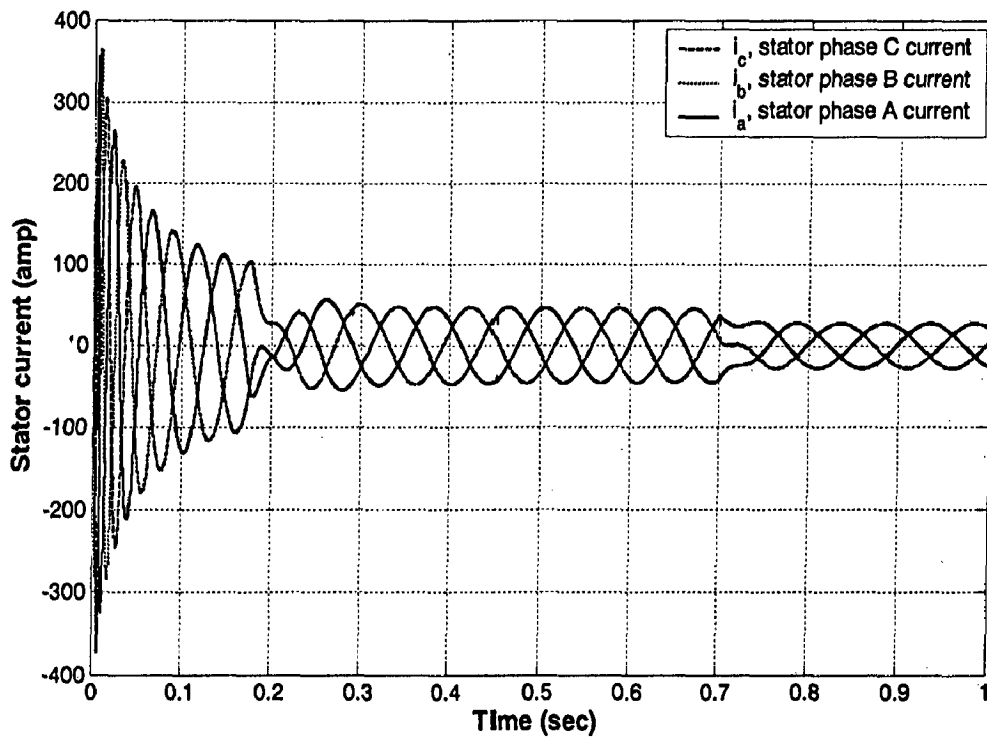


Figure (4.23): Stator phase current response

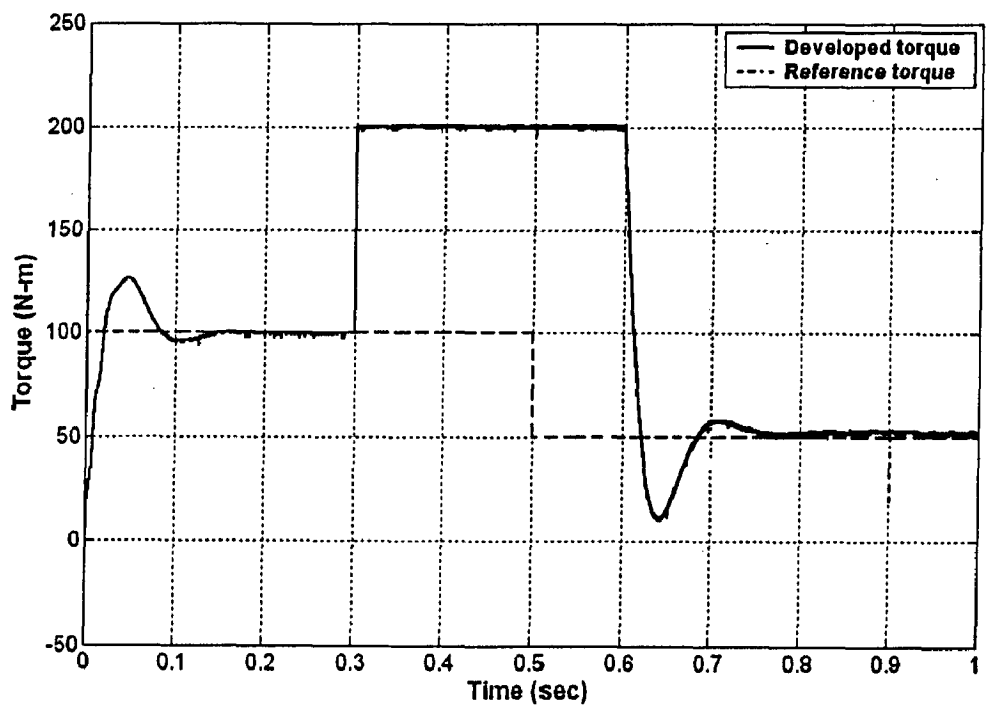
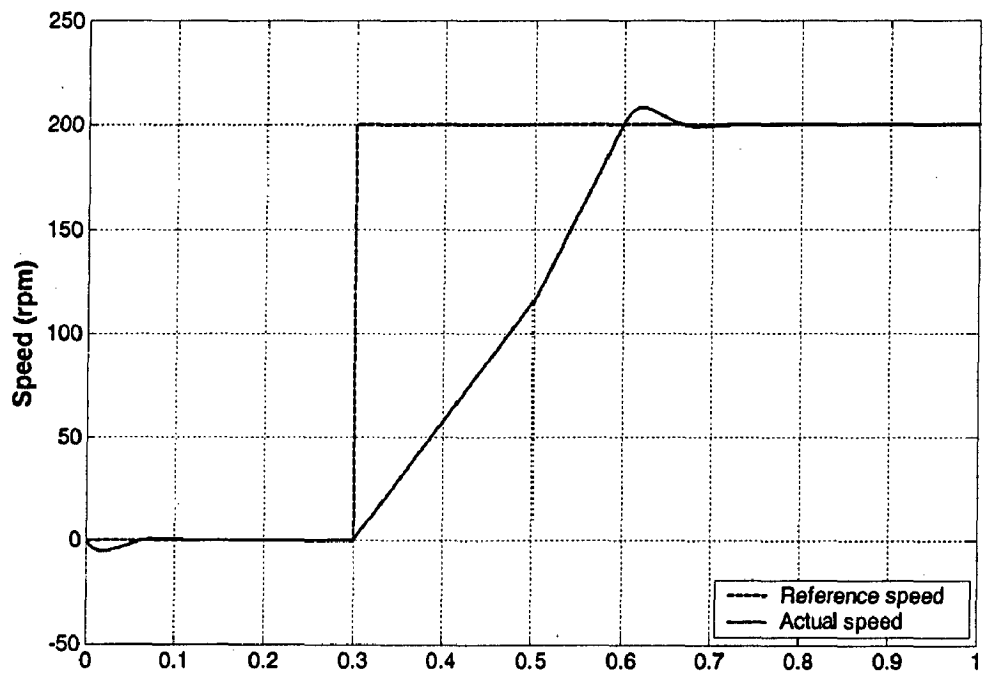


Figure (4.24): Speed and torque response under dynamic load condition
 $\omega_r = 200$ rpm from 0.3 sec to 1.0 sec
 $T_L = 100$ N-m from starting to 0.5 sec and then changes to
 50 N-m at 0.5 sec

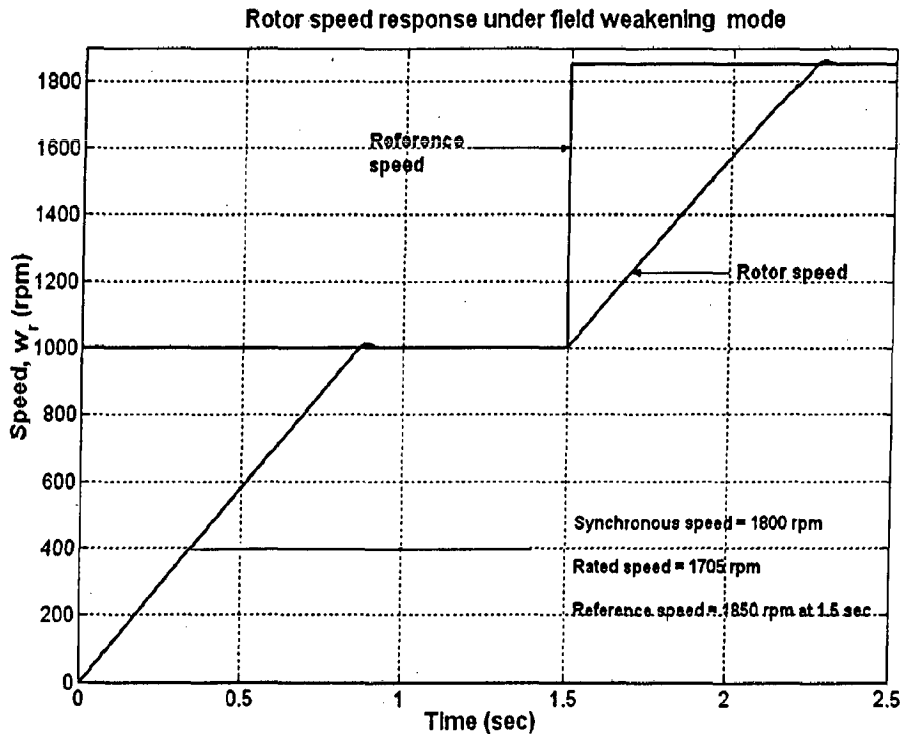
4.7 Response during field weakening mode.

For operation of simple drive system above the rated speed, a simple control strategy is included in the Field weakening block of SIMULINK design. The dynamic equations are:

$$\lambda_{rc} = \lambda_b; \quad 0 \leq \pm\omega_r \leq \pm\omega_{rated} \quad (4.7)$$

$$\lambda_{rc} = \frac{\omega_b}{|\omega_r|} \lambda_b; \quad \pm\omega_b \leq \pm\omega_r \leq \pm\omega_{r(max)} \text{ and } |\omega_r| \geq \omega_b \quad (4.8)$$

For simulation analysis of the drive system in field weakening mode, a step speed command of 1000 rpm which changes to 1850 rpm at 1.5 sec is taken as the reference speed signal. The response shown in the figure (4.25) shows that the system is stable in field weakening mode and speed of the motor follows the reference speed above the rated speed range. Figure (4.26) shows the rotor flux response in the field weakening mode of operation. Base value of the rotor flux is 0.96 Weber. Rotor flux decreases to a lower value as the speed goes above the base speed.



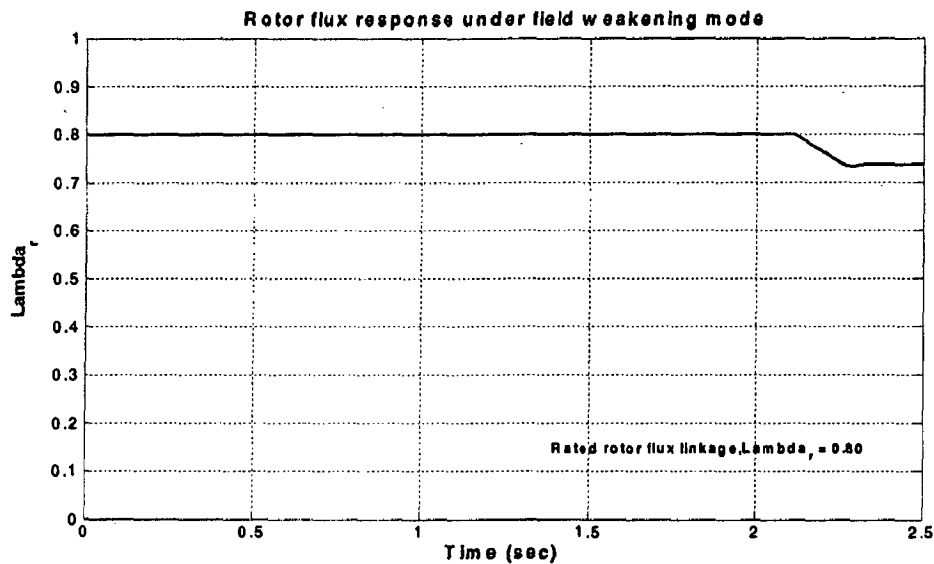


Figure (4.26): Rotor flux (λ_r) response

4.8 Parameter Sensitivity of the Indirect Vector Control Scheme:

A mismatch between the vector controller and induction motor parameter occurs as a result of either of the motor parameter changing with operating conditions such as temperature rise or of the wrong instrumentation of the parameters in the vector controller [5] [11] [12] [13]. The latter phenomenon is controllable, but the former is dependent on the operating conditions of the motor drive and hence is uncontrollable. The mismatch produces a coupling between the flux- and torque- producing channels in the machine

This has the following consequences:

- a) The rotor flux linkage deviates from the commanded value.
- b) The electromagnetic torque, hence, deviates from its commanded value, producing a nonlinear relationship between the actual torque and its commanded value.
- c) During torque transient, an oscillation is caused both in rotor flux linkages and in torque responses, with a settling time constant equal to the rotor time constant.

In torque drive, first two consequences are most undesirable. Although, in speed controlled drive, the nonlinear torque-to-torque command characteristic doesn't have a detrimental effect on the steady- state operation, its effect is considerable during the transients only.

4.8.1 Response of Uncompensated System.

For analysis of the uncompensated system, a step change in rotor circuit resistance is applied at 0.2 sec. In the first case rotor resistance is equal to the value, used in the vector controller block. In the second case it is 1.5 times its actual value and in the third case rotor resistance is 0.5 times its actual value. Responses shown below are for open loop speed control system. From the figure (4.29) and (4.30), it is clear that if the rotor circuit resistance increases then stator dq-axis current lags the current under matched condition. So, the component of q-axis current along d-axis increases the rotor flux, resulting in overfluxing, shown in figure (4.28) and hence the torque increases figure (4.27). But if the rotor circuit resistance decreases then stator dq-axis current leads the current under matched condition as shown in figure (4.29) and (4.30). So, the component of q-axis current along d-axis decreases the rotor flux resulting in underfluxing, shown in figure (4.28) and hence the torque decreases figure (4.27). Figure (4.31) shows the open loop speed response for different values of rotor resistance.

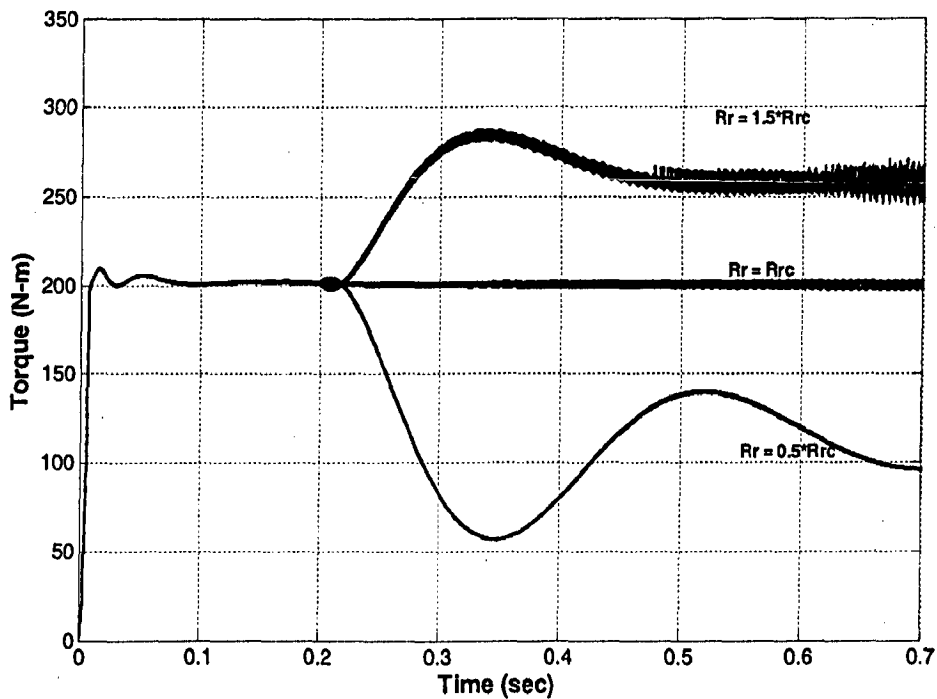


Figure (4.27): Torque response for different values of rotor resistance

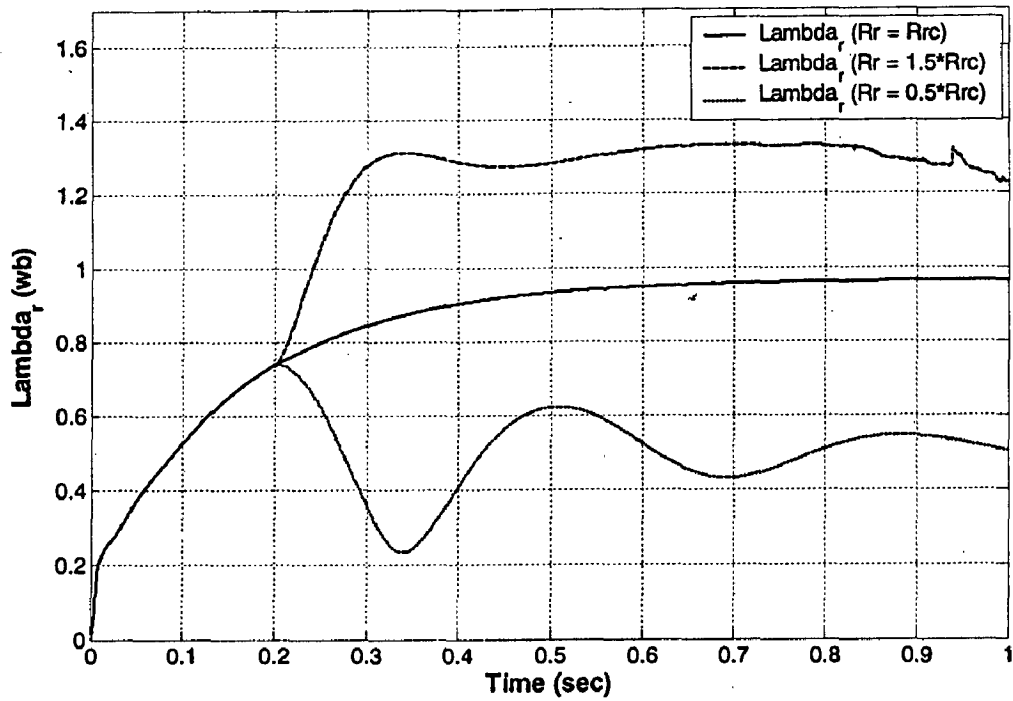


Figure (4.28): Rotor flux response for different values of rotor resistance

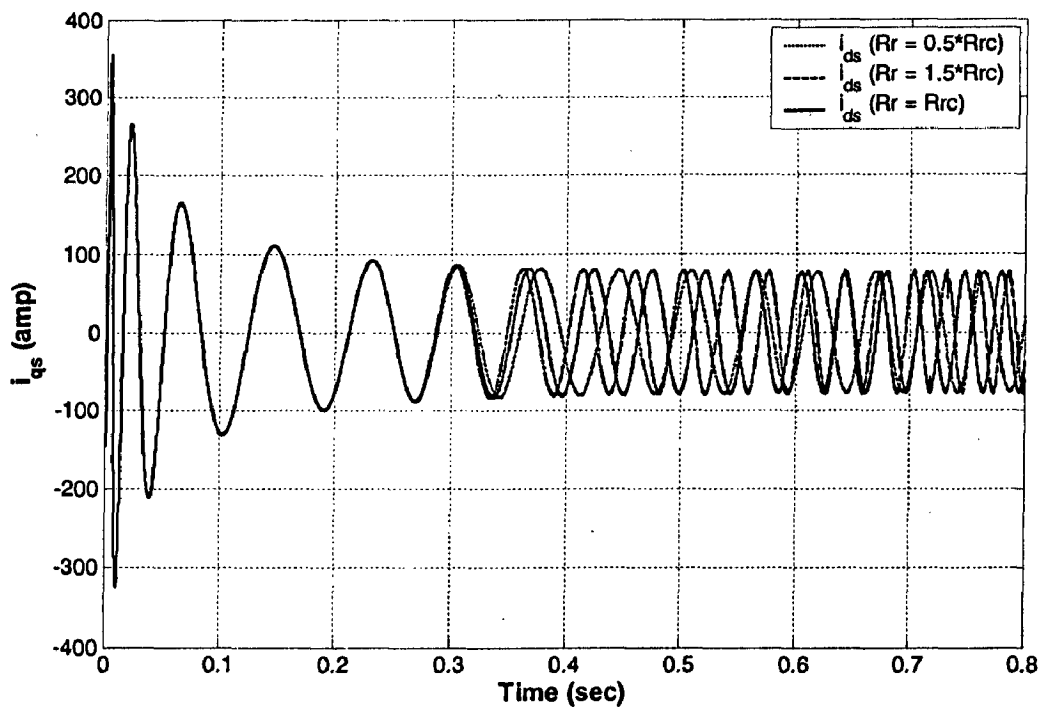


Figure (4.29): Stator q-axis current response

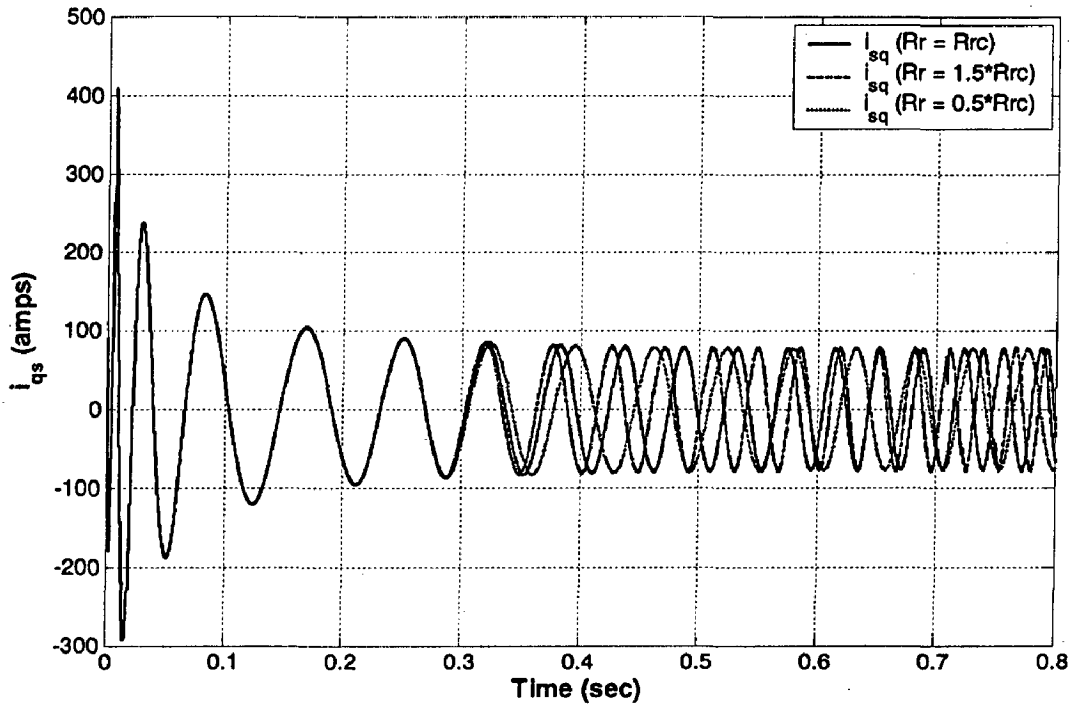


Figure (4.30): Stator d-axis current response

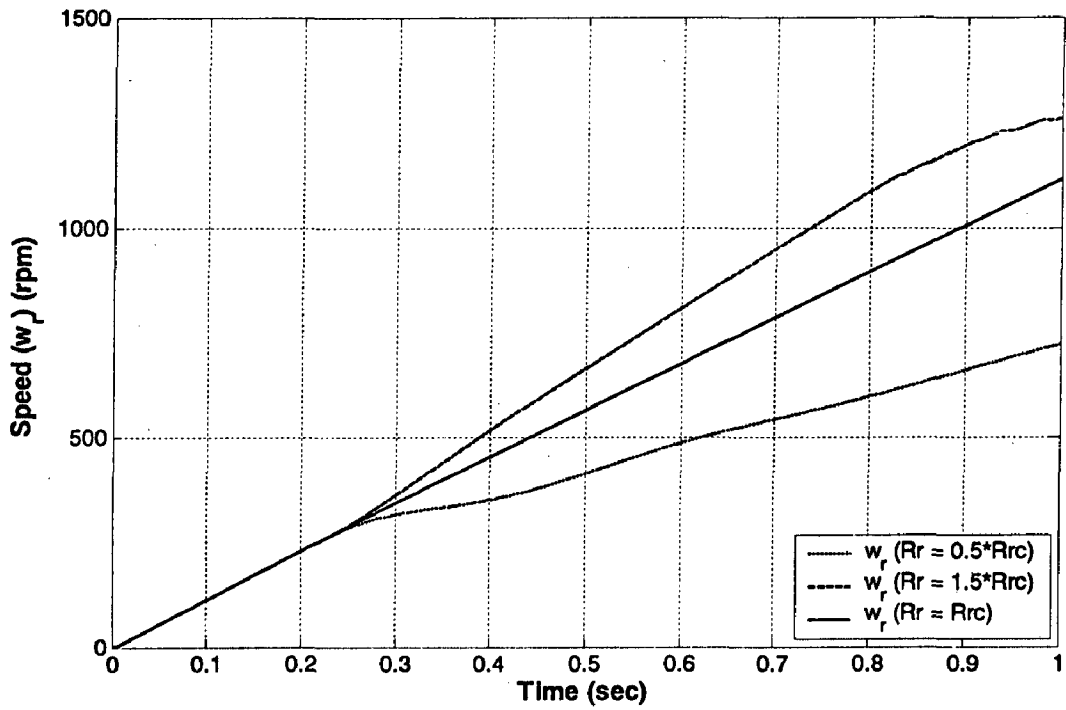


Figure (4.31): Speed response

4.9 Parameter Sensitivity Compensation.

The effects of mismatch of parameters between the induction motor and vector controller can be minimized by adapting the parameters in the vector controller to the actual machine parameters, at all times. This is called the tuning of vector controller.

4.9.1 Slip gain tuning based on MRAC:

Slip frequency in vector control scheme is given as:

$$\omega_{sl} = \frac{L_m R_r}{L_r \lambda_r} i_{qs} \quad (4.9)$$

$$\text{or, } \omega_{sl} = K_s i_{qs} \quad (4.10)$$

$$\text{Where slip gain, } K_s = \frac{L_m R_r}{L_r \lambda_r}$$

With the closed loop flux control, the estimated value of λ_r (input to K_s is known), therefore, variation of three parameters (L_m, L_r , and R_r), is of concern. The saturation effect of magnetizing inductance L_m almost cancels the variation of $\frac{L_m}{L_r}$, thus leaving the dominating effect of rotor resistance variation on K_s .

For tuning of vector controlled drive, Slip gain model reference adaptive control (MRAC) method is used [1]. Here, the reference model output signal X^* that satisfies the tuned vector control is a function of command currents i_{ds}^* and i_{qs}^* machine inductance and operating frequency. The adaptive model X is estimated by the machine feedback voltages and currents as shown in figure (4.32). The reference model output is compared with that of the adaptive model and the resulting error generates the estimated slip gain K_s through a PI compensator. Thus, slip gain tuning occurs when X matches with X^* . The MRAC used, is based on torque model [12] [13]. The K_s parameter is tuned such that $T_e = T_e^*$ at all operating conditions. The reference model output is given as

$$X^* = T_e^* = \frac{3}{2} \left(\frac{p}{2} \right) \frac{L_m^2}{L_r} i_{ds}^* i_{qs}^* \quad (4.11)$$

The actual torque is estimated from motor stationary frame variables as follows:

$$X = T_e = \frac{3}{2} \left(\frac{p}{2} \right) (\lambda_{ds}^s i_{qs}^s - \lambda_{qs}^s i_{ds}^s) \quad (4.12)$$

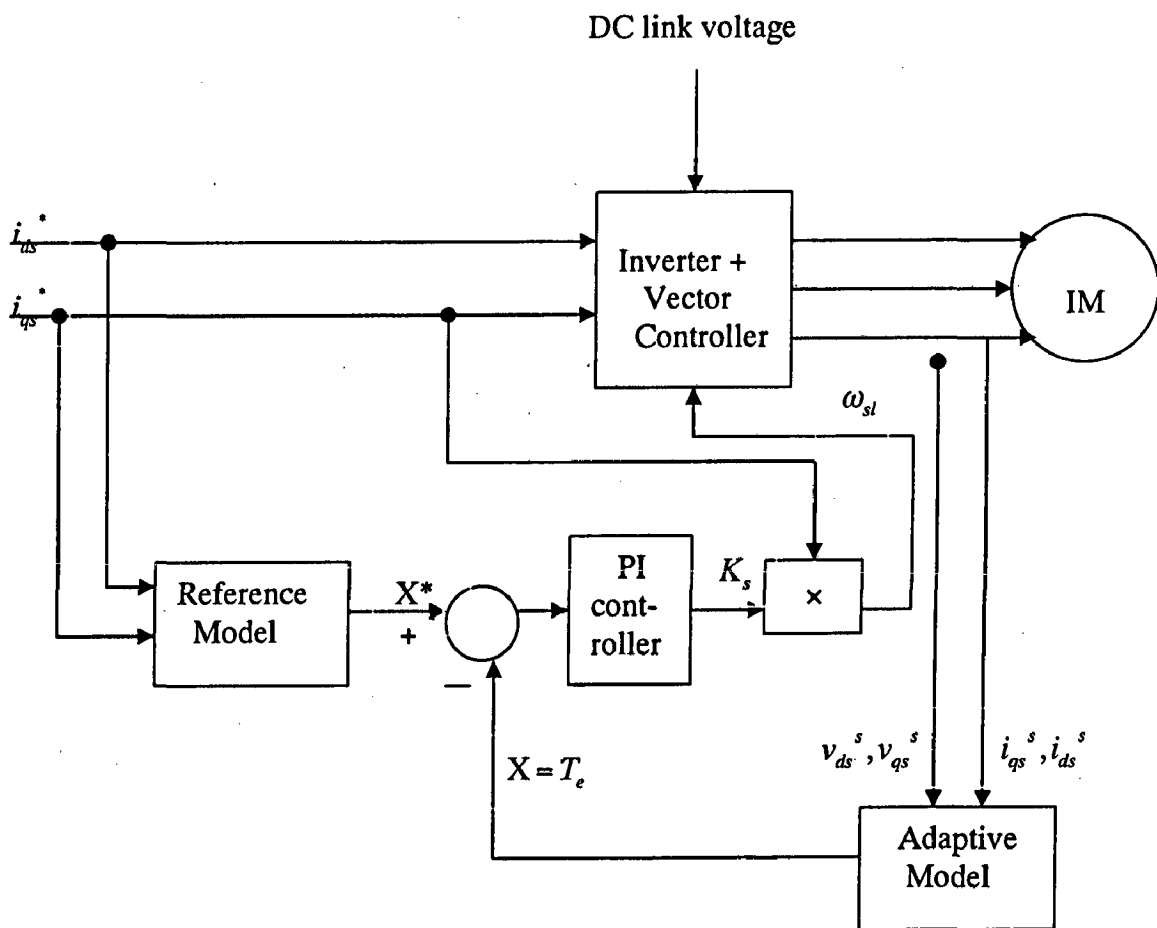


Figure (4.32): Slip gain tuning by model reference adaptive control principle

4.9.2 Response of compensated system.

For simulation of compensated system, a step change in resistance at 0.2 sec is applied. From 0.0 sec to 0.2 sec system runs under parameter matched condition and from 0.2 sec to 0.5 sec, it operates under mismatched condition (i.e. different rotor resistance condition). At 0.5 sec parameter compensation is applied. From figure (4.28), it is clear that during uncompensated mode operation, rotor flux increases or decreases if the rotor resistance is greater or less than the actual value, respectively. When system is compensated, rotor flux gains its original value of 0.96 Weber and torque reaches to its rated value until machine achieves its no load speed. These responses are shown in figures from (4.33) to (4.38) are for open loop speed control system.

From 0.0 to 0.2 sec: Parameter matched operation.

From 0.2 sec to 0.5 sec: Parameter mismatched and uncompensated operation.

From 0.5 sec to 1.8 sec: Parameter mismatched and compensated operation.

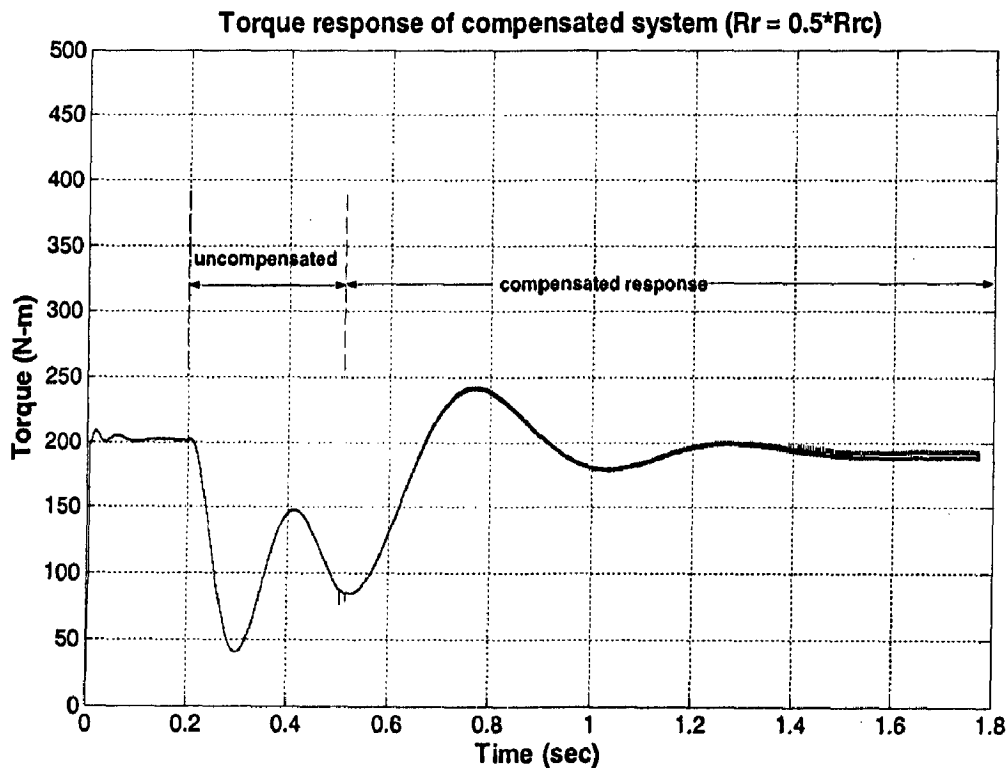


Figure (4.33): Torque response ($R_r = 0.5 * R_{rc}$)

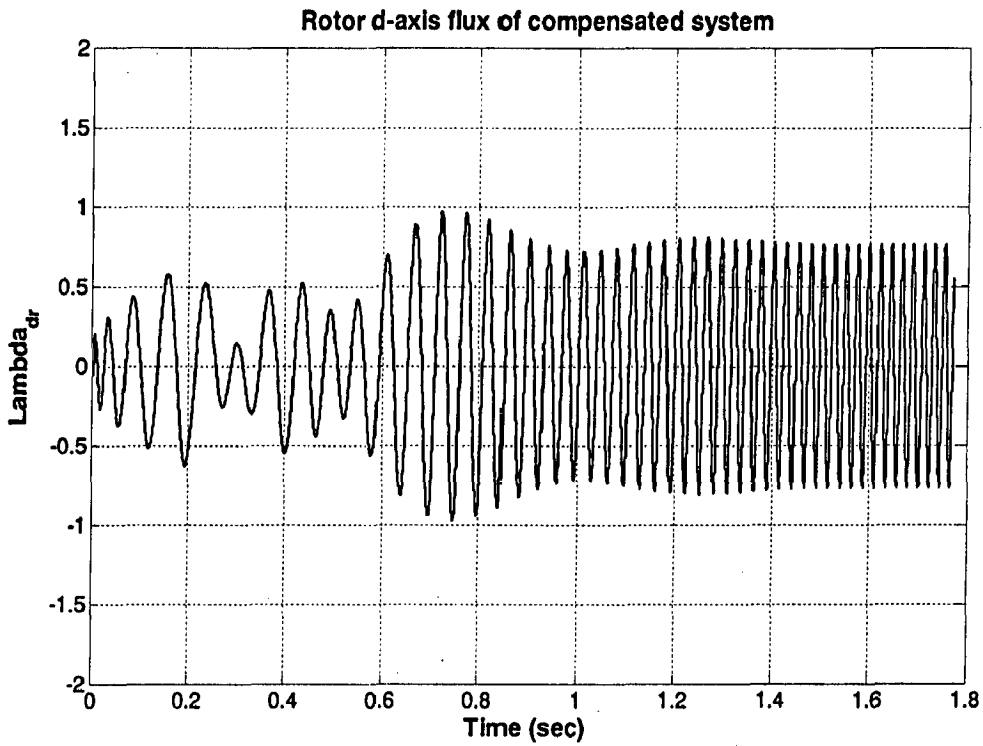


Figure (4.34): Rotor d-axis flux response ($R_r = 0.5 * R_{rc}$)

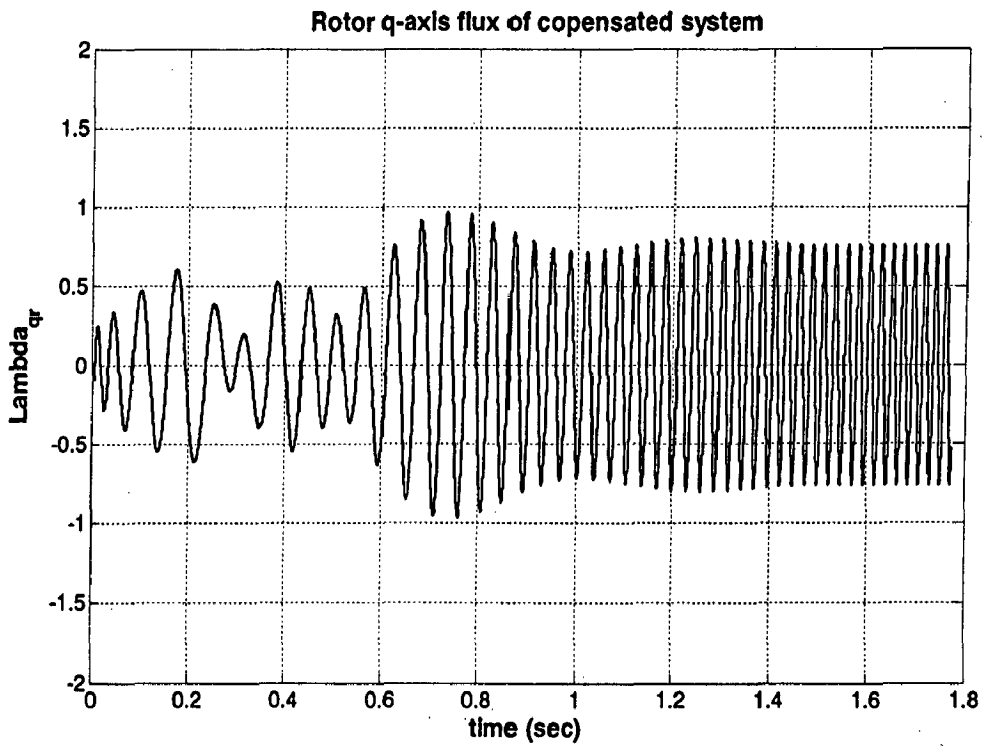


Figure (4.35): Rotor q-axis flux response ($R_r = 0.5 * R_{rc}$)

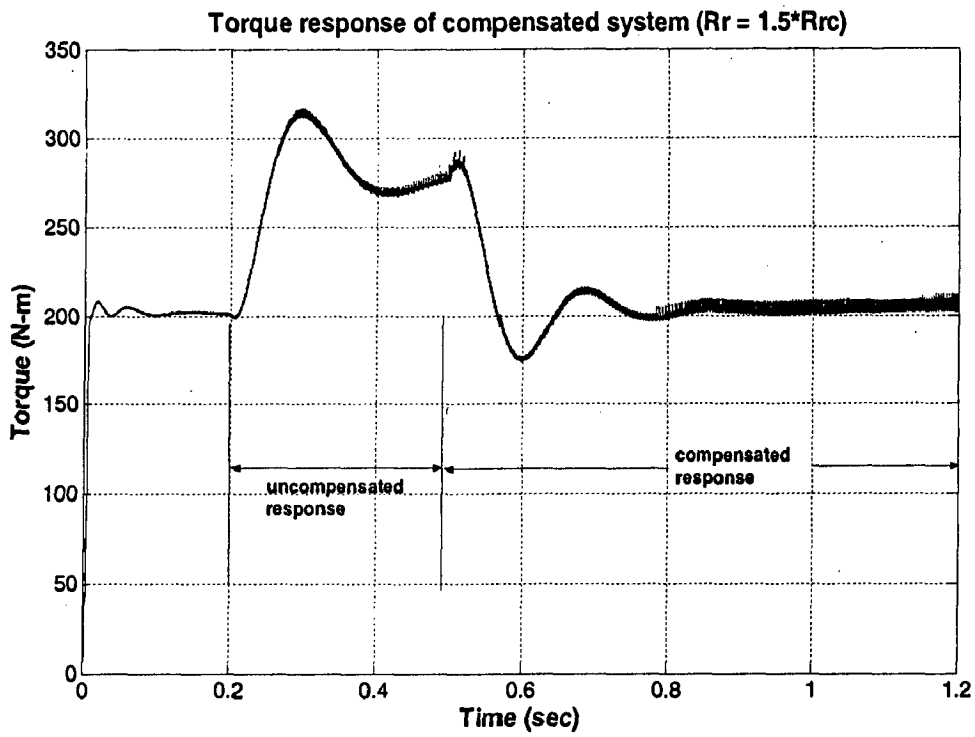


Figure (4.36): Torque response ($R_r = 1.5 \cdot R_{rc}$)

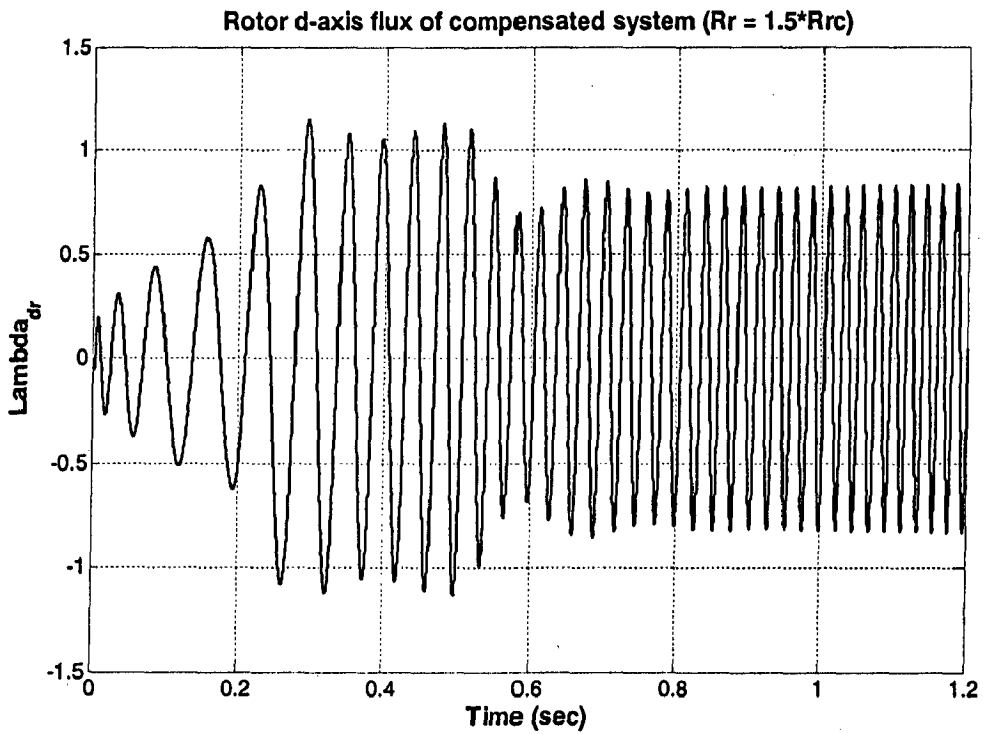


Figure (4.37): Rotor d-axis flux response ($R_r = 1.5 \cdot R_{rc}$)

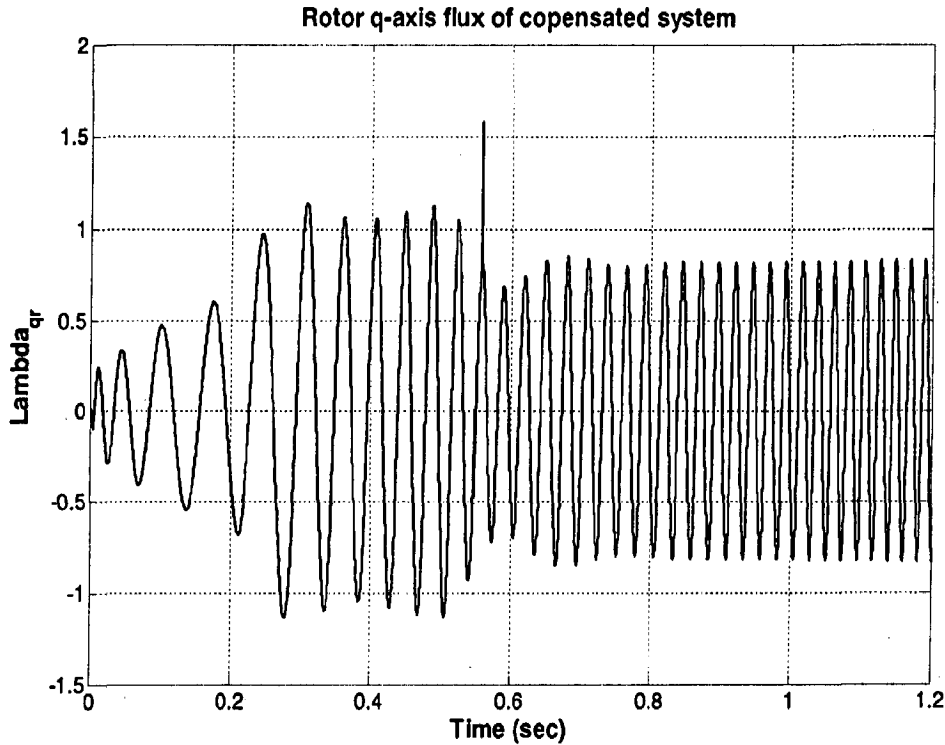


Figure (4.38): Rotor q-axis flux response ($R_r = 1.5 * R_{rc}$)

4.10 Parameter sensitivity effect on closed loop speed control system.

The closure of outer speed loop ensures that the electromagnetic torque command T^* is modified until the actual output torque (T_e) is equal to the load torque (T_L) in steady state, regardless of the parameter variations in the induction motor. For behavior analysis in closed loop system during parameter mismatched condition, simulation is carried out for three different values of actual rotor resistance. In the first case rotor resistance is equal to the actual value and then in second and third case, it is changed to 150% and 50% of the actual value. The major variables considered for study are the actual torque, actual rotor flux linkage, stator flux and speed. Figure (4.39) shows the speed response for three different values of rotor resistance. It shows that as the rotor resistance is decreased, speed response becomes sluggish and takes more time to reach the steady state. Under steady state all the three speed responses follows the reference speed signal irrespective of the values of rotor resistance.

Simulation input parameters:

$$\omega_{ref} = 200 \text{ rpm}$$

$$T_e = 50 \text{ N-m}$$

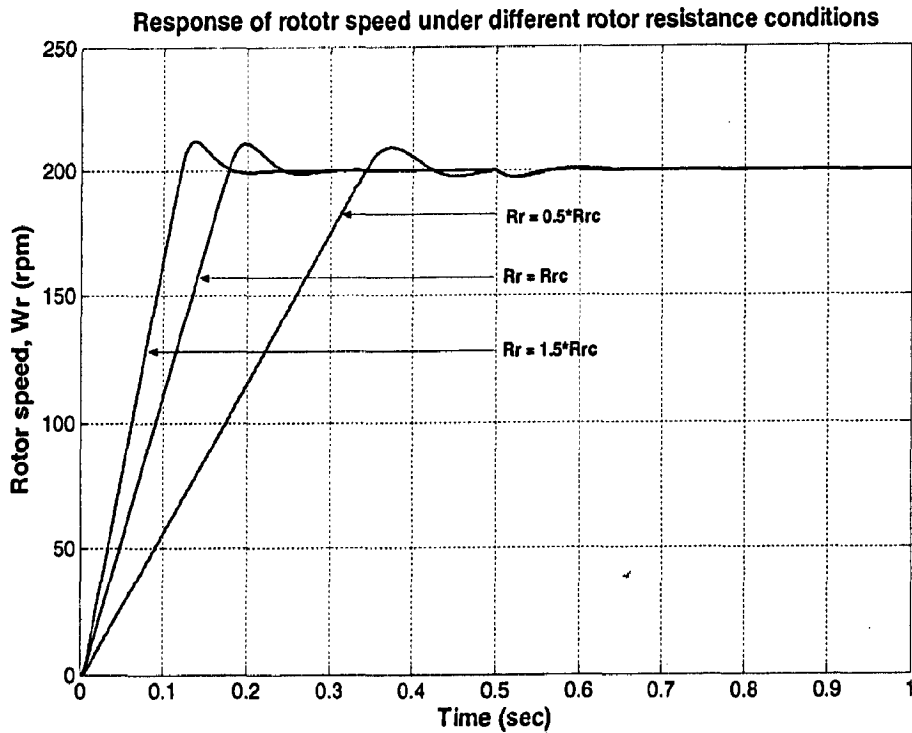


Figure (4.39): Speed response for different values of rotor resistance

Motor developed electromagnetic torque response for different values of rotor resistances is shown in figure (4.40). From this figure, it is clear that, if the rotor resistance is increased, then the starting torque and torque oscillation of the motor increases. But in steady state, generated electromagnetic torque follows the load torque, irrespective of the parameter mismatch. Figure (4.41) shows the response of commanded torque for different values of rotor resistance. This figure shows the modification of commanded torque which makes the electromagnetic torque to follow the load torque.

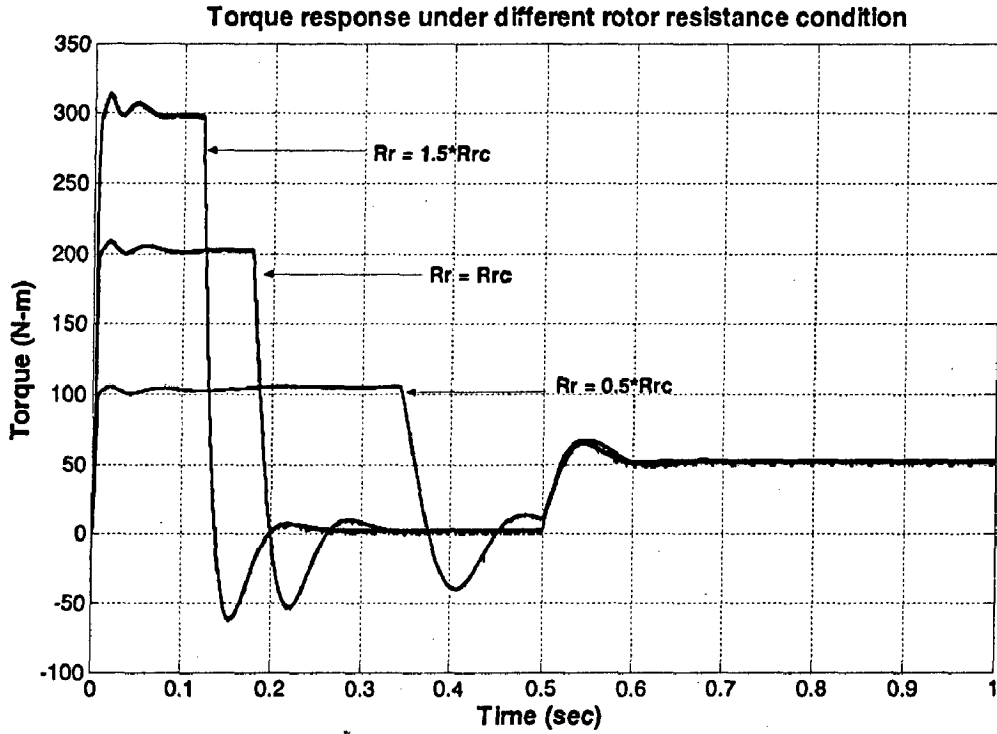


Figure (4.40): Torque response for different values of rotor resistance

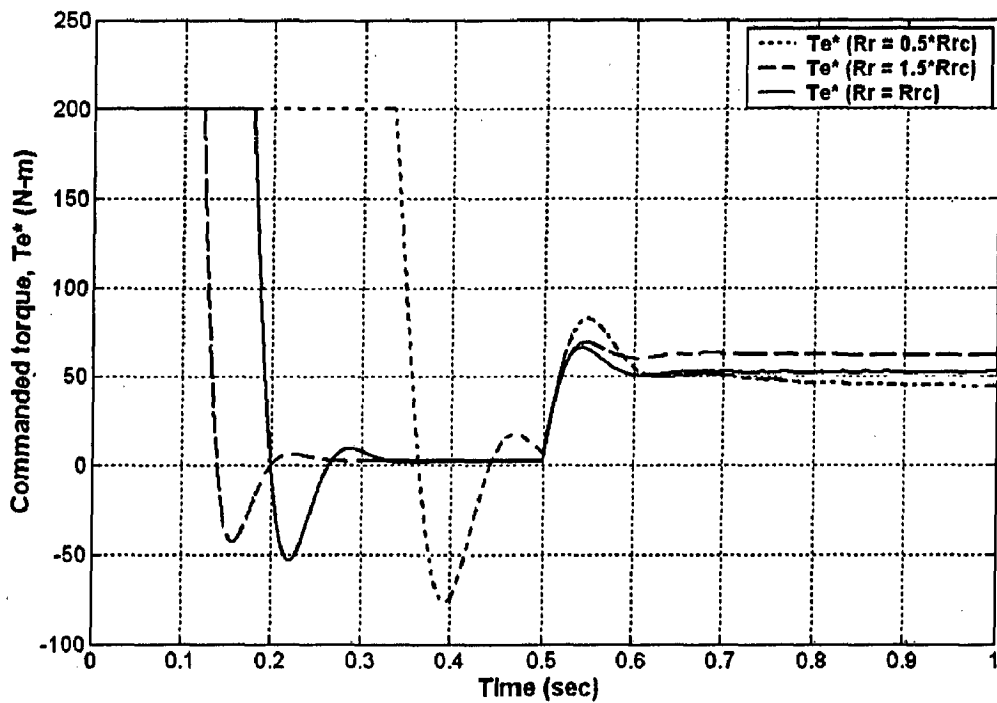


Figure (4.41): Commanded Torque response for different values of rotor resistance

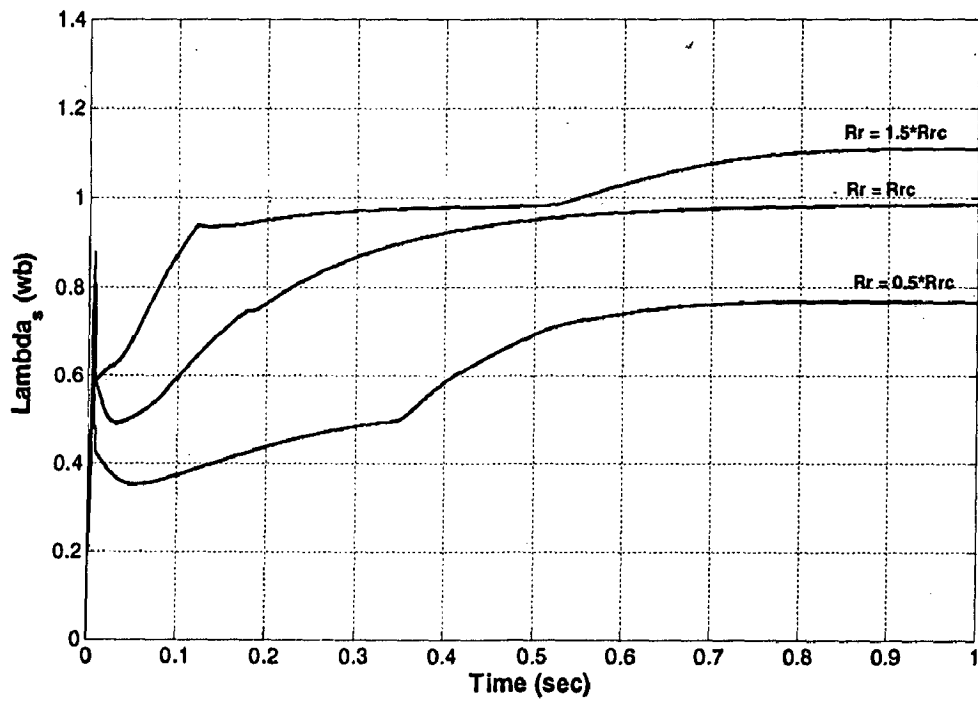


Figure (4.42): Stator flux response for different values of rotor resistance

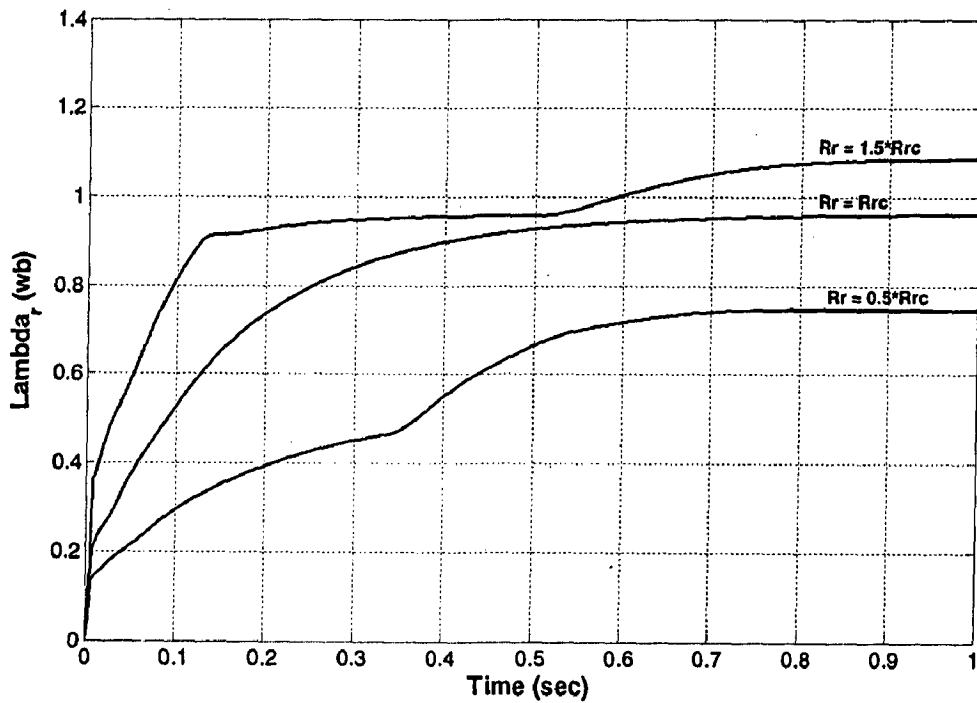


Figure (4.43): Rotor flux response for different values of rotor resistance

Response of stator and rotor flux response for different values of rotor resistance is shown in figure (4.42) and (4.43). It shows that if the rotor resistance is increased then stator and rotor flux also increases.

4.11 Interim conclusions:

In indirect vector control method, the rotor flux position θ_r , relative to the stationary reference frame, has been determined from rotor position θ , added to the relative position θ_{sl} between the rotor flux vector λ_r and the rotor position. The rotor position θ , has been calculated by integration of rotor speed whereas θ_{sl} is determined by integration of slip frequency. Figure (4.29) and (4.30), it has been observed that when a load torque of 50 N-m was applied in a step fashion at speed of 200 rpm, the change in speed was not very much noticeable. It was in a way expected from a proper vector control. Figure (4.24) that shows the stable dynamic performance of drive when it was started at a load of 100 N-m with zero speed. This figure also shows that during acceleration, the actual speed changes linearly, indicating that the torque of induction motor responded in a step fashion from 100 N-m to the rated torque of 198 N-m. Drive system operates successfully in four quadrants indicating motoring and braking conditions. From the 3rd and 4th chapter it is clear that the orthogonal vectors i_{qs} and λ_r of the induction motor correspond respectively to the armature current and excitation flux of the DC motor.

CHAPTER 5

HYBRID VECTOR CONTROL

5.1 Introduction.

In the previous chapters, different vector control schemes have been modeled and analyzed. Between the two methods of vector control, i.e. the direct and indirect methods, the former doesn't need speed signal if the closed loop speed control is not required and the machine doesn't operate typically below 5% of the base speed. The flux and the corresponding unit vector signals in this case can be easily estimated from the machine terminal voltages and currents by solving the stator voltage equations. As the speed approaches zero, the stator frequency (also voltage) becomes very small which is very difficult to integrate because of the DC offset problem. The indirect vector control (IVC), on the other hand, is dependent on the speed signal in the whole speed range and suffers parameter variation problems.

Here a vector-controlled drive is simulated that starts at zero speed, and run at any speed. The drive control system uses DVC mode with rotor flux orientation in whole speed range. However the control uses IVC mode for start-up at zero speed and shut down. Figure (5.1) shows the IVC – DVC transition control diagram.

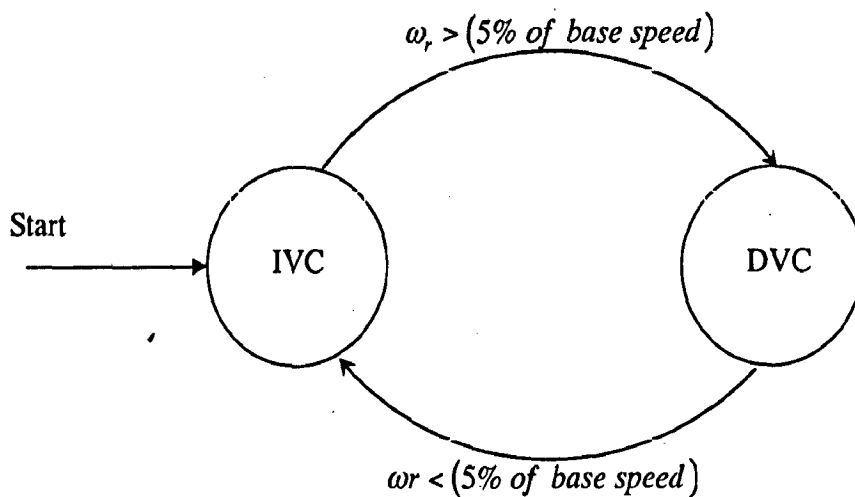


Figure (5.1): IVC – DVC transition control diagram

The drive uses synchronous current control where the polar unit vector signal ($\cos \theta_e$ and $\sin \theta_e$) is supplied from IVC mode at start-up operation, and as the speed begins to develop, the signal is switched to DVC mode. Again, as the speed approaches zero, the drive is switched back to IVC mode.

5.2 Simulation results.

The drive system with the proposed control strategy is simulated with MATLAB/SIMULINK. The space phasor model of the induction motor has been used for simulation purposes using the nominal parameters as given in Appendix (1). The complete simulink diagram has shown in figure (5.2). A switching technique has been used that makes the control strategy to operate in between IVC and DVC. Switch makes the transition at 5% of base speed i.e. when speed increases above 5% of base speed, during acceleration, control transits to DVC mode. Similarly during deceleration, when speed goes below 5% of base speed, the drive goes into IVC mode. The high level of switch signal indicates the IVC mode and low level indicates the DVC mode. Amplification level of the switching signal has changed for some time for visibility in graph plotting.

There are two command inputs to the drive, reference speed, ω_{ref} and load torque, T_L . For speed simulation a bipolar step speed command of ± 150 rpm is set as reference signal. Polarity of speed changes at 0.3 sec. Figure (5.3) shows the transition signal response that makes the drive operation either in IVC mode or in DVC mode. A step load torque of 50 N-m is applied at 0.5 sec.

Figure (5.4) shows the stable speed response of motor. The base speed of the chosen motor is 1705 rpm, so as the speed reaches to 5% of base speed (i.e. 85 rpm) at the starting, the switch changes the operating mode from IVC to DVC. Similarly when speed approaches to zero, i.e. during deceleration, mode changes to IVC. In all other steady state speed range, drive operates in DVC mode.

Figure (5.5) shows the torque response of the drive system. Developed torque closely follows the load torque with minimum ripple. Only during acceleration and deceleration, developed torque is at the base torque of ± 198 N-m. Figure (5.6) and figure (5.7) shows the behavior of unit vectors. From figure (5.6), (5.7) and (5.8) that shows the rotor dq- flux response, it is clear that the unit vectors are in correct phase alignment with the dq- flux, leading to vector decoupled control.

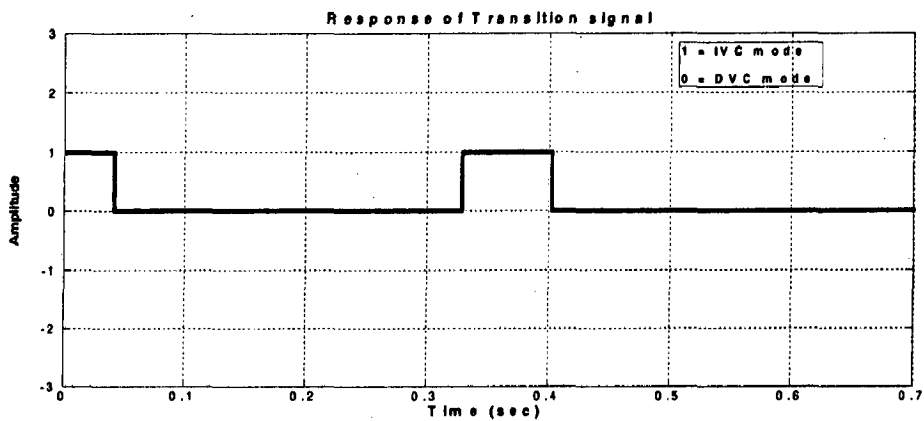


Figure (5.3): Response of Transition signal

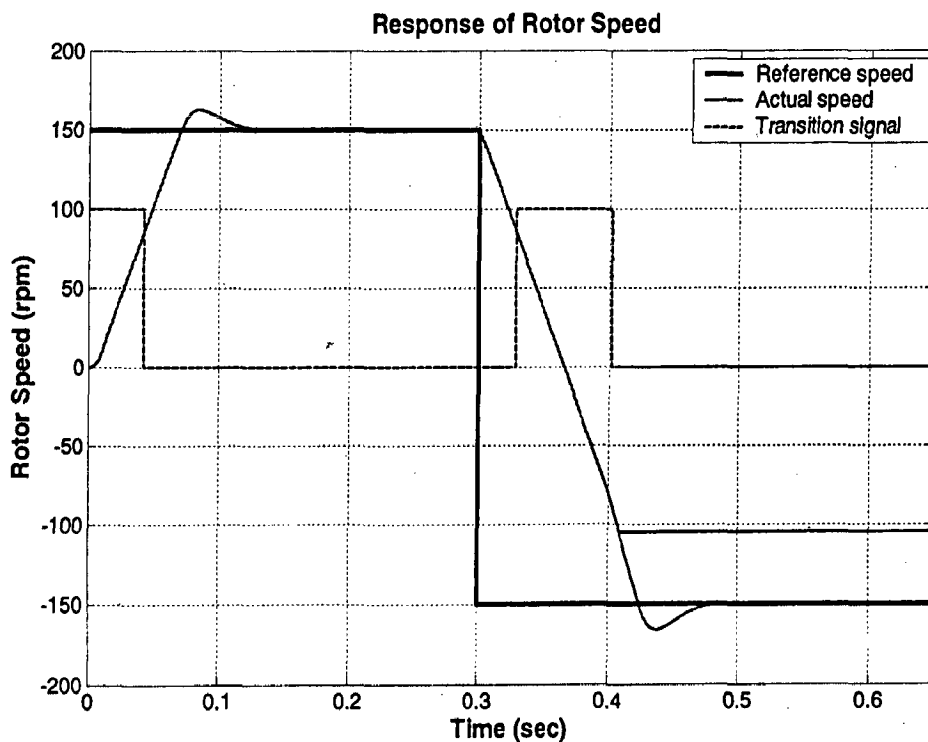


Figure (5.4): Speed response

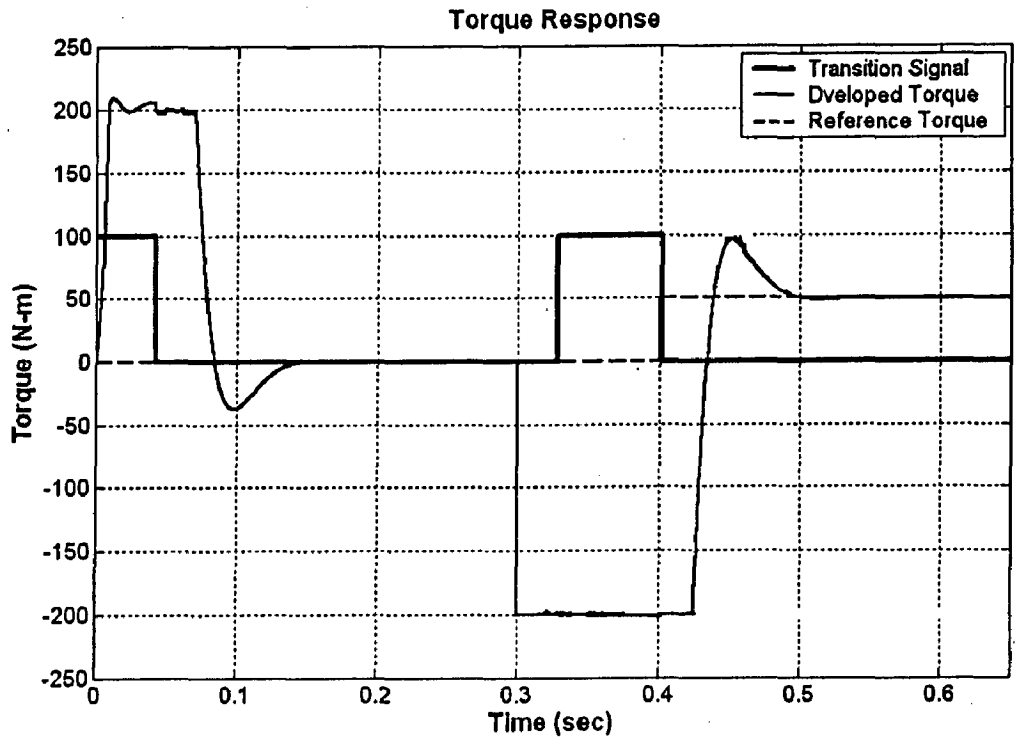


Figure (5.5): Torque response

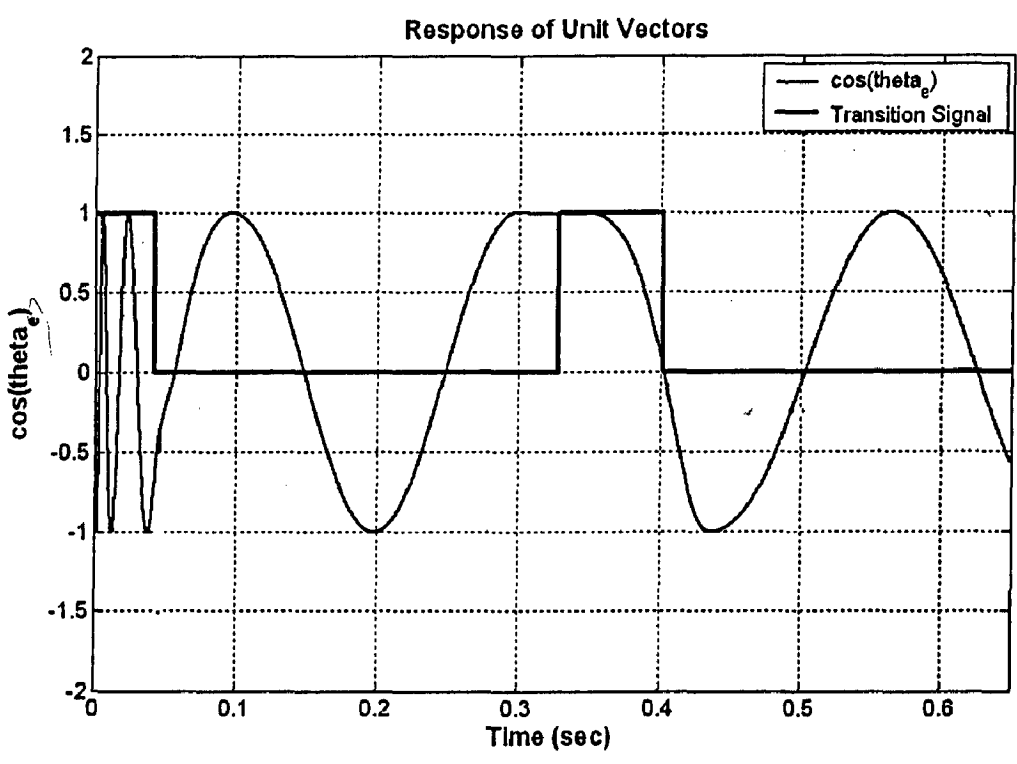


Figure (5.6): Response of $\cos\theta_e$

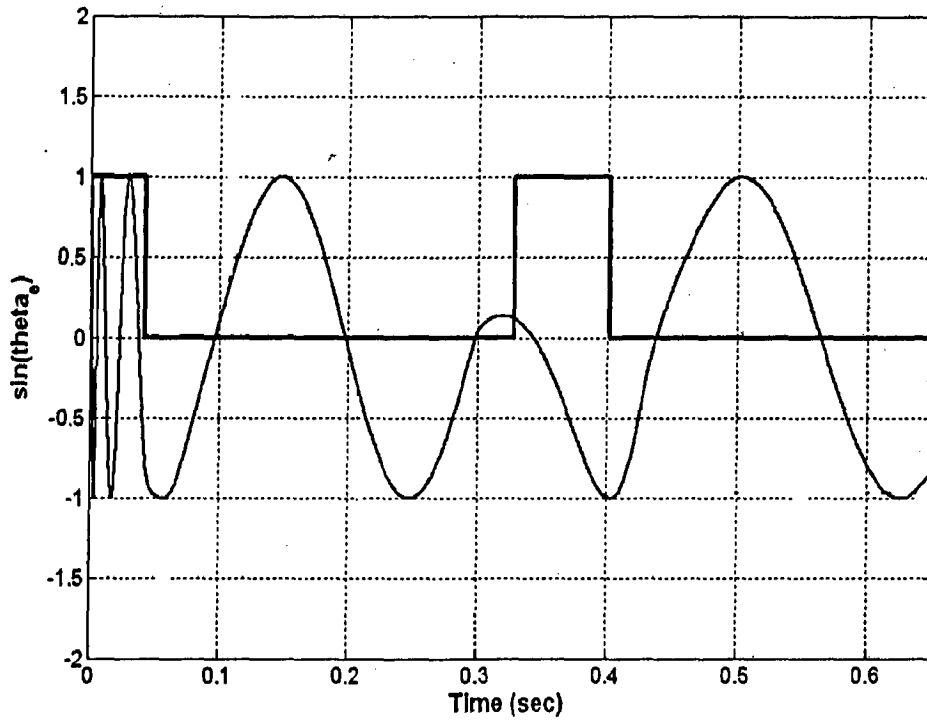


Figure (5.7): Response of $\sin\theta_e$

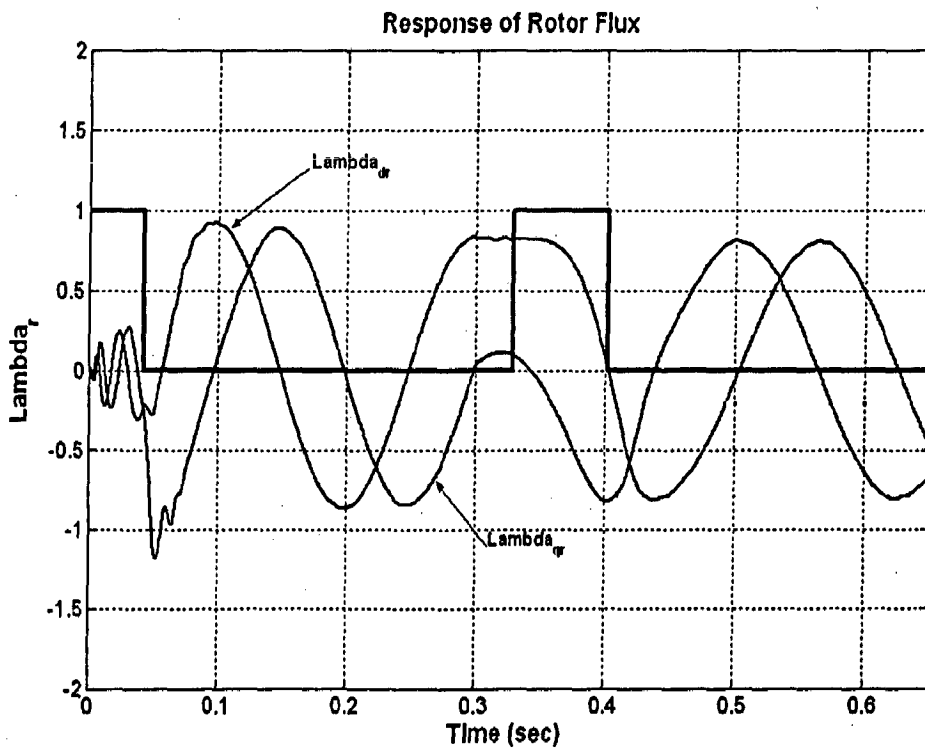


Figure (5.8): Response of rotor dq-flux

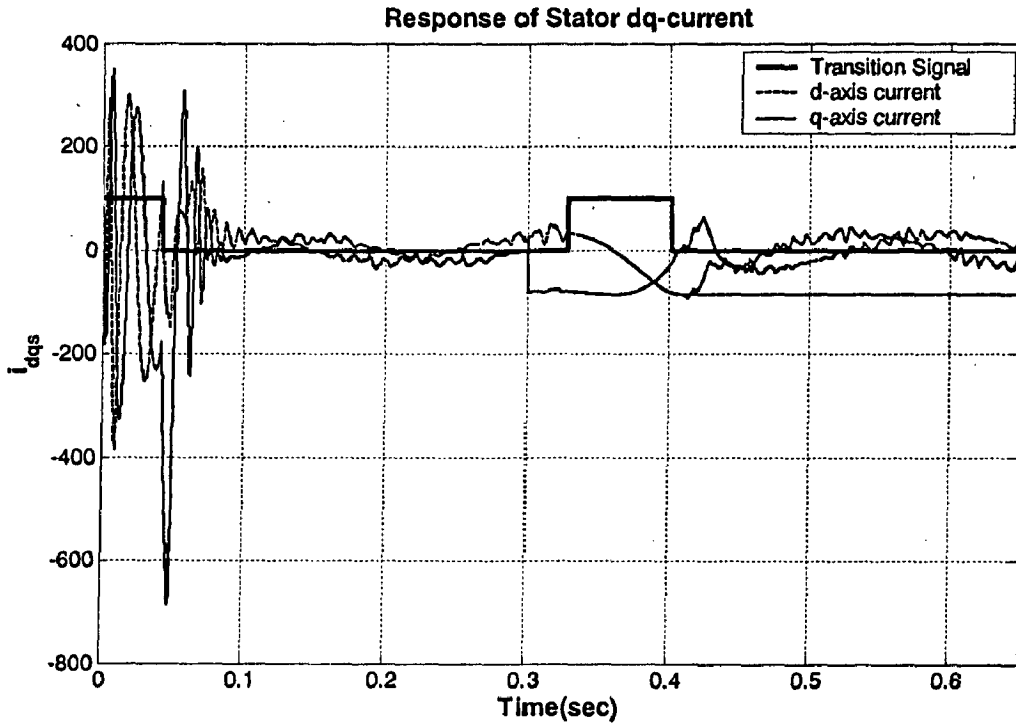


Figure (5.9): Response of stator dq- current

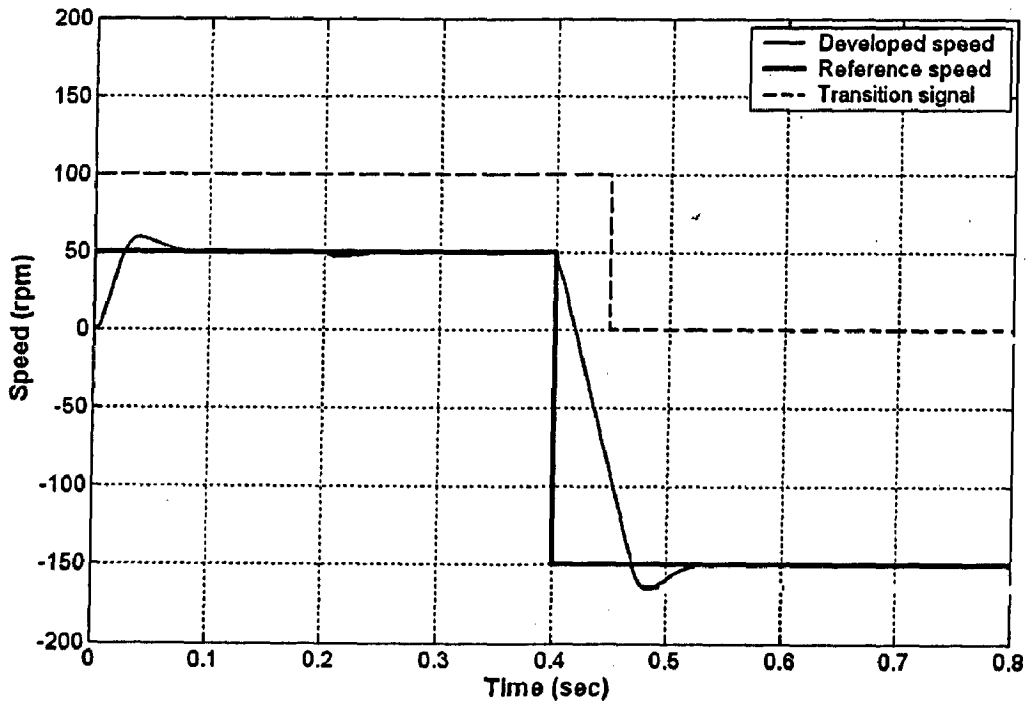


Figure (5.10): Speed response

Figure (5.10) shows the speed response when the drive system operates in IVC mode for 0.45 sec and then transits to DVC mode. For this a speed signal of 50 rpm is applied for 0.4 sec that changes to -150 rpm for 0.8 sec. A load torque of 50 N-m is applied at 0.4 sec. Until the rotor speed follows the 50 rpm command (< 85 rpm), it operates in IVC mode. Stator d-axis and q-axis current response in this mode is shown in figure (5.12) and (5.13). Figure (5.11) shows the torque response. Some oscillatory torque is evident at transition. This is due to mismatch of field angle (θ_e) between the two operating mode i.e. IVC and DVC. Stator dq- current response in DVC mode is shown in figure (5.12) and (5.13). From the dq- current response figure, it is clear that when operating mode changes from IVC to DVC mode, large d-axis transient current occurs unlike q-axis current transient. Reverse behavior is observed when motor operates in IVC mode. During IVC mode, when the speed of motor is low, frequency of the stator current is also low and as the speed increases frequency increases. Hence it is “self frequency tuned” drive system.

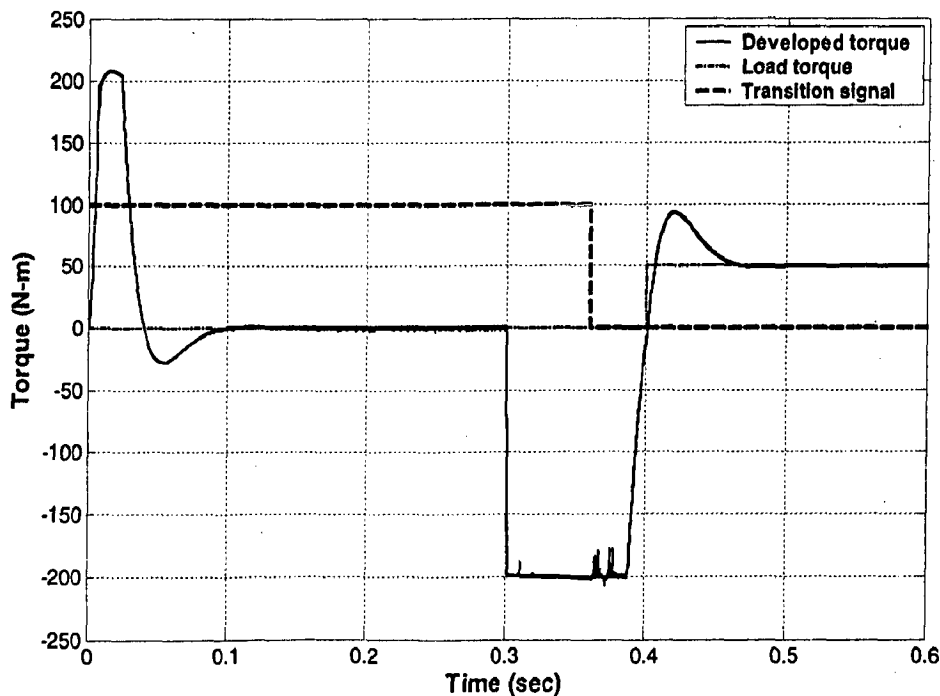


Figure (5.11): Torque response

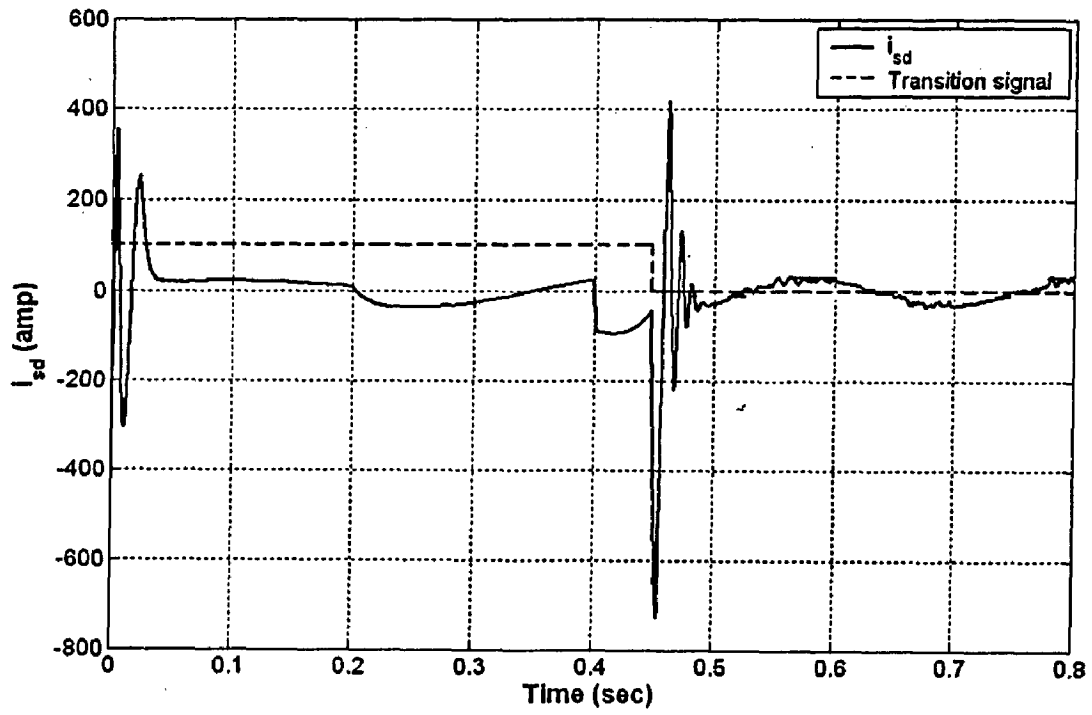


Figure (5.12): Stator d-axis current response

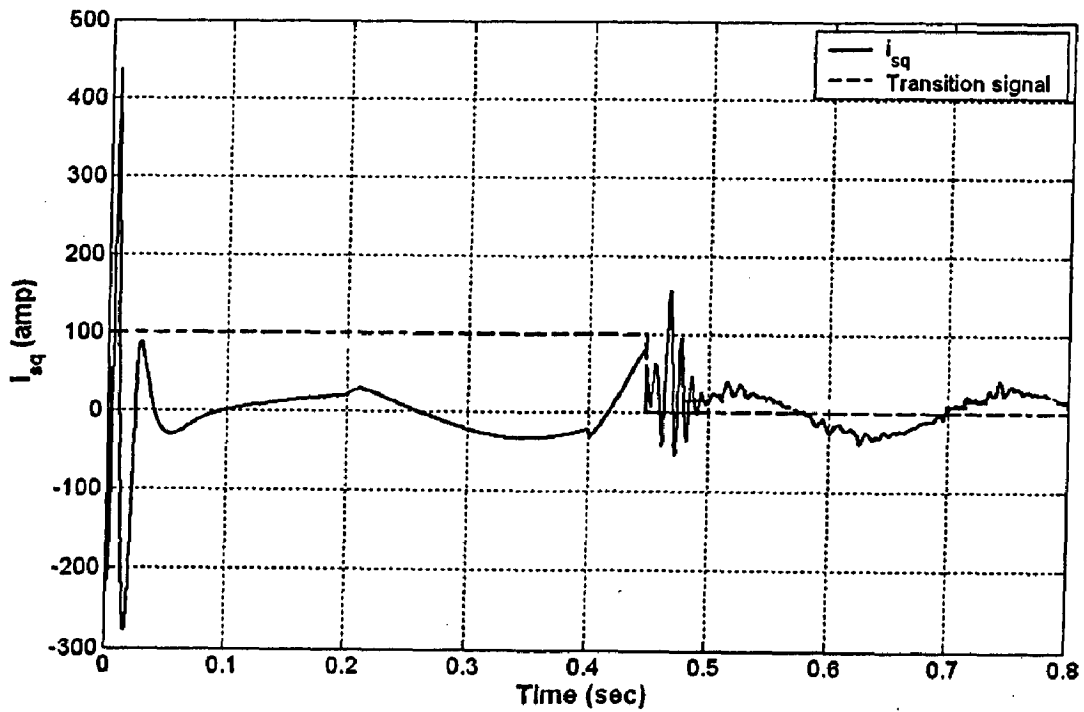


Figure (5.13): Stator q-axis current response

In the responses shown in figures (5.14) to (5.17) the drive system goes from forward motoring operation with positive load torque to reverse motoring operating with negative load torque. The reference speed signal changes from +100 rpm to -80 rpm and applied load torque polarity changes from +50 N-m to -50 N-m at 0.4 sec. Speed and torque response shows a stable behavior. From figure (5.17) and (5.18), it is clear that as the direction of rotor speed becomes negative i.e. when motor starts rotating in reverse direction, the stator dq- current and unit vectors automatically changes their phase direction.

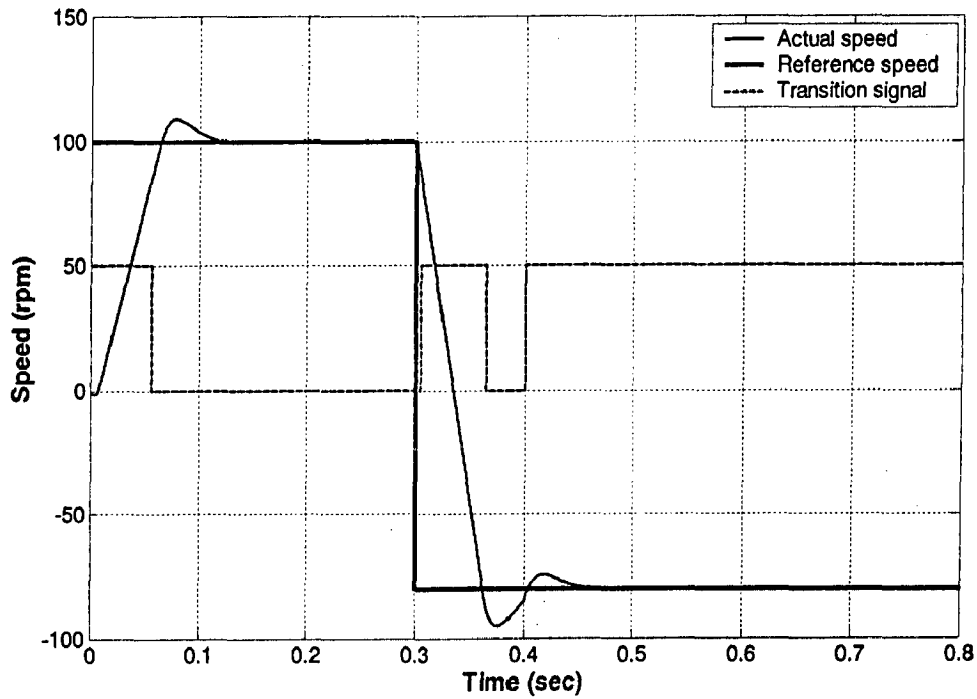


Figure (5.14): Speed response in forward and reverse motoring mode

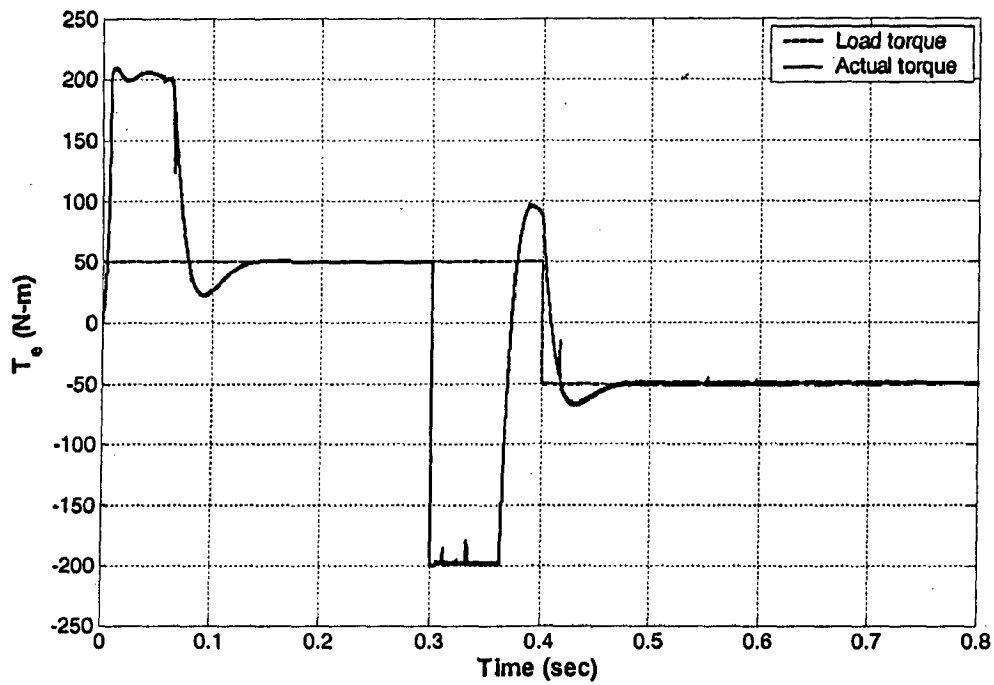


Figure (5.15): Torque response in forward and reverse motoring mode

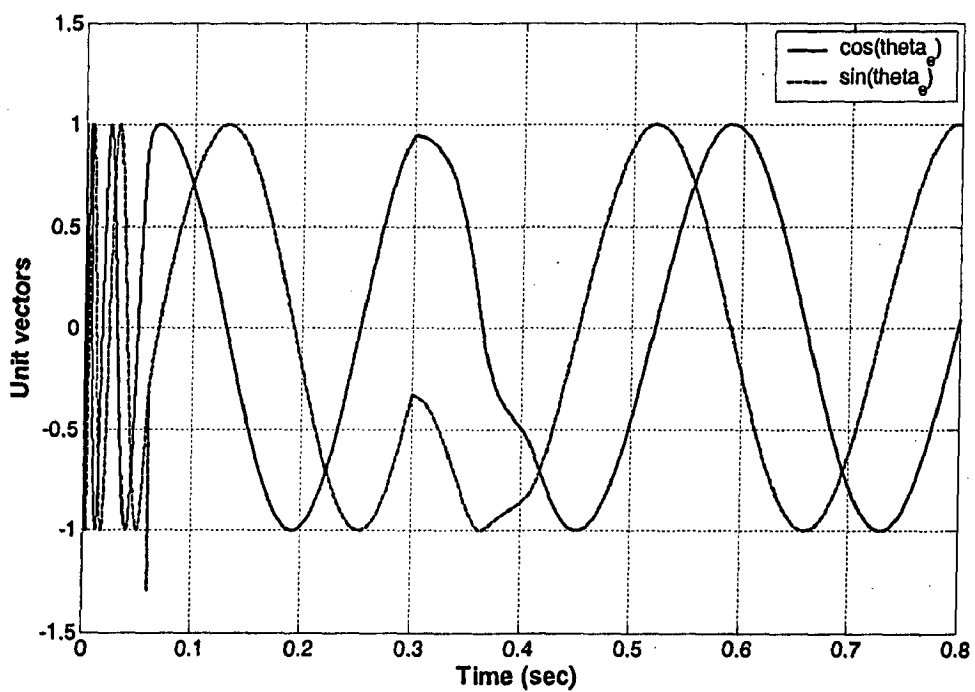


Figure (5.16): Unit vectors response in forward and reverse motoring mode

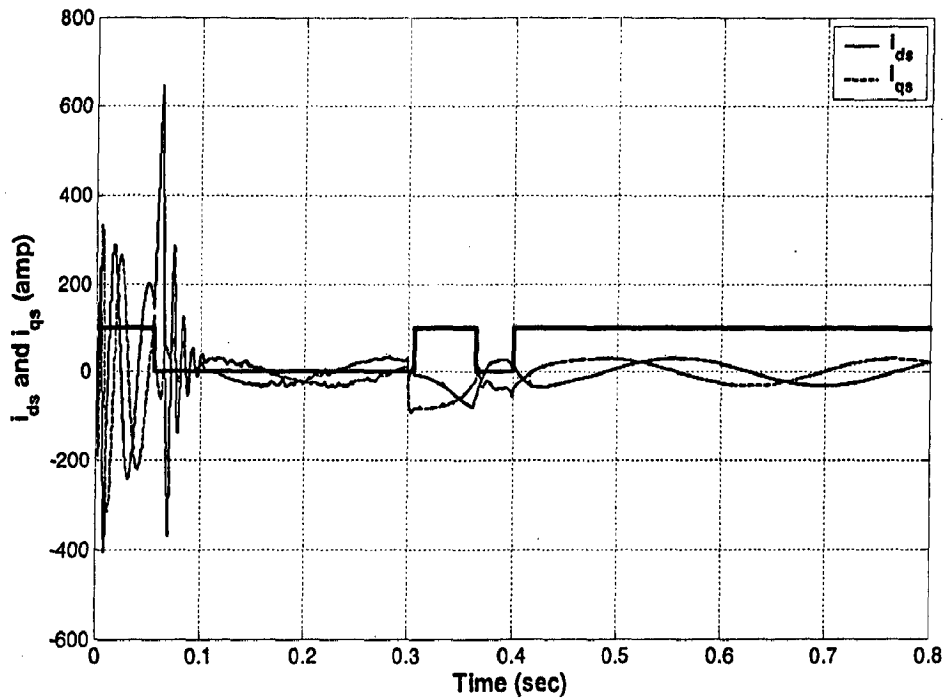


Figure (5.17): Stator dq-current response in forward and reverse motoring mode

5.3 Response under four quadrant operation .

Behavior of motor torque and speed in four quadrants is shown in figures from (5.18) to figure (5.26). For operation of drive in different quadrants, a constant speed command of +150 rpm or -150 rpm, is set as reference speed command. This speed signal decays to zero at 0.4 sec. The load torque reference is set at either +50 N -m or -50 N-m, from 0 sec to 0.5sec. Transition signal changes the drive operation mode whenever speed crosses the 85 rpm speed signal (i.e. 5%of base speed). Figure (5.20) and (5.21) shows the rotor dq-flux and unit vectors response during 1st quadrant operation. Figure (5.22) shows the stator current response.

ω_r = Actual rotor speed.

T_e = Developed electromagnetic torque.

5.3.1 Response during First Quadrant operation: $(+\omega_r, +T_e)$

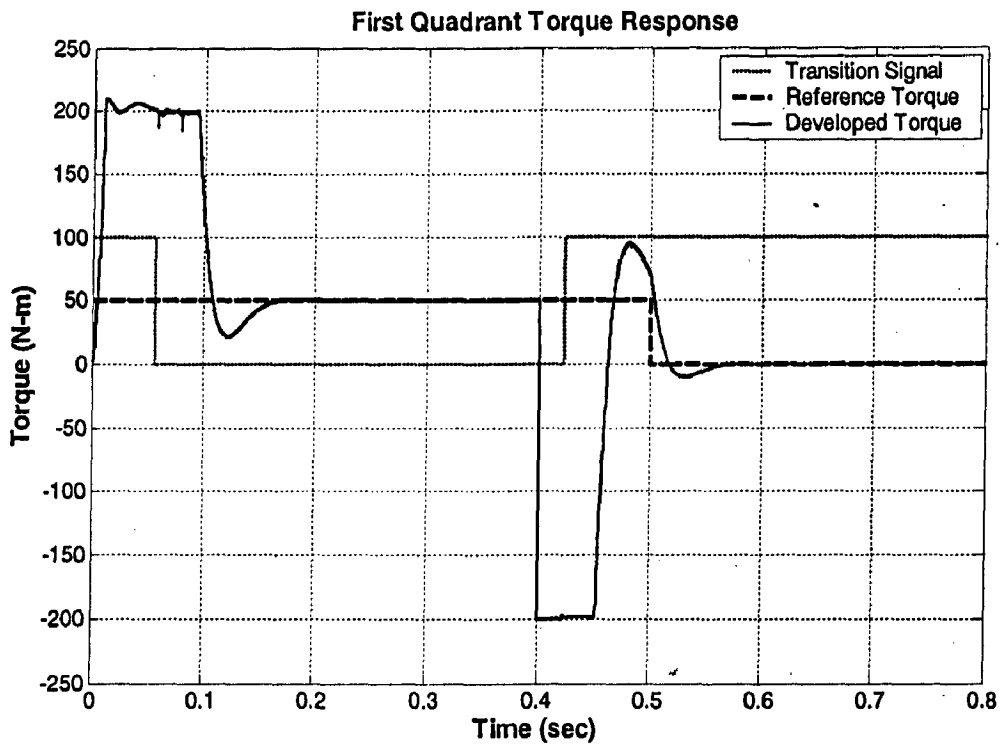
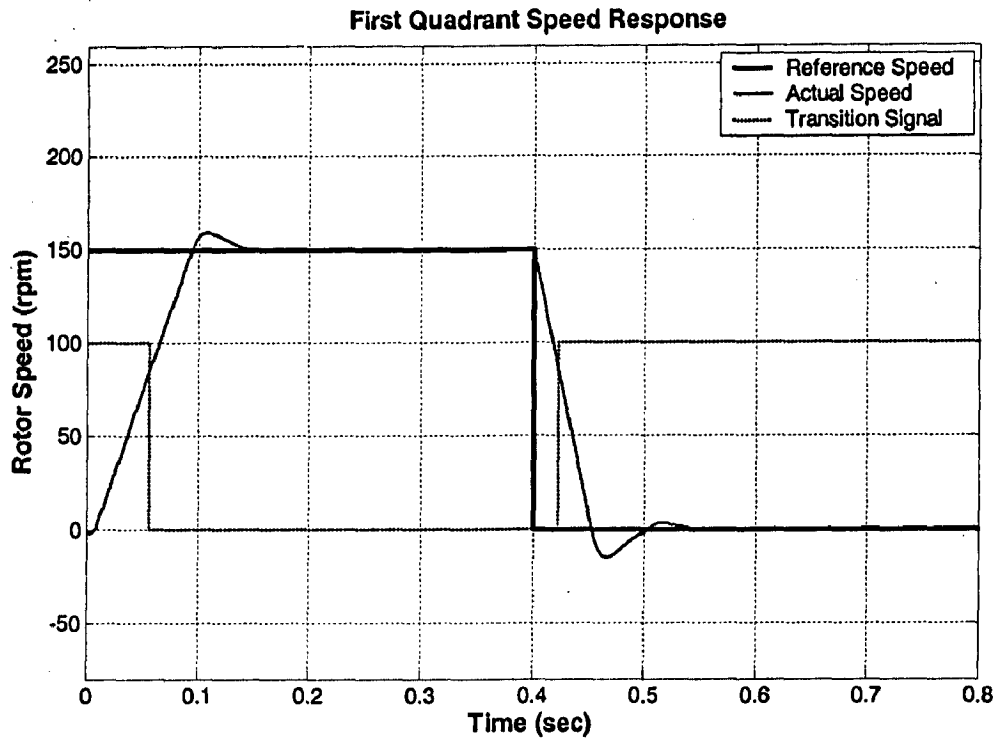


Figure (5.18): Speed (above) and Torque (below) response in 1st quadrant

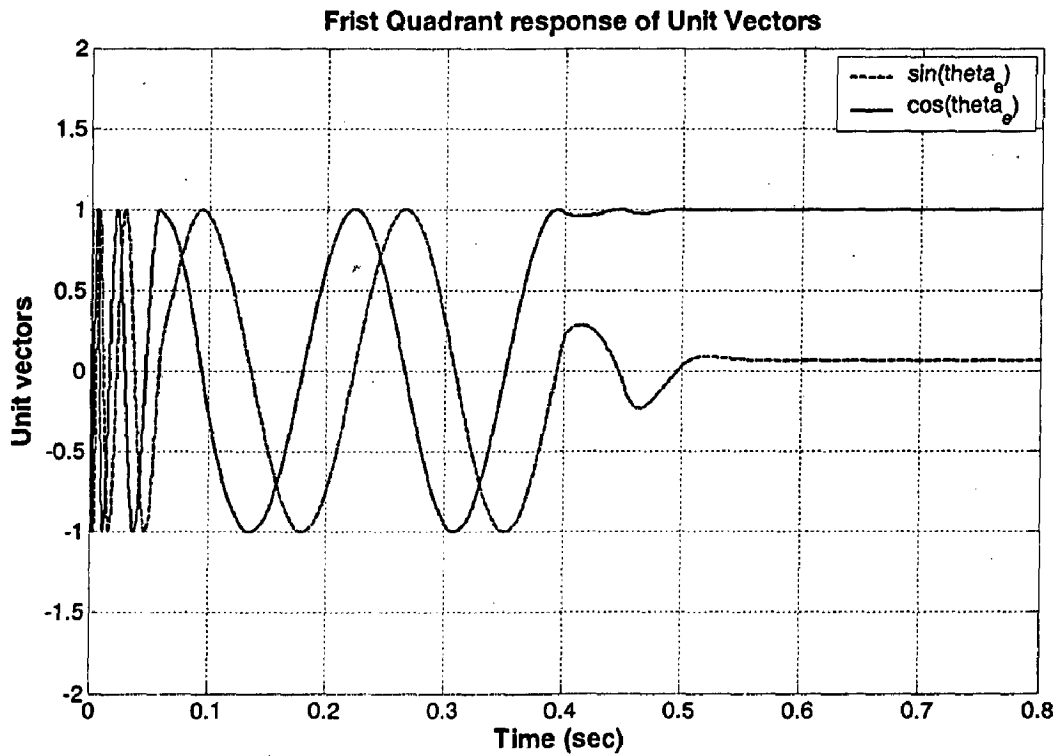
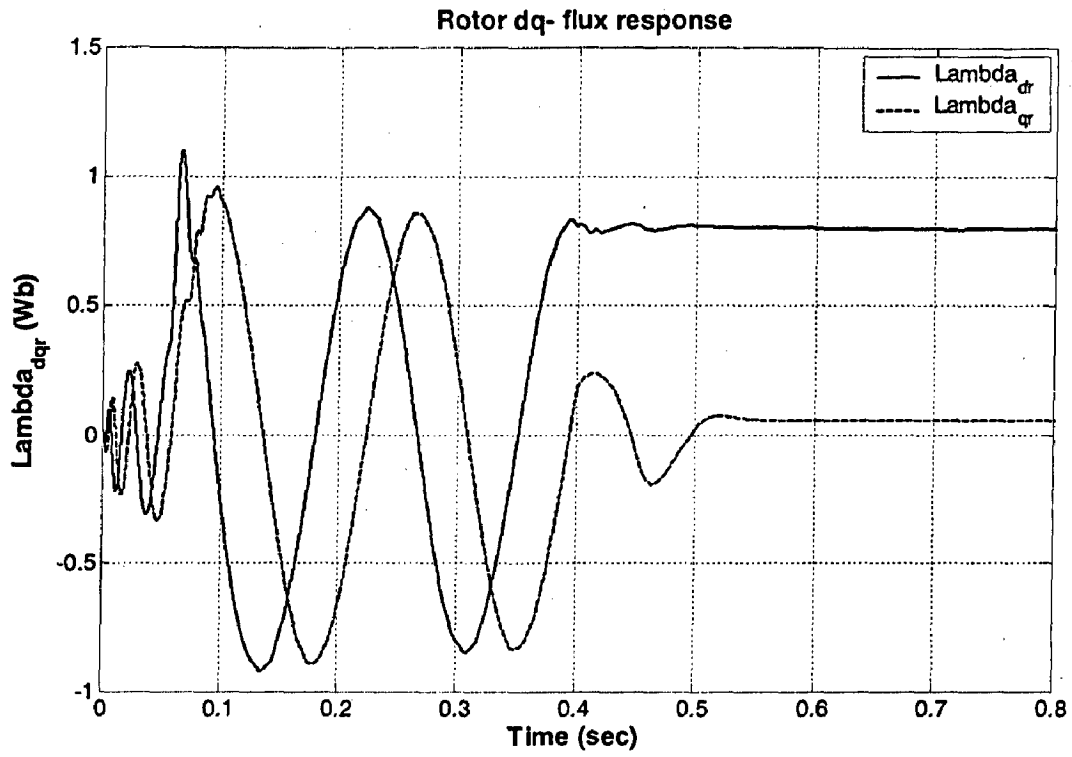


Fig (5.19): Response of Rotor flux (above) and Unit vectors (below) in 1st quadrant

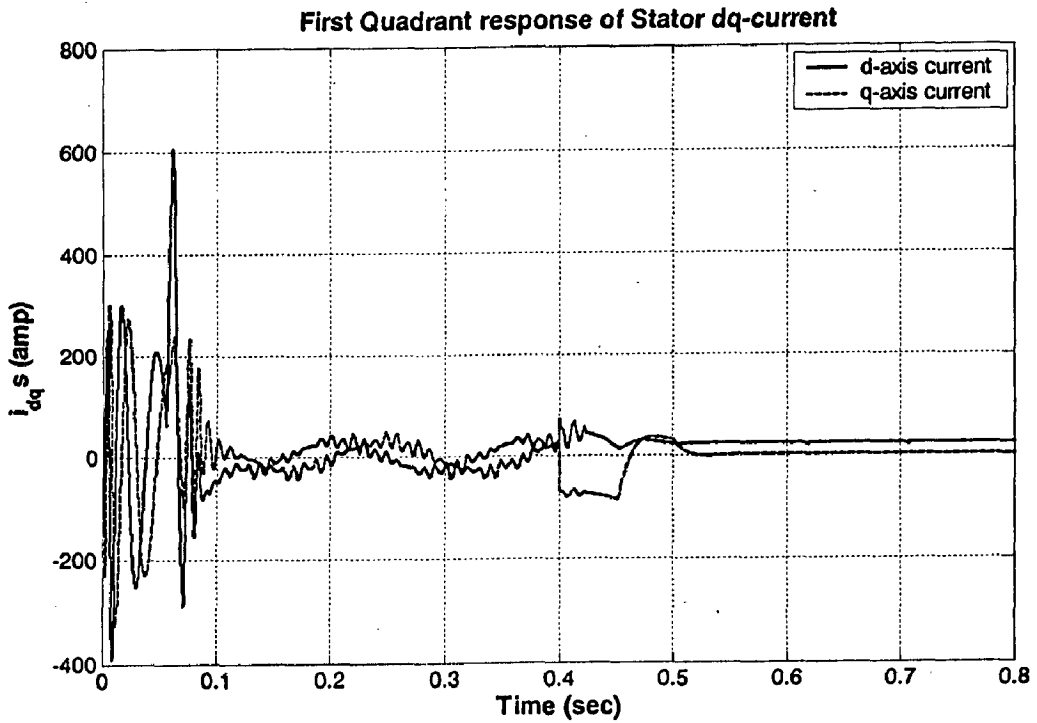


Figure (5.20): Response of stator dq-current in 1st quadrant

5.3.2 Response during Second Quadrant operation: $(+\omega, -T_e)$

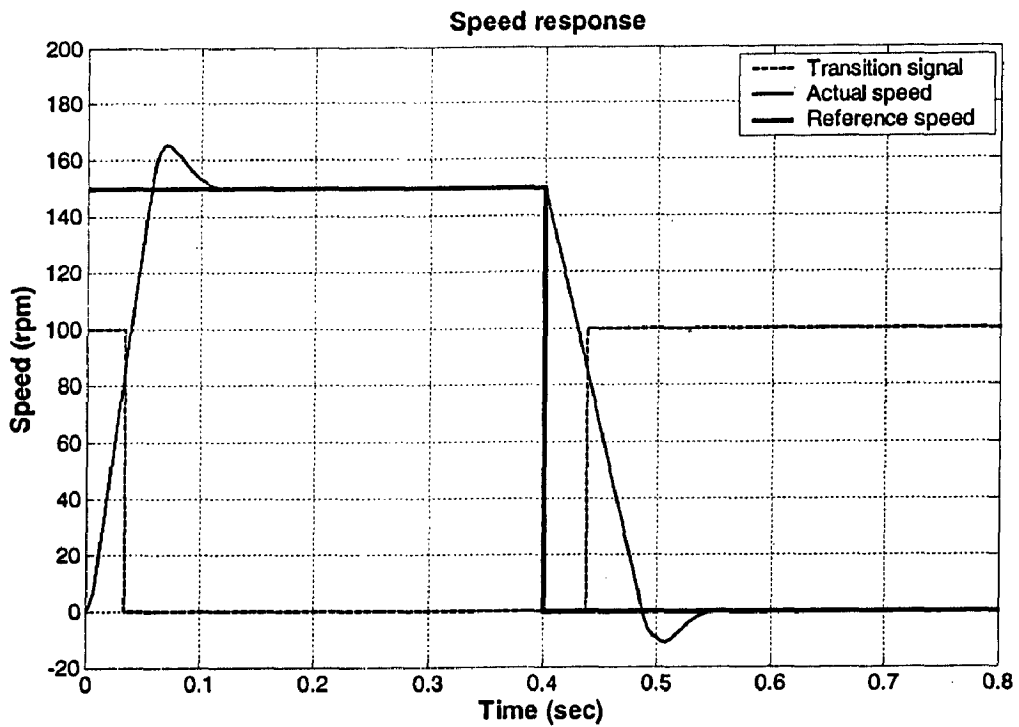


Figure (5.21): Speed response in 2nd quadrant

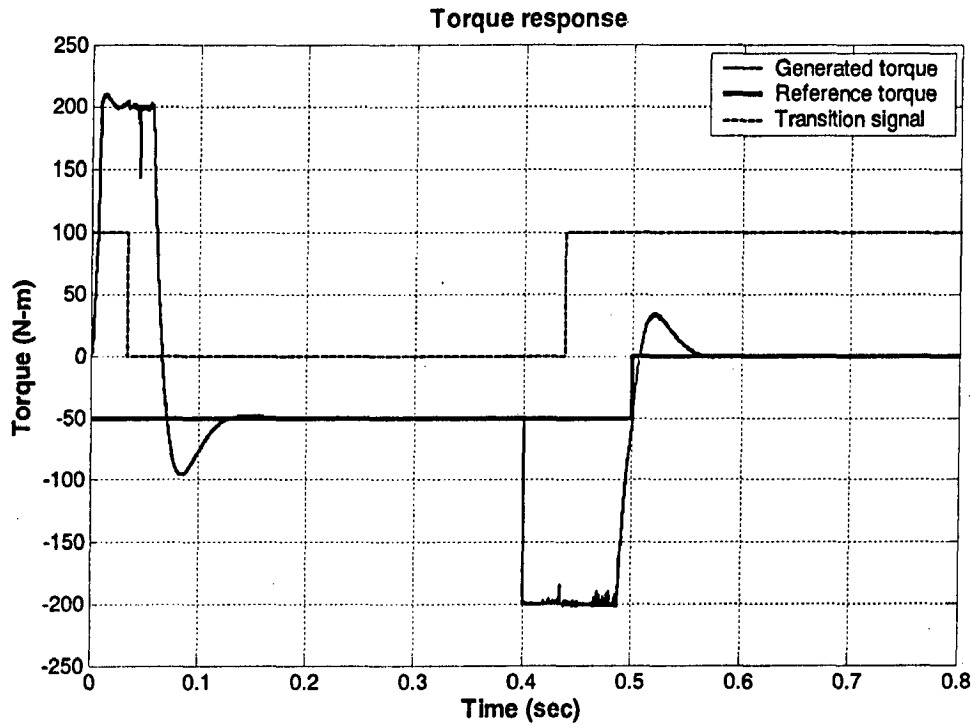


Figure (5.22): Torque response in 2nd quadrant

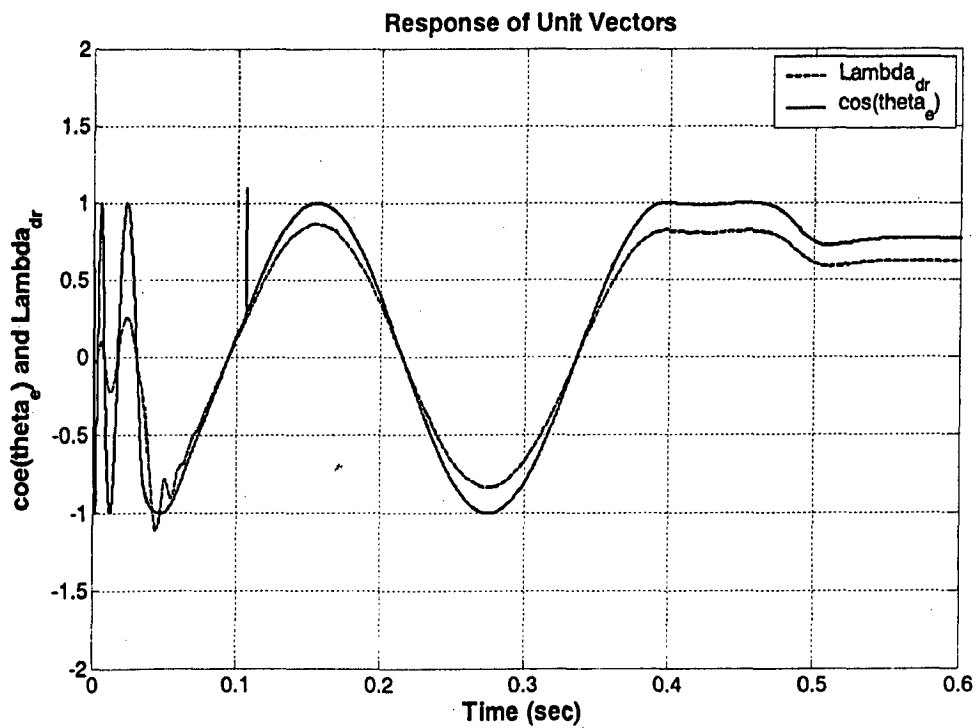


Figure (5.23): Response of $\cos\theta_e$ and λ_{dr} in correct phase sequence

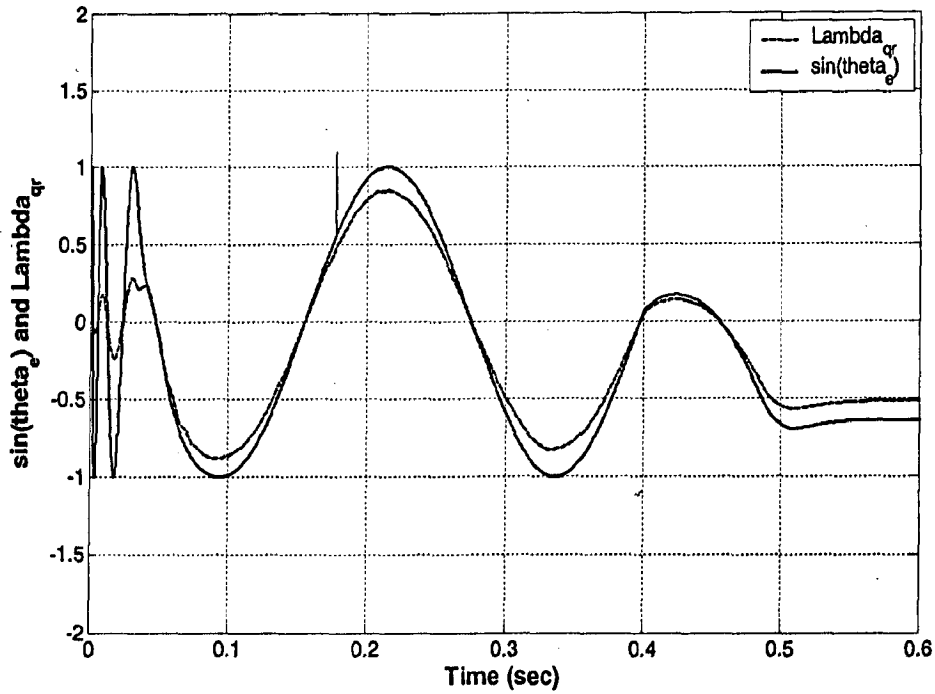


Figure (5.24): Response of $\sin \theta_e$ and λ_{qr} in correct phase sequence

For third and fourth and fourth quadrant operation, only torque and speed responses are shown. Unit vectors and rotor flux responses are shown but it has been found correct according to the quadrant.

For 3rd Quadrant,

$$\omega_{ref} = -150 \text{ rpm for } 0.0 \text{ sec to } 0.4 \text{ sec.}$$

$$T_{Load} = -50 \text{ N-m for } 0.0 \text{ sec to } 0.5 \text{ sec.}$$

Speed and torque response for 3rd quadrant is shown in figure (5.25) and (5.26).

For 4th Quadrant,

$$\omega_{ref} = -150 \text{ rpm for } 0.0 \text{ sec to } 0.4 \text{ sec.}$$

$$T_{Load} = -50 \text{ N-m for } 0.0 \text{ sec to } 0.5 \text{ sec.}$$

Speed and torque response for 3rd quadrant is shown in figure (5.29) and (5.30).

5.3.3 Response during Third Quadrant operation: $(-\omega_r, -T_e)$

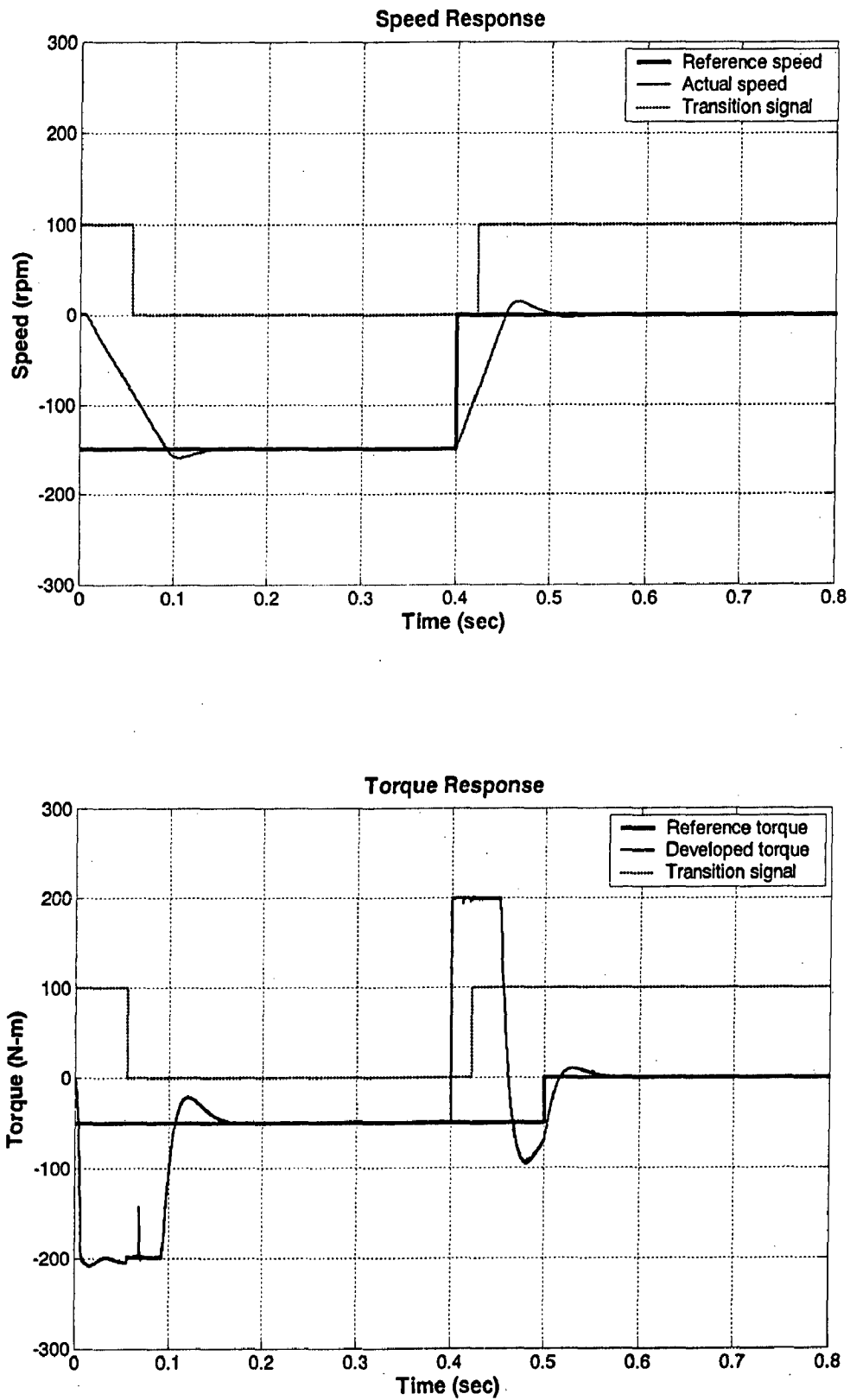


Figure (5.25): Speed (above) and Torque (below) response in 3rd quadrant

5.3.4 Response during Fourth Quadrant operation: $(-\omega_r, +T_e)$

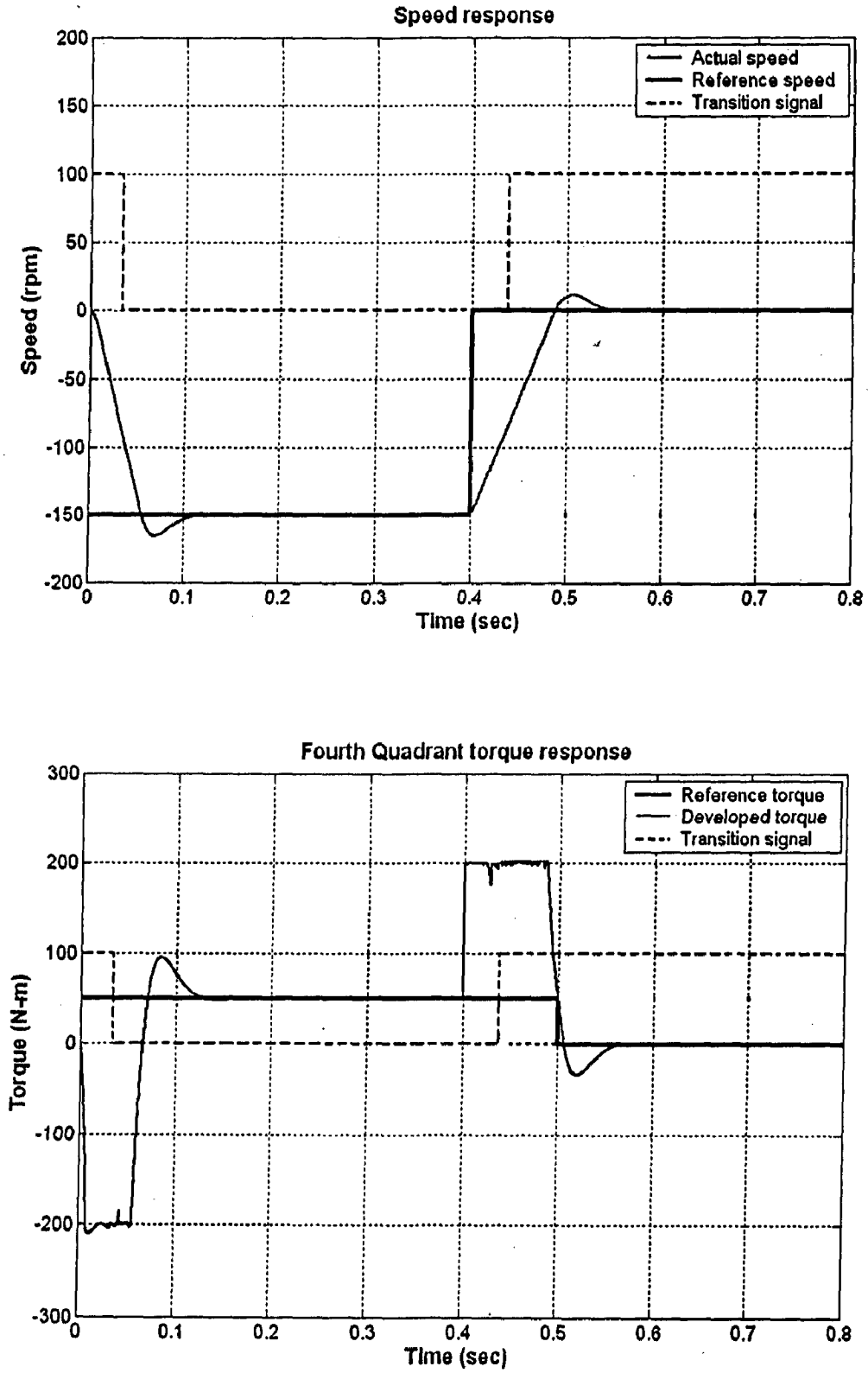


Figure (5.26): Speed (above) and Torque (below) response in 4th quadrant

5.4 Interim conclusions.

The hybrid mode operation has made the drive to operate in all speed ranges, unlike direct vector control (DVC) which has poor speed and torque performance in low speed range and indirect vector control (IVC) which has the problem of higher speed sensing. This hybrid control drive system operated successfully in IVC and DVC mode with the speed variation. The machine has started at zero speed in indirect vector control mode, transits to direct vector control mode as the speed develops, and then transits back to indirect vector control mode at zero speed. The system utilizes the rotor flux orientation in whole speed range, which is most preferable for vector control to yield linear torque response. But this drive system is not a seamless one. It requires switching of indirect and direct orientation scheme. It is a speed control drive system. So, it is not affected by parameter (like rotor time constant) variation in steady state.

CHAPTER 6

CONCLUSION AND SCOPE FOR FUTURE WORK

This work has investigated the hybrid vector control scheme that has been simulated for various speed and load torque inputs. To starting direct vector control and indirect vector control scheme has been simulated and analyzed because hybrid vector control scheme uses both direct and indirect scheme. For the indirect vector control scheme parameter (rotor resistance) mismatch condition between vector controller parameter and machine parameter has also been analyzed.

6.1 Key Results:

1. State space vector model of the induction motor in stationary reference frame have given the desired results, both under free acceleration and rated load condition. Responses shown have been found according to motor ratings.
2. The work done on closed loop speed controlled direct vector control scheme has been found satisfactory. This scheme has used the voltage model of the machine to estimate the rotor flux position. For the calculation of torque current and flux current component simulink design of PI controllers have been used. The gains of the controllers are adjusted according to the band width of controller currents and torque oscillation. Response time and steady state error have also been taken into account. The designed speed controlled drive system has been simulated under different load torque and reference speed conditions. Results have been found very close to the expected one. The developed speed follows the commanded speed and the developed electromagnetic torque nearly traces the load torque.
3. Simulation of the close loop speed controlled indirect vector control scheme has also been found satisfactory. This scheme has used the speed signal to estimate the rotor flux position. Simulations have been conducted for various reference speed and torque commands and the responses have been found as expected. Again for the

design of torque current and flux current PI controllers hit and trial method has been used keeping in view of the current oscillations and torque pulsation. Four quadrant operation of the drive has shown desired performance. Simulation of machine under dynamic load condition has shown a stable behavior. When a load torque was applied under running condition only a little dip was observed during transient but in steady state speed and torque profiles have been following their commanded values, independent of each other.

4. Effects of rotor resistance variation (different from controller resistance value) both in open loop and closed loop have been analyzed. It has been found that as the value of rotor resistance changes, rotor flux also deviates from its set value causing a coupling effect of stator d-axis and q-axis current. It has been shown that actual electromagnetic torque didn't follows the commanded torque during parameter mismatch. In closed loop system, increase in rotor resistance has decreases the speed response time but under steady, it follows the reference speed irrespective of parameter variation. Similar behavior has been observed with the torque. MRAC method has been applied for rotor resistance variation compensation. Slip gain tuning has been used for the application of this method. When the system was compensated system, it has been found that rotor flux linkage follows the set value under parameter mismatch condition. Thus compensated system has avoided the coupling effect when rotor and controller parameter (resistance) was different. Four quadrant operation of this closed loop drive system was also analyzed. The responses have been found, as expected.
5. It has been found that designed hybrid vector controlled operates successfully starting from zero speed in the indirect vector control mode, transitions to direct vector control mode as the speed develops, and then transition backto indirect vector control mode at zero speed. The designed system was simulated successfully for different load and speed conditions and it has given the desired performances. A switching technique has performed this mode transfer operation whenever speed approaches in the range of $\pm 5\%$ of base speed. It has found that it (i.e. step switching) leads to the torque oscillation during transition. But it is not enough to cause system instability. The closed

loop drive system has been simulated for different values of speed and torque commands. The results have been found satisfactory. Four quadrant operation of this drive system has also been performed and the results were found good enough with little error. In all the vector strategies that have been simulated, has used rotor flux orientation since it has found easy to implement.

6. The work effort has also shown that the frequency ω_c of the drive is not directly controlled as in scalar control. The machine is essentially “self-controlled”, where the frequencies as well as the phase are controlled indirectly with the help of unit vectors. The transient response has been found fast like a DC machine, because torque controlling component (i_{qs}) of stator current does not affect the flux component (i_{ds}). The speed control is possible in four quadrants without any additional control elements (like phase sequence reversing circuit). In forward motoring condition, figure (5.14), if the torque T_c is negative figure (5.15), the drive initially goes to regenerative braking mode, which slows down the speed. At zero speed, the phase sequence of the unit vectors automatically reverses figure (5.16), giving reverse motoring operation.

6.2 Scope for Future Work:

The present work may be extended in any of the following directions

1. This hybrid control drive system requires a switch for mode transfer. It can be made seamless. So that, machine can make a smooth transition between the two modes, without causing any torque or flux oscillation.
2. Speed encoder has been used for speed measurement. The developed drive system can be made speed sensorless. For flux sensing in direct vector control scheme, calculation can be made that based on stator flux thus avoiding too much parameter variation. Rotor flux based calculation utilizes the stator resistance R_s , inductances L_{sl} , L_{rl} and L_m , so variation of these parameters reduces the accuracy of estimated signals. It can also be possible to compensate the varying parameters.

3. MATLAB is a program that models all the physical processes involved with the motor controller mathematically. It does not consider variables such as heat, magnetic saturation etc. But these parameters have significant effects on the formulation and behavior of any drive system. So the effects of these parameters should be examined.
4. Real time simulation and hardware implementation of the hybrid vector control drive system can be made. Effect of various motor parameters like stator resistance, magnetizing inductance, and leakage inductances of rotor and stator can be analyzed and drive can be compensated against these parameters variation. Further online estimation and compensation of parameters can be simulated and implemented.

REFERENCES

1. R. W. Doncker, and D. W. Novotny, "The universal field oriented control", IEEE trans. Ind. Appl. Vol 30, Jan/Feb., 1994, pp. 92-100.
2. B. K. Bose, M. G. Simoes, D. R. Crecelius, K. Rajshekara and R. Martin, "Speed sensorless hybrid vector controlled induction motor drive", IEEE IAS Ann. Mtg. 1995, pp. 137-143.
3. B. K. Bose, *Power Electronics And Electric Drives*, Prentice-Hall, Engle wood Cliffs, New Jersey, 1986.
4. Philip T. Kerin, Francisco Disilvestro, Ioannis Kanellakopoulos, Jonathan Locker, "Comperative Analysis of Scalar and Vector Control Methods for Induction Motors", University of Illinois , 1993, IEEE.
5. Bimal K. Bose, "Modern Power Electronics And AC Drives". 3^d Reprint, Pearson Education (Singapore) Pte. Ltd., Delhi, 2003.
6. Bimal K. Bose, M. Godoy Simoes, Department of Electrical Engineering, "Speed Sensorless Hybrid Vector Controlled Induction Motor Drive", The University of Tennessee, Knoxville, 1995, IEEE.
7. S. Shinnaka, "New Hybrid Vector Control for Induction Motor without Velocity and Position Sensors", Department of Electrical Engineering, Kanagawa University, Yokohama, JAPAN.
8. C. Schauder, "Adaptive speed identification for vector control of induction motors without rotational transducers", IEEE, Ann. Meet Conf. Rec., pp 493499, 1989.
9. Krishnan, R., "Electric Motor Drives, Modelling, Analysis, and Control", Prentice-Hall India, New Delhi, July 2003.
10. "Field Oriented Control of 3-Phase AC-Motors", Literature Number: BPRA073, Texas Instruments Europe, February 1998.
11. "Digital Signal Processing Solution for Induction Moto", Application Note BPRA043, Texas Instruments, 1996.

12. Trounce, C., Round, S.D. , Duke, R.M. , “ *Comparison by Simulation of Three-Level Induction Motor Torque Control Schemes for Electric Vehicle Applications*”, University of Canterbury, New Zealand.
13. Jose Andres Santisteban, Member, IEEE, and Richard M. Stephan, Member, IEEE, “*Vector Control Methods for Induction Machines: An Overview*”, IEEE TRANSACTIONS ON EDUCATION, VOL. 44, NO. 2, MAY 2001.
14. A. Vagati and F. Villata, “AC servo system for position control”, Proceedings of ICEM , pp. 871-874, 1984.
15. T. Tajima, H. Umida and H. Tetsutani, “ Zero-crossing speed control by sensorless vector control with instantaneous speed estimation”, IEE Japan Industrial application society, 1996, pp. 219-220.
16. P. Caminos and N. Munro, “*PID Controllers: recent tuning methods and design to specification*”, IEE Proceedings, Control Theory Application., Vol 149, N0.1, January 2002.
17. Kanokvate Tungpimolrut*, Fang-Zheng Peng and Tadashi Fukao, “*A Robust Rotor Time Constant Estimation Method for Vector Control of Induction Motor Under Any operating Conditions*”, Department of Electrical and Electronics Engineering, Tokyo Institute of Technology, Japan. 1994 IEEE.
18. Hernik Mosskull, “*Tuning of Field Oriented Controller for Induction Machines*”, Bombardier Transportation, Sweden, Power Electronics, Machines and Drives, 16-18 April 2002, Conference Publication No. 487. IEE 2002.
19. Xing Yu, Matthew W. Dunnigan, Member IEEE, and Barry W. Williams, “*A Novel Rotor Resistance Identification Method for an Indirect Rotor Flux Oriented Controlled Induction Machine System*”, 2002 IEEE.
20. G. Terorde and R. Belmans, “ *Speed , Torque and Flux Estimation of Induction Motor Drives with Adaptive System model*”, Katholieke Universiteit Leuven, Belgium, Power Electronics, Machines and Drives, 16-18 April 2002, Conference Publication No. 487. IEE 2002.

21. Karen L. Butler, Member, IEEE, Mehrdad Ehsani, Fellow, IEEE, Preyas Kamnath, Member, IEEE, "A Matlab-Based Modeling and Simulation Package for Electric and Hybrid Electric Vehicle Design", 1999, IEEE.
22. J.W.L. Nerys, A. Hughes and J. Corda, "Alternative Implementation of Vector Control for Induction Motor and its experimental evaluation", IEE Proc.-Electr. Power Appl., Vol. 147, No. 1 January 2000.
23. Hachicha M., Masmoudi N., Kharrat M. W., Kamoun L., "DSP Implementation of Fuzzy Speed Control System for Electric Vehicle Application", National Engineering school of Sfax, B. P. W 3038 SFAX TUNISIE.
24. Ciro Attaianesi, Member, IEEE, Vito Nardi, and Giuseppe Tomasso, Member, IEEE, "A Self-Commissioning Algorithm for VSI-fed Induction Motors", IEEE Transactions on Power Electronics, Vol. 17, No. 6, November 2002.
25. Dorin O. Neacsu, Senior Member, IEEE, and Kaushik Rajashekara, Fellow, IEEE, "Comparative Analysis of Torque – Controlled IM Drives with Applications in Electric and Hybrid Vehicles", IEEE Transactions on Power Electronics, Vol. 16, No. 2, March 2001.
26. Bimbhra, P.S., "Generalized Theory of Electrical Machines", Eighth Edition Khanna Publishers, Delhi,
27. Mukherjee, P. K., Chakravorti, S., "Electrical Machines", Dhanpat Rai Publications, Second Edition, 2000.
28. Rudra Pratap, 2003, "Getting Started with Matlab", Oxford University Press.
29. Chapman, S. J., 2002, "Matlab Programming for Engineers", Bookware Champion Series.
30. Dubey, G. K., "Power Semiconductor Controlled Drives", Prentice Hall Publication, 1998.
31. file://E:\IEEEWORKE BOOKS\NASAR_EL\top9.htm
32. Math Works. (2001). What is SIMULINK. The Math Works, Inc. Available: <http://www.mathworks.com/access/helpdesk/help/toolbox/SIMULINK/ug/ug.s>

Induction Motor parameters

Horse power rating	50 hp
Type of motor	3- phase , Star connected, Squirrel cage
Frequency rating	60 Hz
Voltage rating	460 volts (Line-to-Line)
Number of poles	4
Inertia constant, J	1.662 (kg-m ²)
Frictional constant, Bm	0.1 (Nm/ (rad/sec))
Rotor flux linkage, λ_r	0.08 (Wb)
Base speed	1705 rpm
Stator resistance, R_s	0.087 ohm
Rotor resistance, R_r	0.228 ohm
Stator leakage inductance, L_{st}	0.8e-3 Henry
Rotor leakage inductance, L_{rt}	0.8e-3 Henry
Stator mutual inductance, L_m	34.7e-3 Henry
Rated current, i_s	46 amp

Matlab Programme for Direct Vector Control

g:\work\DVC_1.m Page 1

June 27, 2005 2:27:40 AM

```
close all,clear,clc;
```

```
%induction motor parameters: -- 50Hp, 3-phase, 60Hz, 460V, Star connected.
```

```

Hp=50;           %Power rating of Induction motor
p=4;            %Number of poles
Bm=0.1;         %Friction coefficient in rad/sec
J=1.662;        %Moment of inertia in Kg-m^2
fro=0.96;       %Rotor flux linkage in weber
wb=178.54;      %Base speed in rad/sec
fo=60;          %Base frequency in Hz
Lsl=0.8e-3;     %stator leakage inductance in hanery
Rs=0.087;       %stator resistance in ohm
Lm=34.7e-3;     %stator mutual inductance in hanery
Lrl=0.8e-3;     %rotor leakage inductance in hanery

```

```
%%%%%%%% Vector controller or commanded parameters%%%%%%%%
```

```

Lslc=0.8e-3;    %commanded stator leakage inductance in hanery
Rsc=0.087;      %Commanded stator resistance in ohm
Lmc=34.7e-3;    %Commanded mutual inductance in hanery
Lrlc=0.8e-3;    %Commanded rotor leakage inductance in hanery
Rrc=0.228;      %Commanded rotor resistance in ohm
Rt=Rrc;         %stator resistance in ohm (variable)

```

Lrc=Lrlc+Lmc;

Lr=Lrc;

%%%

Vdc=sqrt(2)*460; %DC link voltage

fc=20000; %carrier frequency in Hz

MI=0.8; %modulation index

wo=2*pi*fo;

Kp1=1.55;Ki1=95; %gain of flux current PI controller

Kp2=5;Ki2=95; %gain of torque current PI controller

Kps=100;Kis=5200; %gain of speed PI controller

Trc=Lrc/Rrc %commanded rotor time constant

Tr=Lr/Rr %actual rotor time constant

Kte=(3/2)*(p/2)*(Lm/Lr) %torque constant

K_s=1-Lm^2/(Lr*Lr) %Leakage coefficient

Matlab Programme for Hybrid Vector Control

g:\work\HVC_1.m Page 3

June 27, 2005 2:27:40 AM

```
close all,clear,clc;
```

```
%induction motor parameters: -- 50Hp, 3-phase, 60Hz, 460V, Star connected.
```

```
Hp=50;           %Power rating of Induction motor
p=4;            %Number of poles
Bm=0.1;         %Friction coefficient in rad/sec
J=1.662;        %Moment of inertia in Kg-m^2
fro=0.96;       %Rotor flux linkage in weber
wb=178.54;      %Base speed in rad/sec
fo=60;          %Base frequency in Hz
Lsl=0.8e-3;     %stator leakage inductance in hanery
Rs=0.087;       %stator resistance in ohm
Lm=34.7e-3;     %stator mutual inductance in hanery
Lrl=0.8e-3;     %rotor leakage inductance in hanery
```

```
%%%%%%%% Vector controller or commanded parameters%%%%%%%%
```

```
Lslc=0.8e-3;    %commanded stator leakage inductance in hanery
Rsc=0.087;      %Commanded stator resistance in ohm
Lmc=34.7e-3;    %Commanded mutual inductance in hanery
Lrlc=0.8e-3;    %Commanded rotor leakage inductance in hanery
Rrc=0.228;      %Commanded rotor resistance in ohm
Rr=Rrc;         %stator resistance in ohm (variable)
Tlim=200;       %Torque limit (N-m)
```

Lrc=Lrlc+Lmc;

Lr=Lrc;

%%%

Vdc=sqrt(2)*460; %DC link voltage

fc=20000; %carrier frequency in Hz

MI=0.8; %modulation index

wo=2*pi*fo;

Kp1=12.55;Ki1=86; %gain of flux current PI controller

Kp2=12.5;Ki2=86; %gain of torque current PI controller

Kps=100;Kis=5200; %gain of speed PI controller

Trc=Lrc/Rrc %commanded rotor time constant

Tr=Lr/Rr %actual rotor time constant

K_alpha=Tr/Trc

K_beta=Lm/Lmc

Kte=(3/2)*(p/2)*(Lm/Lr) %torque constant

K_s=1-Lm^2/(Lr*Lr) %Leakage coefficient

Matlab Programme for Direct Vector Control

g:\work\DVC_1.m Page 1

June 27, 2005 2:27:40 AM

```
close all,clear,clc;
```

```
%induction motor parameters: -- 50Hp, 3-phase, 60Hz, 460V, Star connected.
```

```

Hp=50;           %Power rating of Induction motor
p=4;            %Number of poles
Bm=0.1;         %Friction coefficient in rad/sec
J=1.662;        %Moment of inertia in Kg-m^2
fro=0.96;       %Rotor flux linkage in weber
wb=178.54;      %Base speed in rad/sec
fo=60;          %Base frequency in Hz
Lsl=0.8e-3;     %stator leakage inductance in hanery
Rs=0.087;       %stator resistance in ohm
Lm=34.7e-3;     %stator mutual inductance in hanery
Lrl=0.8e-3;     %rotor leakage inductance in hanery

```

```
%%%%%%%% Vector controller or commanded parameters%%%%%%%%
```

```

Lslc=0.8e-3;    %commanded stator leakage inductance in hanery
Rsc=0.087;      %Commanded stator resistance in ohm
Lmc=34.7e-3;   %Commanded mutual inductance in hanery
Lrlc=0.8e-3;   %Commanded rotor leakage inductance in hanery
Rrc=0.228;     %Commanded rotor resistance in ohm
Rr=Rrc;        %stator resistance in ohm (variable)

```

Tlim=200; %Torque limit (N-m)

Lrc=Lrlc+Lmc;

Lr=Lrc;

%%%

Vdc=sqrt(2)*460; %DC link voltage

fc=20000; %carrier frequency in Hz

MI=0.8; %modulation index

wo=2*pi*fo;

Kp1=12.55;Ki1=66; %gain of flux current PI controller

Kp2=12.5;Ki2=66; %gain of torque current PI controller

Kps=100;Kis=5200; %gain of speed PI controller

Trc=Lrc/Rrc %commanded rotor time constant

Tr=Lr/Rr %actual rotor time constant

K_alpha=Tr/Trc

K_beta=Lm/Lmc

Kte=(3/2)*(p/2)*(Lm/Lr) %torque constant

K_s=1-Lm^2/(Lr*Lr) %Leakage coefficient

Matlab Programme for Indirect Vector Control

g:\work\IVC_1.m Page 2

June 27, 2005 2:27:40 AM

```
close all,clear,clc;
```

```
%induction motor parameters: -- 50Hp, 3-phase, 60Hz, 460V, Star connected.
```

```
Hp=50;           %Power rating of Induction motor
p=4;             %Number of poles
Bm=0.1;         %Friction coefficient in rad/sec
J=1.662;        %Moment of inertia in Kg-m^2
fro=0.96;       %Rotor flux linkage in Weber
wb=178.54;      %Base speed in rad/sec
fo=60;          %Base frequency in Hz
Lsl=0.8e-3;     %stator leakage inductance in hanery
Rs=0.087;       %stator resistance in ohm
Lm=34.7e-3;    %stator mutual inductance in hanery
Lrl=0.8e-3;    %rotor leakage inductance in hanery
```

```
%%%%%%%% Vector controller or commanded parameters%%%%%%%%
```

```
Lslc=0.8e-3;    %commanded stator leakage inductance in hanery
Rsc=0.087;      %Commanded stator resistance in ohm
Lmc=34.7e-3;   %Commanded mutual inductance in hanery
Lrlc=0.8e-3;   %Commanded rotor leakage inductance in hanery
Rrc=0.228;     %Commanded rotor resistance in ohm
Rr=Rrc;        %stator resistance in ohm (variable)
Tlim=200;      %Torque limit (N-m)
```

Lrc=Lrlc+Lmc;

Lr=Lrc;

%%%

Vdc=sqrt(2)*460; %DC link voltage

fc=20000; %carrier frequency in Hz

MI=0.8; %modulation index

wo=2*pi*fo;

Kp1=1.55;Ki1=95; %gain of flux current PI controller

Kp2=5;Ki2=95; %gain of torque current PI controller

Kps=100;Kis=5200; %gain of speed PI controller

Trc=Lrc/Rrc %commanded rotor time constant

Tr=Lr/Rr %actual rotor time constant

Kte=(3/2)*(p/2)*(Lm/Lr) %torque constant

K_s=1-Lm^2/(Lr*Lr) %Leakage coefficient

Matlab Programme for Hybrid Vector Control

g:\work\HVC_1.m Page 3

June 27, 2005 2:27:40 AM

```
close all,clear,clc;
```

```
%induction motor parameters: -- 50Hp, 3-phase, 60Hz, 460V, Star connected.
```

```
Hp=50;           %Power rating of Induction motor
p=4;            %Number of poles
Bm=0.1;        %Friction coefficient in rad/sec
J=1.662;       %Moment of inertia in Kg-m^2
fro=0.96;      %Rotor flux linkage in weber
wb=178.54;     %Base speed in rad/sec
fo=60;         %Base frequency in Hz
Lsl=0.8e-3;    %stator leakage inductance in hanery
Rs=0.087;     %stator resistance in ohm
Lm=34.7e-3;   %stator mutual inductance in hanery
Lrl=0.8e-3;   %rotor leakage inductance in hanery
```

```
%%%%%%%% Vector controller or commanded parameters%%%%%%%%
```

```
Lslc=0.8e-3;    %commanded stator leakage inductance in hanery
Rsc=0.087;     %Commanded stator resistance in ohm
Lmc=34.7e-3;   %Commanded mutual inductance in hanery
Lrlc=0.8e-3;   %Commanded rotor leakage inductance in hanery
Rrc=0.228;     %Commanded rotor resistance in ohm
Rr=Rrc;        %stator resistance in ohm (variable)
Tlim=200;      %Torque limit (N-m)
```

```

Lrc=Lrlc+Lmc;
Lr=Lrc;
%%%%%%%%%%%%%%%%%%%%%%%%%%%%%%%%%%%%%%%%%%%%%%%%%%%%%%%%%%%%%%%%%%%%%%%%
Vdc=sqrt(2)*460;           %DC link voltage
fc=20000;                 %carrier frequency in Hz
MI=0.8;                   %modulation index
wo=2*pi*fo;
Kp1=12.55;Ki1=86;        %gain of flux current PI controller
Kp2=12.5;Ki2=86;        %gain of torque current PI controller
Kps=100;Kis=5200;       %gain of speed PI controller
Trc=Lrc/Rrc              %commanded rotor time constant
Tr=Lr/Rr                 %actual rotor time constant
K_alpha=Tr/Trc
K_beta=Lm/Lmc
Kte=(3/2)*(p/2)*(Lm/Lr) %torque constant
K_s=1-Lm^2/(Lr*Lr)     %Leakage coefficient

```